Brown Dwarfs in the solar neighborhood

a high resolution study of their physical properties
and the search for planetary mass companions

Dissertation

zur Erlangung des akademischen Grades
***doctor rerum naturalium* (Dr. rer. nat.)**

vorgelegt dem Rat der Physikalisch-Astronomischen Fakultät
der Friedrich-Schiller-Universität Jena
von

Diplom-Physikerin

Micaela Bianca Stumpf

geboren am 19.06.1973 in Stuttgart

Gutachter

1. **Prof. Dr. Thomas Henning**
   (Max-Planck-Institut für Astronomie Heidelberg &
   Friedrich-Schiller-Universität Jena)
2. **Prof. Dr. Artie Hatzes**
   (Thüringer Landessternwarte Tautenburg & Friedrich-Schiller-Universität Jena)
3. **Prof. Dr. Peter H. Hauschildt**
   (Hamburger Sternwarte & Universität Hamburg)

Tag der Disputation : 19. Januar 2010

Zusammenfassung

Beobachtungen von Braunen Zwergen sind von entscheidender Bedeutung, da ihre Eigenschaften zwischen denen von späten Sternen und Riesenplaneten liegen. Da die Braunen Zwerge nie das stabile Wasserstoffbrennen der stellaren Hauptreihe erreichen, existiert für sie keine eindeutige Masse-Leuchtkraft-Beziehung, was eine exakte Bestimmung ihrer physikalischen Eigenschaften und die Überprüfung der Entstehungstheorien erschwert. Eine besondere Lösung dieses Problems bieten räumlich aufgelöste Doppelsysteme von Braunen Zwergen, die eine dynamische Massenbestimmung der Einzelkomponenten unabhängig von vorhandenen Modellen ermöglichen.

Die vorliegende Dissertation stellt die Ergebnisse einer laufenden Studie von solchen Doppelsystemen mit relativ kurzer Umlaufperiode dar, basierend auf hochaufgelösten photometrischen und spektroskopischen Nahinfrarot - Beobachtungen mit dem *Very Large Telescope* und seiner durch natürlichen und Laserleitstern gestützten adaptiven Optik. Die ausgewählten Objekte umfassen hierbei den gesamten Spektralbereich von den frühen L Zwergen, dem auffälligen Übergangsbereich von L nach T, bis hin zu den späten T Zwergen. Für das Doppelsystem Kelu-1 AB werden die erhaltenen Bahnparameter, sowie die erste dynamisch bestimmte Systemmasse diskutiert. Die zusätzlich erhaltenen ersten Einzelspektren weisen auf eine dritte Komponente im System hin, die Kelu-1 AB damit zu einem exzellenten Kandidaten für ein Braune Zwerge - Dreifachsystem machen. Die photometrischen Untersuchungen von 2MASS 0310+1648 AB, eines Doppelsystems im L / T Übergang, lassen eine auffällige Erscheinungsform erkennen, die höchstwahrscheinlich auf die Entdeckung des erst fünften L / T Doppelsystems mit einer Umkehrung des Helligkeitsverhältnisses der beiden Komponenten schliessen lässt. Anschliessend erlaubten die erhaltenen, ausgedehnteren Einzelspektren des T Zwerge Systems ϵ Indi Bab, sowie die Ergebnisse für Kelu-1 AB, eine Überprüfung der Vorhersagen der Atmosphären- und Entwicklungsmodelle. Die Analysen scheinen einen bereits früher aufgetretenen Trend zu bestätigen, dass die derzeitigen Modelle die Massen der ultrakühlen Sterne und Braunen Zwerge zumindest teilweise unterschätzen.

Des Weiteren wurden Beobachtungen von zwölf relativ jungen L Zwergen aus der sonnennahen Umgebung mit dem *Hubble Space Telescope* durchgeführt, um nach Begleitern mit planetarer Masse zu suchen. Die Ergebnisse wurden mit Hilfe der differentiellen Abbildung erzielt, die sich die verschiedene spektrale Eigenschaften der Objekte zu Nutzen macht. Es konnten zwei neue Doppelsysteme aus Braunen Zwergen aufgelöst werden. Die erhaltenen Parameter, wie z. B. Abstände und Massenverhältnisse, stehen

im Einklang mit den Ergebnissen aus früheren Multiplizitäts-Studien Brauner Zwerge. Schliesslich konnte noch ein möglicher Begleiter zu 2MASS 0337-1758 identifiziert werden, dessen erste Massenabschätzungen an der Grenze zwischen Braunen Zwergen und Planeten liegen. Dies macht ihn zum Kandidaten als kühlsten und masseärmsten bisher aufgelösten Begleiter eines L oder T Zwerges.

Abstract

The observations of brown dwarfs play a crucial role because of their properties intermediate between those of late-type stars and giant planets. As brown dwarfs never stabilize on the hydrogen burning main sequence, there is no unambiguous mass-luminosity relation. This makes it hard to determine their physical properties and to test theories of formation processes. Spatially resolved brown dwarf binaries provide the unique opportunity to determine the dynamical masses of the binary components independently of theoretical models.

This thesis presents the results of an ongoing near-infrared high-resolution spectroscopic and photometric monitoring program with the *Very Large Telescope* Natural Guide Star and Laser Guide Star Adaptive Optics systems to observe binary brown dwarfs with relatively short orbital periods. The chosen objects cover the entire spectral range from early L dwarfs, across the particularly interesting L / T transition to the late T dwarfs. For the L dwarf binary system Kelu-1 AB the results of the orbital fits are discussed, including the first dynamical mass estimate of the system. In addition, the first resolved spectra provide evidence for a third system component, making the system an excellent candidate to be the first pure brown dwarf triple system discovered so far. Photometric investigations on the L / T transition binary 2MASS 0310+1648 AB revealed a very striking nature of the system, most likely resulting in the detection of the only fifth resolved L / T transition binary with a flux reversal between the components. Furthermore, extended resolved spectra of the T dwarf binary ϵ Indi Bab allowed, together with the Kelu-1 AB results, to test atmospheric and evolutionary models. The analysis seems to confirm the already previously reported trent that current models, at least partly, underestimate the masses of very low-mass stars and brown dwarfs.

A spectral differential imaging program on a sample of twelve relatively young field L dwarfs in the solar neighborhood was carried out, using the *Hubble Space Telescope*, to search for planetary mass companions around brown dwarfs. Two brown dwarf binaries were resolved and the derived binary parameters like separations and mass ratios, as well as the overall binary fraction of the survey are consistent with the results of previous multiplicity surveys of brown dwarfs. Finally, a companion candidate to 2MASS 0337-1758 is identified. First mass estimates place it at the brown dwarf/planetary mass boundary and make it the coolest and least massive resolved companion candidate to any L or T dwarf.

für meinen Neffen ***Philipp***

den kleinsten, aber hellsten Stern
in meinem Leben

Eines sollten wir nicht verlernen:

den staunenden Blick
eines Kindes

– Augustinus –

CONTENTS

1

INTRODUCTION

THE NEBRA SKY DISC is the oldest known precise illustration of astronomical phenomena and reveals the fascination that the amazing view of a clear night sky exerted on mankind already in prehistoric times several thousand years ago. What started out with the fundamental observations of the motion of the Sun, the Moon and the most prominent stars, soon experienced a wealth of observational advances. In the beginning, their interpretation was heavily influenced by politics and religions, but it finally became what it is today, the science of modern astronomy. One important step into this direction occurred 400 years ago when Galileo Galilei pointed the first telescope into the sky and saw details no eye had recognized before. Since then, further developments of instruments and improved techniques led to more and more groundbreaking discoveries and even more important, the verification of physical theories. In particular in 1995, when substellar astronomy culminated in the first unambiguous discoveries of brown dwarfs, which had been already theoretically hypothesized since 1963, and the first extrasolar planet (exoplanet) around a sun-like star, at the same time.

1.1 Brown Dwarfs – siblings of stars or planets?

The existence of stellar-like objects below a minimum mass of ~ 0.07 - $0.08\ M_{\odot}$, depending on metallicity, which are not massive enough to sustain stable hydrogen fusion in their core, was first predicted independently by both Kumar (1963) and Hayashi & Nakano (1963). These originally called "black dwarfs" were later renamed into *Brown Dwarfs* by Tarter (1975). In contrast to stars they would never stabilize their luminosity, go through normal stellar evolution and reach the main sequence, but would become objects with a completely degenerated core. However (like stars and unlike planets), they are heavy enough to fuse deuterium in the beginning and therefore shine like faint

stars, but then continually evolve to cooler temperatures and dim over time, like planets, once they radiate away their initial contraction energy and their supply of deuterium is exhausted.

While the boundary between stellar and substellar objects is clearly determined by the hydrogen-burning limit, the exact definition of a brown dwarf at its lower mass limit and hence of a planet at its upper limit, is still a difficult and controversial issue. Originally, the terms *star* and *planet* were defined by the distinction based on their formation process, whereby stars form through cloud fragmentation and planets form within a circumstellar disk. Another focus is set on the interior physics: that planets do not drive any nuclear reaction. This automatically defines an upper mass limit for planets at $\sim 13\ M_{\rm Jup}$, the minimum theoretical mass for deuterium burning (Saumon et al., 1996; Chabrier et al., 2000). While the formation processes of brown dwarfs and giant planets are not yet finally specified (see §1.1.1), it has been also pointed out that deuterium is essentially insignificant for the long term evolution of brown dwarfs and their physical properties (see Chabrier et al. 2007 and further discussions therein). Hence, neither the formation criteria nor the mass limit provide a reliable way to clearly distinguish between brown dwarfs and planets. Currently, the most-agreed definition is the "working definition" of the IAU[1], which considers objects with masses above the limiting mass for thermonuclear fusion of deuterium to be brown dwarfs, no matter how they formed nor where they are located, whereas objects with lower masses in orbits around stars or stellar remnants are considered planets.

1.1.1 Different formation models for brown dwarfs

Similar to the lack of a clear boundary between brown dwarfs and planets, it has turned out to be challenging to place firm limits on the formation and evolution of brown dwarfs. Currently exists no common scenario on the dominant mechanism. One of the several proposed mechanism is the traditional star-like formation by direct collapse and fragmentation of molecular clouds (scaled Jeans model), but standard models seem to have difficulties in fragmenting a cloud or stopping the envelope mass accretion at or near the hydrogen burning limit (Boss, 2001; Bate et al., 2002). Hence, additional mechanism are required that halt accretion during the protostellar stage, like the ejection of protostellar embryos from their natal cores (Reipurth & Clarke, 2001; Umbreit et al., 2005) or photoevaporation of their accretion envelope by the radiation of a nearby

[1] www.dtm.ciw.edu/boss/definition.html

high-mass star (Whitworth & Zinnecker, 2004). Additional suggestions for formation processes include the turbulent or gravitationally enhanced fragmentation of molecular clouds, producing very low-mass prestellar cores by shock compression (Padoan & Nordlund, 2004; Bonnell et al., 2008), as well as gravitational instabilities in massive circumstellar disks and subsequent stripping of the substellar companion through encounters with other stars producing free-floating brown dwarfs (Goodwin & Whitworth, 2007; Stamatellos & Whitworth, 2009). Otherwise, brown dwarfs could be also formed like giant planets by core accreation or disk instabilities. If brown dwarfs were formed like giant planets, the question arises, why giant planets seem to remain in orbits around their hosts while there is an apparent paucity of brown dwarf companions orbiting within ~ 3 - 4 AU of solar-type stars, the so-called brown dwarf desert. None of the mentioned formation mechanisms is compatible with all available observations. Hence, none of these mechanisms are mutually exclusive and their relevance might most probably depend on the stellar environment with its varying initial conditions (see also most recent reviews by Luhman et al. (2007) from the observational side and Whitworth et al. (2007) for the theoretical side).

1.1.2 Evolution and physical properties

With masses of $\sim 75\ M_{\rm Jup}$ to 13 $M_{\rm Jup}$ the brown dwarfs fill the gap between low-mass stars and giant planets, and share multiple common characteristics with both of them. In particular their similarities to planets make them an important tool for predicting and studying the properties of exoplanets since those are still extremely challenging to image and study directly.

Since the first unambiguous detection of the very cool brown dwarf Gl 229 B[2] (Nakajima et al. 1995), the first brown dwarf in the Pleiades Teide 1 (Rebolo et al. 1995) and the first extrasolar planet Peg 51b[3] (Mayor & Queloz 1995) hundreds of brown dwarfs were identified in wide-field red and near-IR imaging surveys such as the Two Micron All Sky Survey (2MASS; Cutri et al., 2003), the Deep Near-Infrared Survey (DENIS; Epchtein et al., 1997) and the Sloan Digital Sky Survey (SDSS; York et al., 2000). At present, about 720 brown dwarfs have been discovered and they are known as compan-

[2] Actually, Becklin & Zuckerman (1988) detected the first L dwarf GD 165 B around a white dwarf but an explanation for the unusual spectral features was not immediately apparent and thus it stayed a curious object for another seven years.

[3] Already Wolszczan & Frail (1992) announced the existence of a planet around a pulsar but the planet around 51 Peg was the first around a main sequence star, similar to the Sun.

ions to stars, in nearby star-forming regions and young star clusters or, most commonly, as faint isolated objects in the field.

Their optical and near-IR spectral morphologies, distinct from those of the M dwarfs, led to the extension of the spectral classification sequence with the new spectral types L and T (Kirkpatrick et al. 1999; Martín et al. 1999b). While the early L spectral types contain a mixture of very low mass stars and brown dwarfs, the T type class is composed entirely of brown dwarfs. The following observational and theoretical studies of L and T dwarfs and their classification efforts established a complete spectral sequence from L0 to T9 (e. g. Geballe et al. 2002; Burgasser et al. 2002a; McLean et al. 2003; Knapp et al. 2004). With spectral properties intermediate between those of very low-mass stars and giant planets the observations of brown dwarfs play a crucial role. They exhibit a remarkably varied set of characteristics which hint at the complex physical processes acting in their atmospheres and interiors. The brown dwarfs cover an effective temperature (T_{eff}) range from $\sim$2400 K down to $\sim$650 K. This temperature is very well correlated to the spectral type for early- to mid - L dwarfs (2400 - 1500 K), as well as for mid- to late - T dwarfs (1300 - 650 K), and hence the spectral sequence is also an evolutionary sequence since brown dwarfs cool with time. Yet this correlation is broken in the transition from L to T dwarfs, where over a rather small effective temperature range of 200 K centered around $T_{eff} \sim 1400$ K, spectral properties of brown dwarfs change rather abruptly. The reason for the occurrence over this comparatively narrow effective temperature range is not yet understood and still an area of intense investigations.

Spectral characteristics and atmospheric properties

The spectral classification, based on the morphology of the atomic and molecular absorption features, is the most basic characterization of a brown dwarf, since for most objects these are the only physical properties which can be directly measured. Their spectra are windows through which we can access the physics and chemistry of substellar atmospheres down into the planetary regime. The spectra of the L dwarfs are characterized by: *i*) the disappearance of gas-phase TiO and VO; *ii*) the absorption from neutral alkali metals (e. g. , K and Na) and metallic hydrides (FeH and CrH); *iii*) the increasing depths of the H_2O bands at 0.93 μm and 1.35 - 1.50 μm and the strong molecular bands of CO at 2.3 - 2.5 μm and *iv*) the increasing steepness of the 0.6 - 1.0 μm spectrum. Contrary to that, the near-IR spectra of the T dwarfs are dominated by broad absorption bands of CH_4 ("methane dwarfs"), as well as H_2O absorption lines, and from T5 on also collision-induced absorption by H_2. The transition of late-L to

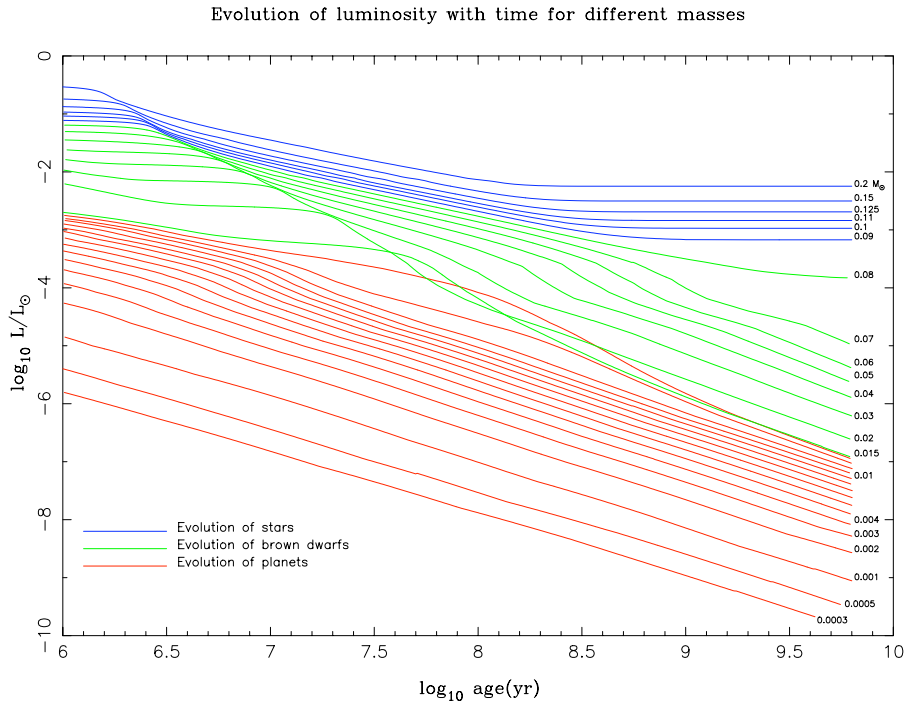

Figure 1.1: Luminosity vs. age evolutionary tracks of low-mass stars (blue), brown dwarfs with masses $\geq 13 M_{\rm Jup}$ (green) and brown dwarfs / giant planets with masses $\leq 13 M_{\rm Jup}$ (red). From Burrows et al. 1997.

early-T dwarfs takes place when the CH_4 absorption starts to appear in both the *H* as well as in the *K* band (Geballe et al., 2002; Cushing et al., 2005). Whereas the *JHK* colors of L dwarfs become redder with decreasing effective temperature, the absorption of these molecules strengthens and causes the T dwarfs to become increasingly bluer. While observational confirmations are still lacking, there is already the prediction of even cooler brown dwarfs than the T spectral type. The hypothesized objects in this class are called Y dwarfs and theoretical models predict the presence of water clouds and ammonia in their spectra (e. g. , Burrows et al., 2003). For more information on the L and T spectral classes, see the recent extensive review of Kirkpatrick (2005).

Since brown dwarfs cool continuously, they pass through the L and T stages with their initial spectral types depending on their masses. Hence their observational properties like effective temperature and luminosity are a function of mass, metallicity and age, which leads to the fact that not all brown dwarfs with the same effective temperature or spectral type are identical (e. g. , a young, slightly less massive brown dwarf can have the same $T_{\rm eff}$ as an older, more massive brown dwarf, see Figure 1.1). To understand all effects of different surface gravities or different colors, several evolutionary models (e. g. , Burrows et al. 1997, 2001; Chabrier et al. 2000; Baraffe et al. 2003), as well

as different models with synthetic spectra for cool atmospheres have been developed, discussing the role of dust, clouds and irradiation (e. g. , Ackerman & Marley 2001; Allard et al. 2001; Tsuji 2002; Burrows et al. 2006). While these current models agree very well with the observations of early L dwarfs (photospheric cloud or dust models) and later T dwarfs (relatively dust-free photosphere or condensate models), they fail to accurately describe the complex processes which are taking place in the atmospheres of those dwarfs at the L / T transition. The surprising brightening in the *J* band, the rapid cloud disappearance, the dramatic shift in the near-infrared spectral energy distribution at $T_{eff} = 1400\ K \pm 100\ K$, as well as conflicting spectral classifications between optical and near-infrared observations for single brown dwarfs cause a wide diversity in the interpretation of these effects (for further discussions on these issues see §4.1 and 5.3.2 and references therein).

To verify the evolutionary models and the theories of inner structure and atmospheres of substellar objects, the observations of brown dwarfs play a leading role. Much effort has been devoted to the modeling of substellar objects during the past decade, improving the understanding of the cool atmospheres, but quite often enough there is still a discrepancy between observed results and theoretical predictions.

1.2 Importance of binaries

The remaining ambiguity between the temperature or luminosity of a brown dwarf and its age or mass throughout its lifetime makes it hard to determine the physical properties of brown dwarfs and to confirm the theoretical models by observations. However, spatially resolved binaries are expected to be coeval, thus removing part of the degeneracy in the mass - luminosity (age - temperature) relation. In addition, they provide the unique opportunity to determine the orbital motion and therefrom derive the dynamical mass for the binary and its components independently from any theoretical model. Such binaries also provide a system with a common age and metallicity, which in turn can help to interpret the physical properties of their cool atmospheres. To check the consistency of the evolutionary models with the observations, one can adjust the theoretical isochrones empirically to fit the observed total masses as well as the individual luminosities of the multiple systems. This can then be followed by the comparison of other indicators like rotation, activity, the presence and strength of spectral features or gravity sensitive features with the corresponding prediction of the ages. In some cases the age of such binary configurations can be determined with considerably higher precision

than for single field brown dwarfs (Liu & Leggett 2005).

Since little is yet known about the responsible mechanism for the formation of brown dwarfs, further studies of the distribution of the binary semimajor-axis separation, their mass ratios and the overall binary fraction will additionally provide important clues and constraints on the origin of brown dwarfs. The various formation mechanisms described in § 1.1.1 are expected to result in differing frequencies and properties of brown dwarfs, e. g. the embryo-ejection scenario predicts only a few brown dwarf binaries in preferentially close orbits, while the isolated fragmentation scenario is expected to generate brown dwarf binaries with similar properties (larger number of binaries or multiples with a wide range of separations) as stellar binaries, only scaled down (for a comprehensive discussion on brown dwarf binary properties see Burgasser et al., 2007).

Therefore, the measurement of the dynamical masses, independent from any model, will not only lead to a much better understanding of their physical properties like interior structure, dust formation, settling and depletion of refractory elements or the underlying opacities, but also to the understanding of their mass distribution and formation processes. Although these dynamical mass measurements are highly required for very low-mass stars and brown dwarfs, only few such measurements have been achieved up to now and large uncertainties remain (see Zapatero Osorio et al. 2004; Bouy et al. 2004; Brandner et al. 2004; Stassun et al. 2006; Ireland et al. 2008; Liu et al. 2008; Dupuy et al. 2008). A search for a larger number of binary brown dwarfs with short orbital periods is necessary to cover a wider parameter space and provide a more accurate picture of the different evolution of objects with the same age but different masses. This will finally lead to a reliable calibration of the theoretical models.

1.3 Outline of this thesis

This PhD thesis investigates on a variety of questions related to the formation and evolution of brown dwarfs like the frequency of very low-mass companions to brown dwarfs, the structure of their atmosphere, as well as other physical and chemical properties. These issues were tackled from two different directions.

Chapter 2 describes the first search for planetary mass objects around a sample of twelve young and isolated brown dwarfs with the spectral differential imaging technique, validating this observing strategy. In addition, the derived separations and mass ratios of three resolved binaries in comparison to previous findings of other surveys are

discussed. The following chapters treat the variety of brown dwarf characteristics using the example of three different binary systems covering the entire spectral range of brown dwarfs. These data were derived as part of a new high-angular resolution brown dwarf binary monitoring project.

Chapter 3 presents the results for the L dwarf system Kelu-1 AB for which the first dynamical mass estimations are derived, permitting the test of evolutionary models. The interpretation of resolved near-IR spectra indicates the presence of a third system component. In Chapter 4 the first photometric and astrometric results of the L / T transition binary 2MASS 0310+1648 are discussed, revealing a puzzling flux distribution which demands further investigations. Chapter 5 concludes with a comprehensive comparison of synthetic atmopheric spectra with resolved spectra of the T dwarf binary system ϵ Indi Bab. While it is shown that the atmospheric models improved in the past to better fit the observations, the results from the evolutionary models still indicate an underestimation of the component masses compared to existing dynamical mass estimates. Finally, Chapter 6 summarizes the most important results and provides an outlook on ongoing and possible future projects in connection with this work.

2

THE SEARCH FOR PLANETARY MASS COMPANIONS WITH HST

2.1 Motivation

SINCE the discovery of the first extrasolar planet around 51 Pegasi by Mayor & Queloz in 1995, more than 330 extrasolar planets (exoplanets) in more than 280 planetary systems have been identified to date[1]. However, most of these detections were made using indirect detection methods like radial velocity (RV) surveys, the transit method or microlensing events. Further, the RV technique can in general only provide minimum masses ($M \sin i$) and therefore, only detect planet *candidates*. From the beginning, these exoplanets revealed a remarkable diversity in their physical and orbital characteristics like separation, eccentricities and masses and thus challenged the planet formation scenario. In particular, the period-mass distribution shows tendencies which are hard to explain within the framework of current models (e. g. massive "hot Jupiters" were mostly found at very small orbits, even down to a semi-major axis of only 0.02 AU). A revision of the standard scenario seemed to be required. However, the discovery space of RV searches does not yet cover planets at distances larger than about 5 AU (for statistics see Marcy et al. 2003). The question is, if the observed period-mass distribution is, at least partly, a selection effect (higher sensitivity at shorter orbital periods) and thus might provide only an incomplete picture of the overall planet population, or if giant planets are really rare at larger separations. In addition, the indirect RV and microlensing techniques do not enable any photometric or spectroscopic information of the exoplanet companions and their physical properties such as brightness, color, effective temperature or composition.

[1] http://exoplanet.eu/catalog.php

Therefore, a lot of attention has been directed towards direct imaging of planetary mass objects (PMO) in the last years. A direct detection would enable extensive follow-up studies to characterize the planets, but the main challenge of this method is to deal with the huge brightness contrast and the small angular separation between the faint planet companion and its host star. With the possibility of high-resolution space-based observations and the improvement of adaptive optics (AO) systems on large ground-based telescopes, the necessary sub-arcsecond spatial resolution became achievable. In addition, exoplanets and brown dwarfs are hotter at younger ages and hence the brightness contrast between the primary and a possible companion will be much smaller. Thus, in order to push the direct detection threshold down to the planetary mass regime, systematic searches focused especially on young stars in nearby associations.

First extensive *Hubble Space Telescope* (HST) programs to search for substellar companions to post-TTauri stars (Brandner et al., 2000), as well as to very low mass (VLM) stars and brown dwarfs in the Pleiades open cluster (Martín et al., 2000a) did not reveal any companion at intermediate orbits. Since then, several other extended HST surveys of free-floating ultra-cool dwarfs and brown dwarfs revealed that roughly 20% of them have substellar companions. Almost all of them constitute close to equal-mass systems (e. g. Bouy et al. 2003; Reid et al. 2001b; Burgasser et al. 2003b) and hence, rather resemble more massive, stellar binaries than planetary systems. These L and T dwarf binaries possibly hint at a similar formation process for ultra-cool dwarfs and stars. Consequently, some interesting questions arose:

Do "single" brown dwarfs evolve similar to single stars?

Are they capable of forming planetary systems?

The detection of circumstellar disks around several young brown dwarfs revealed that they at least posses the raw material to form planets (e. g. Apai et al. 2002; Pascucci et al. 2003; Liu et al. 2003; Jayawardhana et al. 2003; later confirmed by results of e. g. Apai et al. 2005; Luhman et al. 2006a, 2008; Scholz et al. 2008, see also reviews in Luhman et al. 2007 and Henning 2008).
On that account, we started in 2004 the first spectral differential imaging (SDI) survey with HST to directly detect a planetary mass object in a close orbit around nearby free-floating brown dwarfs. A direct image detection would have important implications on our understanding of exoplanets, their origin, the formation of substellar bodies in general and binarity in the brown dwarf domain in particular.

2.2 Observing strategy

Because of the higher achievable contrast and the lack of suitable AO reference stars, the observations were conducted from space with HST as explained in the following. With AO observations at large telescopes, the same (or sometimes even better) angular resolutions can be achieved than with HST. However, the final achievable contrast with ground-based observations is limited by spatially correlated speckle noise caused by imperfect wavefront correction and primarily due to light scattering by optical imperfections of the telescope, leading to quasi-static speckles that remain in AO corrected images. For space-based imaging, these limitations are greatly relaxed because the atmosphere plays no role in degrading the stability of the observed point spread function (PSF). Although HST suffers similarly from quasi-static speckles (here caused by thermal induced movement of the optical elements, known as HST "breathing"), the timescale of their evolution is roughly an HST orbit and not minutes like in the ground-based observations, allowing a precise measurement and reproducibility of the PSF structure.

Furthermore, the high-order AO performance is strongly limited by the requirement of a sufficiently bright (minimum $K \approx 12$ mag), nearby natural "guide star" (NGS) for the correction system. Our target sample is comprised of field brown dwarfs, most of which have fainter K_S magnitudes and no bright enough NGS in their vicinity. Thus, only HST provided the necessary combination of high angular resolution and image stability required to resolve a much fainter companion at a very small separation.

The observing strategy that suited best to reach our goal of detecting planetary mass objects around brown dwarfs and to overcome the remaining brightness contrast, was the spectral differential imaging (SDI) technique (Smith et al., 1987). This technique takes advantage of the fact that a cool (≤ 1300 K) giant planet or low-mass brown dwarf (i. e. T dwarf) is much fainter in certain molecular bands due to strong absorption than in the neighboring continuum. Already Allard & Hauschildt (1995) stated that the spectral energy distribution (SED) of brown dwarfs is very peculiar. The molecular opacities, which globally define the continuum of brown dwarfs, cause the SED to peak around 1.1 μm for solar metallicities, almost independent of their effective temperature. Further, the observed *J*–*K* colors for L dwarfs are red (about + 2 mag), while they are blue (- 0.1 to + 0.4 mag) for the T dwarfs. This is caused by dust grain formation (Allard et al., 2001). Therefore, the brightness difference of any L dwarf – T dwarf pair is smallest around 1.1 μm, making the *J* - band the best spectral regime to detect T - type

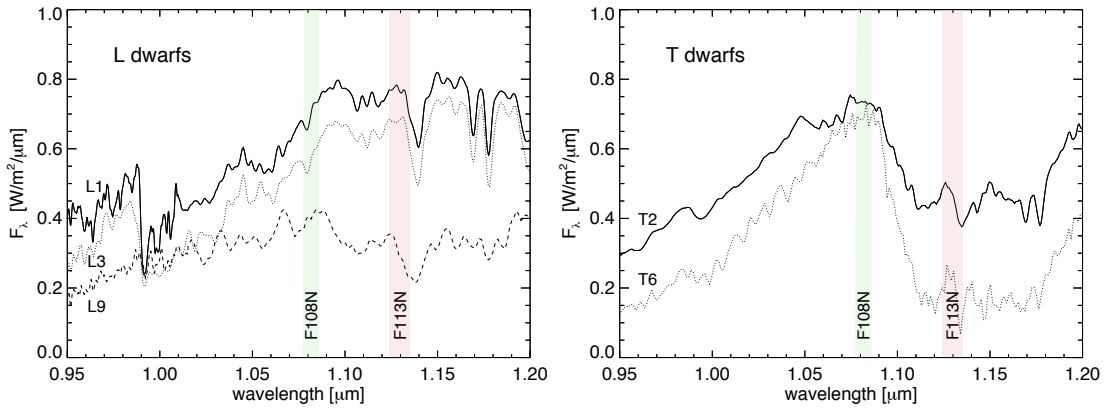

Figure 2.1: Observed spectra of L and T dwarfs (from S. Legett's online archive) with the superimposed bandpass of the HST F108N and F113N filters. For a better comparison the flux is arbitrarily scaled.

or even cooler companions to L dwarfs.

Figure 2.1 shows the spectral features of L and T dwarfs in this wavelength regime in detail. It reveals that L dwarfs have a comparative flat SED between 1.06 μm and 1.15 μm, while the flux of a T dwarf drops significantly at the beginning of the molecular water absorption band at $\sim$ 1.10 μm. Thus, a subtraction of two images obtained simultaneously, one in and one off, yet near this molecular band, will cancel out most of the equally bright PSF structure of the primary (L dwarf), revealing the much fainter signal from a cool, possibly planetary mass companion (see Rosenthal et al. 1996; Racine et al. 1999). The narrow-band filters F108N and F113N of the NICMOS1 camera (NIC1) on board HST match particularly well the relevant bands and are ideally suited for the differential imaging technique.

2.3 Sample selection

Given the angular separation and luminosity ratio problem described above, the list of targets was assembled with the focus on brown dwarfs in proximity to the Sun and with a relatively young age. A closer distance to the Sun translates in a larger angular separation for a given physical separation between the brown dwarf and an eventual planetary-mass object, thus companions on smaller orbits can be detected. In addition, the detection threshold caused by sky background decreases for a fainter planetary mass object, since its apparent brightness becomes larger, the closer it is to the Sun.

Concerning the age, priority was given to targets with estimated ages younger than 1 Gyr. Giant planets are more luminous when they are young due to the remaining

gravitational contraction energy from their formation process. Left without a resource of producing new energy they cool down rapidly and become dimmer with time. Hence any planetary mass companion to an old brown dwarf would be relatively cool and too faint for detection. Based on evolutionary models and synthetic spectra, a young (100 Myr) exoplanet is $\sim 10^5$ times more self-luminous than an old (5 Gyr) exoplanet, whereas their primary is only 2 - 5 times brighter at the younger age (e. g. Burrows et al. 1997; Baraffe et al. 2003).

The age estimation of the targets in this survey was not straightforward since all of them are field brown dwarfs without any hints of being a member of an association or moving group. They were selected according to spectral age indicators, such as the presence of Lithium in the atmosphere. The detection and strength of Lithium absorption is a clear confirmation of the substellar nature of these objects. Combined with the still relatively high effective temperature representative for the spectral type L this is a clear sign of youth ≤ 1 Gyr (Basri 1998; Magazzu et al. 1993). Moreover, the lack of chromospheric activity represented by a weak or non-existence of the H_α emission line is another indicator of youth/substellarity as suggested by Gizis et al. (2000).

The final sample was compiled out of ~ 250 L dwarfs cataloged in D. Kirkpatrick's online archive[2] as of 2004 (start of this project) and consists of 12 young L dwarfs which fulfilled the following requirements:

- the object is within 30 pc to the Sun
- the Li I absorption at 6708 Å is present and therefore a clear confirmation of their substellar nature and youth.
- the objects are isolated in the sense of no known close companion so far.

These age and proximity criteria helped to enlarge the range of mass and separation over which the survey would be sensitive and to maximize the discovery probability. The properties of all selected targets are summarized in Table 2.1. Although there are no Lithium measurements available for the two mid - L dwarfs 2MASSW 004521+1634 and 2MASSI 0835–0819, they were included since they belonged to the 10 closest L dwarfs known and because of their brightness compared to other L dwarfs of the same spectral type. A similar decision was made for Kelu-1 which had only a weak detection of the Lithium absorption line but was apparently overluminos and showed photometric

[2] now: http://www.DwarfArchive.org

and spectroscopic variability (for more details see Chapter 3). Furthermore, the nearby T dwarf 2MASSW 055919–1404 was added to calibrate the spectral differential imaging method for HST/NICMOS.

2.4 Observations and Data reduction

The observations of the twelve isolated L dwarfs and the calibration T dwarf were scheduled as HST program GO 10208 (PI: W. Brandner) from September 2004 to July 2005. The sources were observed with the NICMOS1 (NIC1) camera, providing a high-resolution pixel scale of $0\farcs0432$ and a field of view (FoV) of $11''$ x $11''$, in the two narrowband filters F108N (1.08 μm) and F113N (1.13 μm). The observation sequences consisted of 4 exposures at two different detector positions in each filter. This two-point dither pattern facilitates to optimize the PSF sampling, to effectively reject bad pixels and to gain redundancy against cosmic ray events. Altogether, two orbits per target were necessary to achieve the required S/N ratio of 6 - 8 for a limiting magnitude of $J = 20$ mag and a brightness difference of 6 mag at a separation of $0.3''$. All data were acquired in MULTIACCUM mode and the total integration times per filter were 2560 s (F108N) and 2816 s (F113N), respectively. In order to limit possible HST breathing variations in the PSF, differential imaging observations in the F108N and F113N filters were obtained in each of the orbits.

SDI data reduction

For the analysis of the data sets, the HST pipeline reduced images were used, followed by an additional bad pixel masking in order to compensate for the non-optimal bad pixel mask available in the pipeline. The SDI reduction was then accomplished with an own custom made IDL program: First, a square aperture around the brown dwarf is extracted from all four images in each filter. To make use of the full integration time, the extracted frames were then co-added after they were aligned with respect to the first image of the related filter. This alignment was done with a 2D cross-correlation and a FFT-shift based combination, which provides a sub-pixel accuracy. In the next step, a sub-pixel re-sampling was performed in order to transform the observation in the F108N filter to the same λ/D scale as in the F113N filter (where λ is the respective observing wavelength and D is the HST primary mirror diameter). The final difference between the two filters was then calculated after additional alignment of the two master images with the shift algorithm, followed by a flux calibration to account for any flux losses

Table 2.1: List of selected Targets

Object name	RA (J2000)	DEC (J2000)	SpT	Distance [a] [pc]	Li I EW [Å]	V [b,d] [mag]	J [c,d] [mag]	Observation Date	Ref.
2MASSW 004521+1634	00 45 21.4	+16 34 44.7	L3.5	10.4	?	22.0	13.1	17/11/2004	3,4
2MASSW 005110–1544	00 51 10.8	– 15 44 16.9	L3.5	30	10	24.1	15.2	02/12/2004	1
2MASSW 010332+1935	01 03 32.0	+19 35 36.2	L6	28.6	12	24.5	16.1	08/10/2004	1
2MASSW 031059+1648	03 10 59.9	+16 48 15.6	L9	20	5	24.8	16.4	24/09/2004	1
2MASSW 033703–1758	03 37 03.6	– 17 58 07.9	L4.5	29	8	23.6	15.6	24/09/2004	1
LSR 0602+3910	06 02 30.5	+39 10 59.2	L1	10.6	7	20.8	12.3	15/04/2005	4
2MASSI 0652+4710	06 52 30.7	+47 10 34.8	L4.5	11.1	14	21.4	13.5	24/03/2005	5
2MASSI 082519+2115	08 25 19.6	+21 15 52.0	L7.5	10.7 *	10	22.5	15.1	12/02/2005	1,2
2MASSI 0835–0819	08 35 42.6	– 08 19 23.7	L5	8.3	?	21.0	13.2	14/06/2005	5
2MASSW 124646+4027	12 46 46.8	+40 27 15.1	L4	25.1	11	22.3	15.0	22/10/2004	1
Kelu-1	13 05 40.2	– 25 41 06.0	L2	18.7 *	1.7	22.1	13.4	31/07/2005	2,6
2MASSW 152322+3014	15 23 22.6	+30 14 56.2	L8	18.6 *	9	24.4	16.3	30/09/2004	1
2MASSW 055919–1404	05 59 19.1	– 14 04 48.9	T4.5	10.3	–	25.0	13.8	07/09/2004	2,7

? denotes lacking observations

[a] Spectrophotometric distance estimates from the given references unless otherwise noted. Distance error is $\sim$ 10%

* Distance from trigonometric parallax in the given references

[b] from the CDS Simbad service

[c] from 2MASS All-Sky Point Source Cataloge

[d] Uncertainties of apparent magnitudes are $\sim$ 0.1 mag

References: [(1)] Kirkpatrick et al. (2000), [(2)] Dahn et al. (2002), [(3)] Wilson et al. (2003), [(4)] Salim et al. (2003), [(5)] Cruz et al. (2003), [(6)] Kirkpatrick et al. (1999), [(7)] Burgasser et al. (2003a)

during the previous re-scale process. In cases where a clear positive residual remained in the reduced image, the difference was also obtained separately for the individual dither positions (hence only two images per filter). This provides two independent detections of a real signal, or the exclusion, if it only exists at one position and is most likely caused by a cosmic ray remnant or hot pixel buried in the central core of the PSF.

2.5 Results

The visual examination of the reduced images reveals that for nine of our targets the residuals are at the level expected from photon noise and no significant positive signal stands out. The final images of these data sets are shown in Figures 2.2 - 2.4. The remaining single positive signals in some of the targets in Figures 2.2 and 2.4 just close to the the original PSF center, are examples for residuals caused by bad pixels which could not be corrected by the additional bad pixel masking, since they were buried in the bright core of the PSF. They are not visible in both of the "single" position SDI images simultaneously and thus do not correspond to a real signal of a possible faint companion. For the four brightest and closest sample targets 2MASSW 0045+1634, LSR 0602+3910, 2MASSI 0652+4710 and 2MASSI 0835-0819 (Figure 2.3) the final SDI results show systematic mirrored dark and bright features in the $\sim$ 6 - 7 central pixels of the images. These are common residuals in contrast-limited cases and are most probably caused by the systematic variations in the PSF structure due to the HST "breathing" already mentioned. Since the other five targets are much fainter and their residuals are mostly dominated by photon noise, this pattern is no longer visible. If they were brighter their residuals would look the same. Altogether, the smooth results indicate the absence of a planetary-mass companion with a minimum mass of 5 - 6 $M_{\rm Jup}$ between 0.07″ and $\sim$ 1.4″ around the brown dwarfs ($\sim$ 1 - 40 AU, depending on their distance to the Sun). This validates our observing and data analysis strategy.
For the three remaining L dwarfs, the observations revealed very interesting results which will be discussed in the following sections.

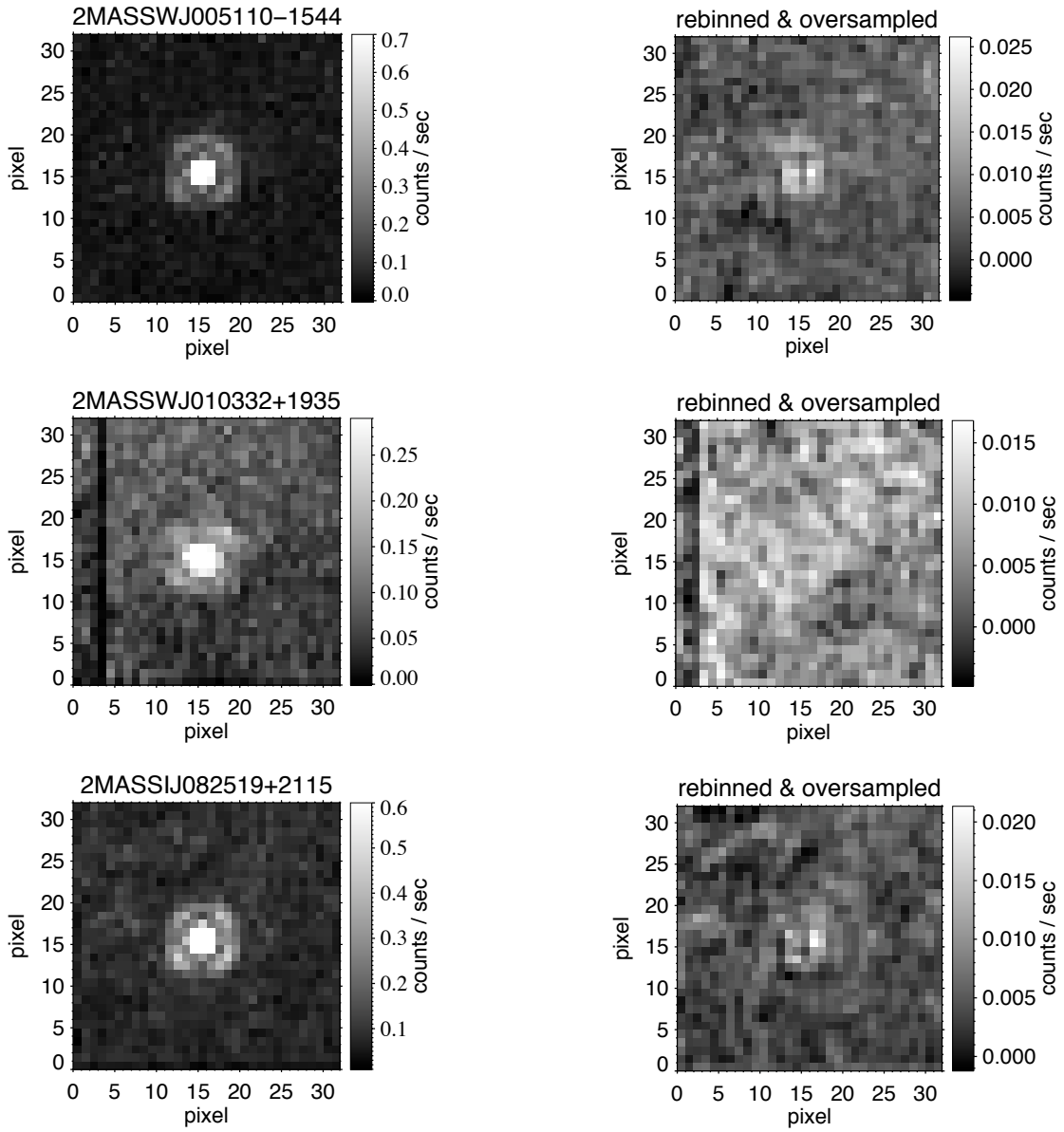

Figure 2.2: Result images for three of the nine targets: The image on the left represents the added image of all 4 exposures taken in the F108N filter with the upper cut-level reduced for a better visibility of the background (thus not representing the real peak values). The right image displays the final reduced image after the subtraction of the two filters. The positive signals visible in the central part of the final images of 2MASS 0051-1544 and 2MASS 0825+2115, are not simultaneously present in each of the individual reduced detector position images and are therefore residuals from bad pixels buried in the original PSF. The overall smooth result images confirm the correctness of our reduction procedure.

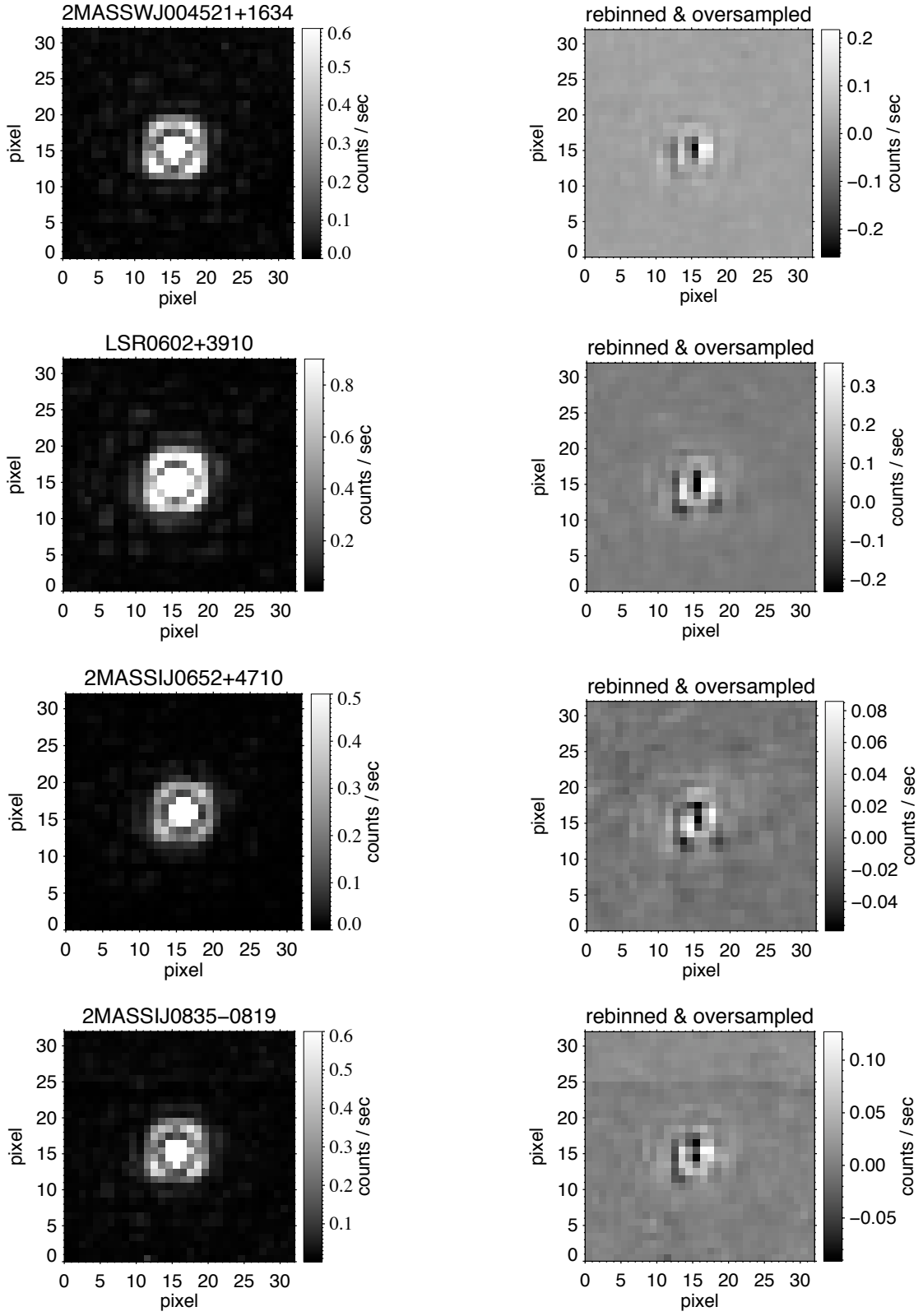

Figure 2.3: same as Figure 2.2. These are the four brightest and closest targets of the sample. The systematic mirrored dark and bright features are most probably caused by the systematic variations in the PSF structure due to the HST "breathing". However, no other convincing positive signal can be found in the vicinity of the brown dwarfs.

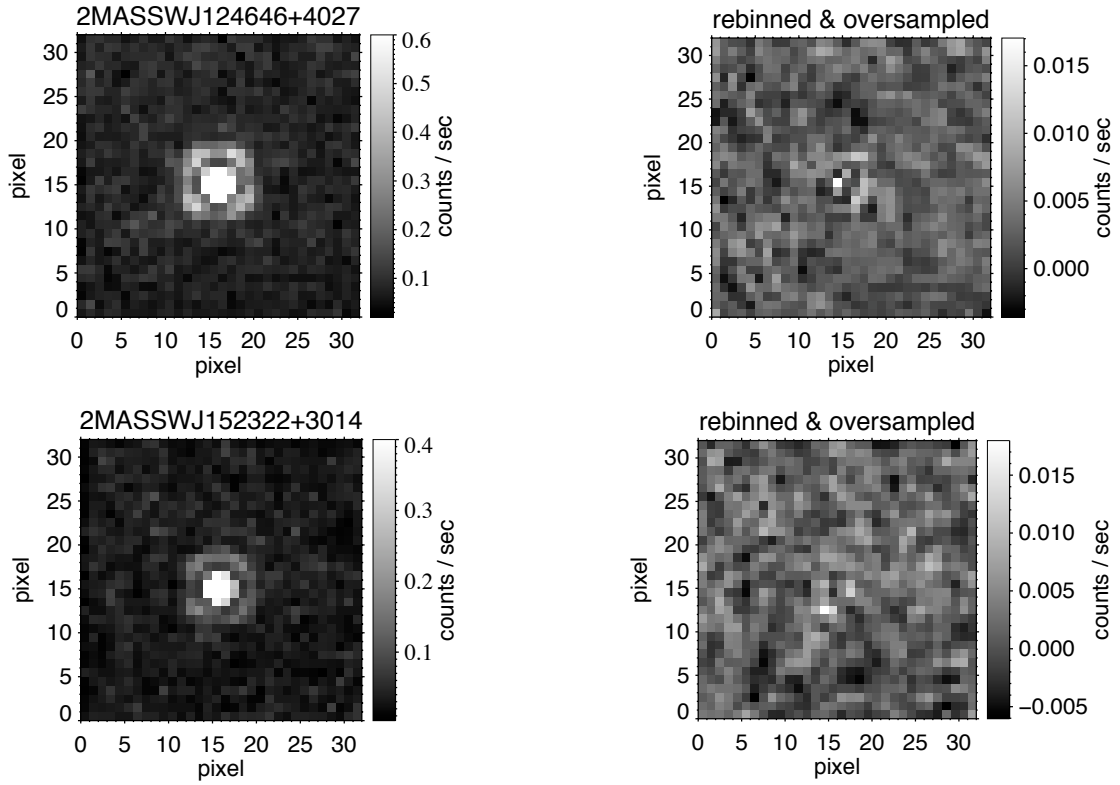

Figure 2.4: same as Figure 2.2. Again, the positive signals visible in both final images are residuals from bad pixels buried in the original PSF and are not present in each of the "single" position SDI images.

2.5.1 Two newly resolved brown dwarf binaries

Despite the effort to select only single brown dwarfs for the sample, the observations revealed that two of the targets are close binary systems. Figure 2.5 shows the NICMOS detection images where both systems are clearly resolved in two components.

Kelu-1 AB

Kelu-1 was independently resolved as a binary system with AO from the ground (Gelino et al. 2006; Liu & Leggett 2005) just four months before the HST observation in July 2005. This solved the by then unexplained overluminosity of the "single" object. The HST observation presented here, is now the first high-resolution confirmation of the physical association of both components. The system shows clear evidence for orbital motion with a fastly increasing separation of 15 mas in four months out to 299.8 $\pm$ 0.2 mas and a position angle (PA) of 221.33° $\pm$ 0.04°, hinting at a short orbit binary. This made Kelu-1 AB a good target for a monitoring program feasible, at least partly, on the timescale of this PhD program. Therefore, extensive follow up observations were obtained and all results concerning this system are discussed in its own Chapter 3.

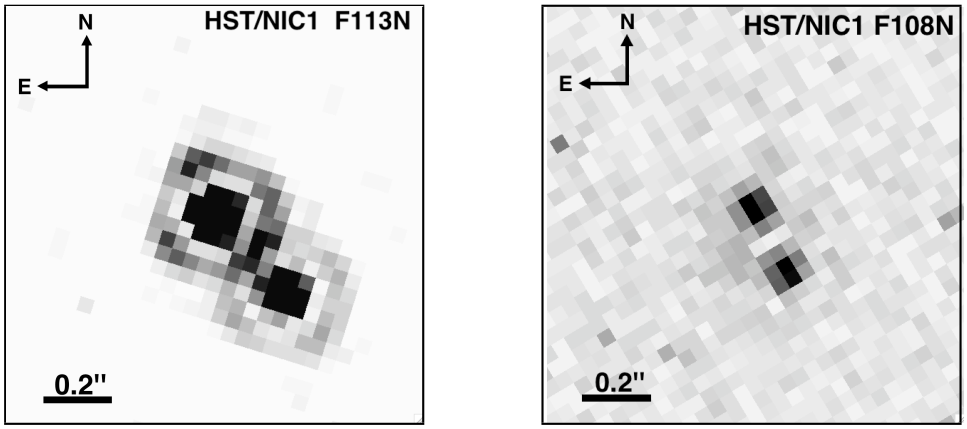

Figure 2.5: NICMOS images of the two resolved L dwarf binaries: on the left the bright, originally classified L2 dwarf Kelu-1 AB and to the right the much weaker L9 dwarf 2MASS 0310+1648 AB

2MASSW 0310+1648 AB

The second discovered very low mass binary is 2MASSW 0310+1648 AB. With an original spectral type of L9, this brown dwarf belongs to the still peculiar L/T transition objects which exhibit several unusual characteristics. Resolved for the first time as a binary system with almost equally bright components, it extends the already higher binary fraction among the brown dwarfs that span the transition between the L and T spectral class. The first astrometric measurements yield a separation of 204.3 ± 0.4 mas and a PA of $206.35° \pm 0.1°$ on September 24, 2004. Including follow up observations, this target will be further discussed in Chapter 4.

2.5.2 A planetary companion candidate

The HST observations of the L4.5 brown dwarf 2MASSW 0337-1758 revealed a clear residual signal in the final SDI reduced image, close to the center of the brown dwarf. Unlike for all the other L dwarfs in this survey, this signal is also visible in the two individually reduced detector position images. Therefore, it cannot be caused by a remaining bad pixel. Further, with a S/N ratio of 7 at its peak in the final image, it is well above the noise level. Figure 2.6 displays the resulting images with the single detector position results in the middle and the final result, including all observation exposures, at the bottom.

The F108N image of 2MASSW 0337-1758 and its final SDI reduced image were used to specify the magnitude difference between the brown dwarf and the companion candidate, as well as their separation and position angle. This was achieved by applying

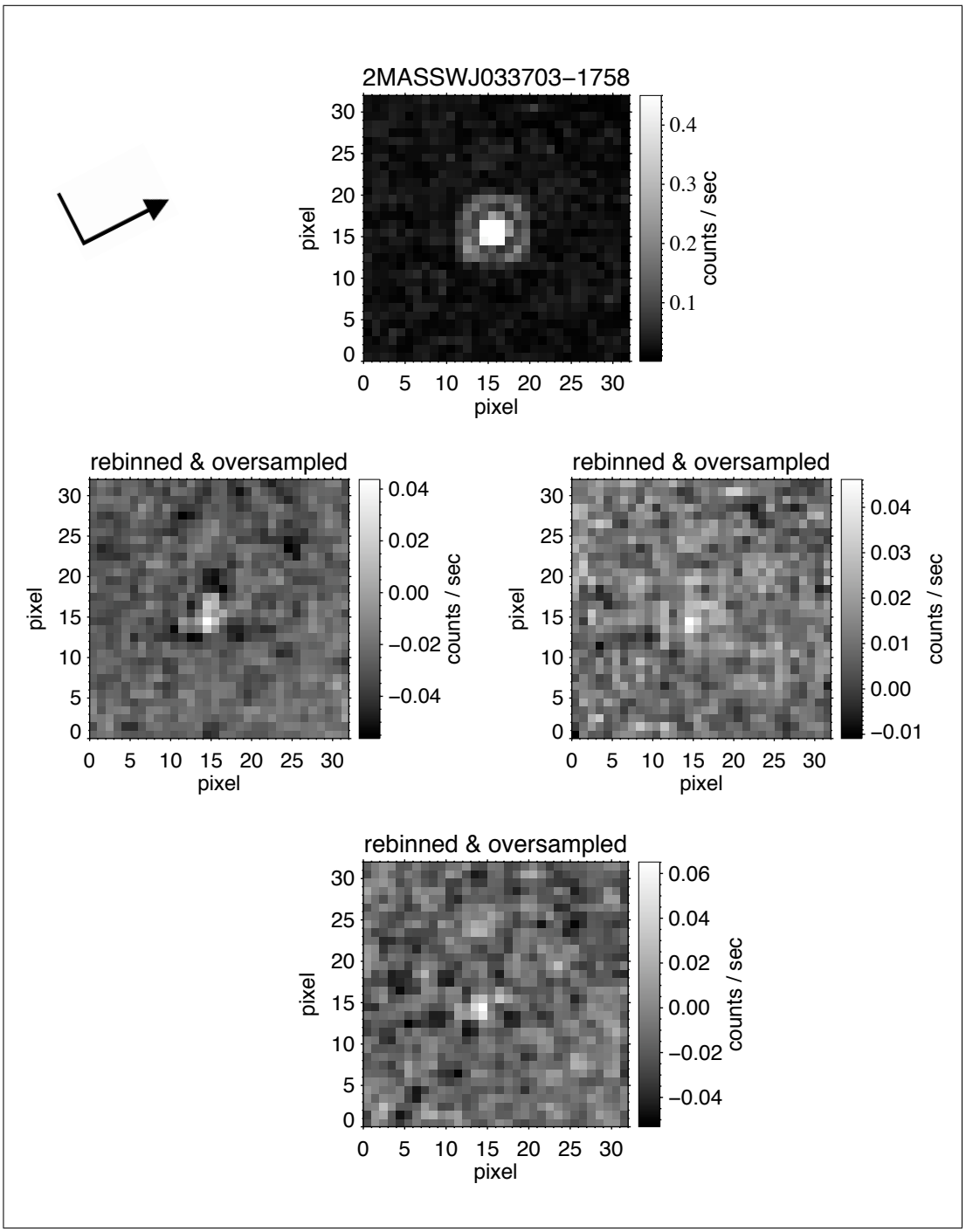

Figure 2.6: The result images for the L4.5 dwarf 2MASSW 0337-1758. The top image represents the added image of all 4 exposures in filter F108N and the bottom one the residual image of all exposures after the SDI reduction (same as in Figures 2.2 - 2.4). In the middle panel, the left inlay displays the residual image at position 1 on the detector, while the right displays the residuals at position 2. The clearly remaining positive signal is visible in all three residual images and thus any contamination by a bad pixel can be ruled out. The brightness difference in the final image is Δ F108N = 3.88 mag. The orientation of all inlays is the same and the north direction is indicated by the arrow.

aperture photometry with the IRAF *phot* routine in the *apphot* package. From the identified centroid positions of the photometric apertures a separation of $0.087'' \pm 0.015''$ (corresponding to 2.52 ± 0.44 AU at a distance of 29 pc) and a position angle of 195.6° ± 5.5° was calculated.

For the photometry, the preliminary assumption that the flux of the companion only contributes to the F108N filter and not the F113N filter was necessary, since the result of the applied SDI technique does not provide any information about the actual flux distribution of the companion candidate in each of the filters. This approximation is roughly valid for very late T dwarfs and even later spectral type objects (see Figure 2.1), but implies that the derived magnitude in F108N for the companion is only a lower limit. For further comparison with other observations and theoretical models, the instrumental count rates were converted into the Vega magnitude scale after aperture correction and using the most recent photometric keyword-value as provided by the STScI webpage[3]. Using this method, we derived a F108N magnitude of 16.54 ± 0.02 mag for 2MASSW 0337-1758 A, a brightness difference of 3.88 ± 0.03 mag between the brown dwarf and its companion candidate and hence a F108N magnitude of 20.42 ± 0.04 mag for the candidate. This corresponds to $M_{F108N} = 14.27 \pm 0.02$ mag and 18.15 ± 0.04 mag, respectively, at a distance of 29 pc.

Together with the age estimation of the primary brown dwarf, the comparison of the derived values with the COND evolutionary models for brown dwarfs and EGPs (extrasolar giant planets) by Baraffe et al. (2003) provides a first approximation of the mass and T_{eff} for the companion candidate. Since the F108N wavelength range lies much closer to the *Y*- band ($\lambda_C = 1.03$ μm) than to the *J* - band, it was assumed that the objects are equally bright in F108N and *Y*. For the following comparison with the isochrones, an extended version of the above mentioned evolutionary models including the *Y*- band (I. Baraffe, private communication) was used. The results for both objects are given in Table 2.2. A comparison of the derived mass and effective temperature for the primary 2MASSW 0337-1758 A with those, one would derive with its 2MASS *J* magnitude, proves the assumption of $M_{F108N} = M_Y$ to be acceptable. For the companion candidate we derive a minimum mass of 10 $M_{\rm Jup}$ to 15 ± 1 $M_{\rm Jup}$ with a T_{eff} between $\sim 600 \pm 20$ K and $\sim 620 \pm 20$ K for an age of 0.5 and 1 Gyr, respectively.

As of spring 2009, there are only six T dwarfs known, which are classified as T8 or

[3] http://www.stsci.edu/hst/nicmos/performance/photometry/postncs_keywords.html

Table 2.2: Mass estimations for the companion candidate of 2MASSW 0337-1758

Object	M_Y [mag]	0.5 Gyr		1 Gyr	
		$M_{\rm Jup}$	$T_{\rm eff}$ [K]	$M_{\rm Jup}$	$T_{\rm eff}$ [K]
Brown Dwarf	14.27 ± 0.02	36 ± 2	1455 ± 60	48 ± 1	1502 ± 30
companion candidate	18.15 ± 0.04	≥ 10	600 ± 20	15 ± 1	620 ± 20

later[4] and only four of them have a $T_{\rm eff} \sim 600$ K (Warren et al. 2007; Delorme et al. 2008; Burningham et al. 2008; Burgasser et al. 2008b). Hence, the companion adds up to a still very small number of just recently detected very cool brown dwarfs and the mass estimation places it right at the theoretical mass limit of $\sim 13\ M_{\rm Jup}$ for deuterium burning, which is mostly used as the boundary to distinguish between brown dwarfs and giant planets (see § 1.1 for the controversial discussion on that definition). Nevertheless, the dominant uncertainty in translating the derived magnitude difference to brown dwarf and even planetary masses, is the uncertainty of the evolutionary models, which are not yet fully calibrated by observations, especially the mass-luminosity relation as a function of age (see further discussions below and in Chapters 3 and 5).

A possible background object?

To clarify if the remaining signal is possibly caused by a background object, the position of 2MASSW 0337-1758 on previous HST/WFPC2 images was analyzed. These images were taken on December 25, 2000 in the broadband filter F814W and the medium band filter F1024M . No source could be detected in the WFPC2 frames above the noise level at the 2004 NICMOS position of the brown dwarf, but the comparison of the two positions allowed the first proper motion determination for 2MASSW 0337-1758 with $\mu_\alpha \cos\delta$ = $0.247 \pm 0.02''$/yr and μ_δ = - $0.024 \pm 0.028''$/yr. This result will be a crucial help to confirm the companionship in follow-up observations.

Analyzing the probability of a background source from a more physical/statistical side, the signal can already be excluded to be caused by a faint, stellar background source (like a M dwarf), since features with similar brightness in both filters are eliminated by the SDI technique and M dwarfs have, like L dwarfs, a relatively flat continuum between 1.08 - 1.13 μm. On the contrary, it does not exclude a distant galaxy or a quasar. To estimate the probability to detect such an object in a radius of $0.09''$ (= $1.96 * 10^{-9}$ square degree area) around 2MASSW 0337-1758 the following analysis was performed:

[4] http://www.DwarfArchives.org

Based on the fact that we have a point-like remaining signal with an approximate magnitude of $J \sim 19.5$ mag, the candidate is unlikely a "normal" galaxy and even too bright to be an active galactic nuclei (AGN), however it may still be a quasar. Taking into account that the remaining signal could have also been caused by a redshifted emission line, the strong [OIII] emission line was used for a first evaluation. A redshift z = 1.141 - 1.183 was found to place it on the F108N filter. Assuming that quasars are uniformly distributed over the sky (roughly valid for $z \leq 2$; Schneider et al. 2007) and using the cross-correlated SDSS-DR5/2MASS catalog for spectroscopic quasars (Ofek et al., 2007), results in 0.0023 quasars/square degree (corresponding to $4.37 * 10^{-12}$ quasars in the radius of 0.09″ around any position on sky) for the preliminarily determined [OIII] - redshift interval. This value was multiplied with a factor of 5 to account for other possible emission lines, an additional factor of 100 to allow for much weaker AGNs and a factor of 10 for the number of the HST survey objects (excluding the clear binary systems). This results in the very small probability of $2.18 * 10^{-8}$ that the candidate is a compact AGN in a radius of 0.09″ around 2MASSW 0337-1758. Thus, the companion candidate is with sufficient confidence not a background object.

2.6 Discussion

The direct detection of exoplanets still remains a challenging endeavor. In the past few years many systematic high-contrast direct imaging surveys for planetary mass companions around a large number of young, nearby stars have been conducted with HST (Luhman et al. 2005; Lowrance et al. 2005) and with AO at large ground - based telescopes (e. g. Masciadri et al. 2005; Metchev 2006; Lafrenière et al. 2007; Biller et al. 2007; Kasper et al. 2007a, the latter two employing SDI). However, only very few planetary mass or very low mass brown dwarf companions have been discovered in these surveys. The first directly imaged planetary mass companion was detected around the young brown dwarf 2MASS 1207-3932 (hereafter 2M1207) by Chauvin et al. (2004, 2005a) with an estimated mass of 5 - 8 $M_{\rm Jup}$ and a separation of $\sim$ 55 AU. Shortly after, several more planetary mass object detections were reported to very young primaries with an age $\leq$ 60 Myr: GQ Lupi b (Neuhäuser et al. 2005), AB Pic B (Chauvin et al. 2005b), DH Tau B (Itoh et al. 2005; Luhman et al. 2006b), Oph 1622-2405 B (Jayawardhana & Ivanov 2006; Close et al. 2007), CHXR 73 B (Luhman et al. 2006b) and 1RXS J1609-2105 B (Lafrenière et al. 2008). With mass estimates between $\sim$ 7 - 20 $M_{\rm Jup}$ (thus at or just above the brown dwarf/planet boundary) and projected separations

of 55 - 300 AU from their primary, their nature is still extensively debated and the exact number of planetary mass companions remains controversial. These large separations suggest a formation process more similar to brown dwarfs (via fragmentation) rather than giant planets (via core accretion, out to a maximum distance of $\sim$ 10 AU; or via gravitational disk instability which demands a very high massive initial disk). Alternatively, planets could form close-in to the star and then migrate outward to a larger radii. Martin et al. (2007) show that such an outward migration could in principle be possible. Very recently, Marois et al. (2008) announced the first directly imaged possible multiple planetary system (HR 8799 b,c,d) with masses between $\sim$ 7 - 10 $M_{\rm Jup}$ at separations between 24 and 68 AU. At almost the same time, Kalas et al. (2008) detected the so far lowest mass companion Formalhaut b ($\sim$ 3 $M_{\rm Jup}$) and Lagrange et al. (2009) claimed the discovery of the closest companion ever directly imaged to a star (β Pictoris b with $\sim$ 8 AU). While Formalhaut b is again at a relatively large separation, HR 8799 b,c,d as well as β Pictoris b, are the first directly imaged companions around a star, whose formation could be explained by the common core accretion or disk instability scenarios.

But not only the formation process hinders the exact assignment of all these companions to the planetary regime. So far, the masses of these planet candidates are entirely based on evolutionary models. These models have been developed in significant detail over the past years (Burrows et al. 1997; Burrows 2005; Baraffe et al. 2003, 2008) but remain purely theoretical, especially for planets and very young ages due to the lack of direct detections of well - characterized giant exoplanets. For example, the original mass estimate for GQ Lup b ranged from 1 to 42 $M_{\rm Jup}$ (Neuhäuser et al. 2005). This wide range in mass estimate is primarily caused by the use of different theoretical evolutionary models (with different initial conditions, see Burrows et al. 1997; Baraffe et al. 2002; Wuchterl & Tscharnuter 2003) to determine the mass as a function of luminosity, temperature and estimated age. The resulting huge discrepancy shows the difficulty of determining an absolute mass for such directly imaged low mass objects and especially at such young ages.

As mentioned in § 2.1, the first surveys for brown dwarf binaries already revealed that the resolved systems showed a tendency toward a high mass ratio distribution ($M_2/M_1 = q \geq 0.8$) with a clear peak at $q \sim 1$. Further high-resolution surveys on ultracool dwarfs searching for binary systems strengthened this trend (see Figure 2.7 on the left). Although an underestimation of the number of low mass ratio systems cannot be excluded due to the lack of sensitivity for $q \leq 0.5$ in most of these surveys, the clear peak to equal mass binary systems is not an observational bias effect (for a detailed

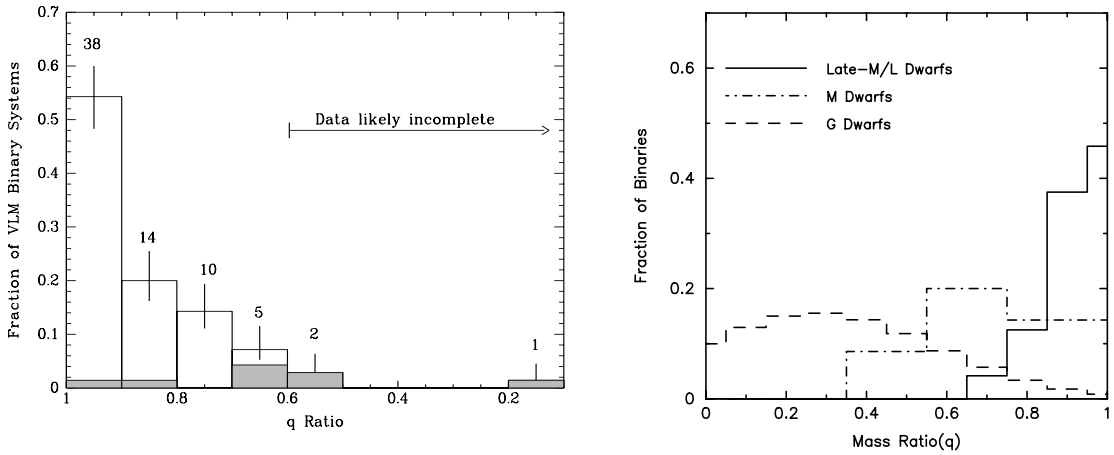

Figure 2.7: The left image illustrates the pure mass ratio distribution of known VLM binary systems with the clear evidence of a peak near unity. The shaded bins represent the systems with ages ≤ 10 Myr (from Burgasser et al., 2007). The right image is from Allen (2007) and displays the comparison of mass ratio distributions for G stars, early M stars and ultracool dwarfs. The mass ration appears to increas with decreasing mass of the primary.

review see Burgasser et al. (2007) and for an extensive Bayesian study Allen (2007)). The same surveys unfolded a semi-major axis distribution which peaks around 3 - 5 AU with only very few separations beyond $\sim$ 15 AU (e. g. Bouy et al. (2003); Table 1 in Burgasser et al. (2007); supported by numerical simulations of Umbreit et al. (2005) and Allen (2007)).

In the following, the results of our HST survey will be compared with respect to the findings discussed above. The resolved and confirmed brown dwarf binary Kelu-1 AB with its mass ratio q = 0.82 (see Chapter 3) and a separation of 5.59 AU at the time of discovery, as well as 2MASSW 0310+1648 AB with its mass ratio $q \sim 1$ (see Chapter 4) and a separation of 5.17 AU, are in full agreement with the previous findings and add up important values to the brown dwarf binary statistics. The non-detection of any companion in this survey at separations larger than 10 AU is also consistent with the separation statistics. The general observed binary fraction of very low mass stars (VLMS) and brown dwarfs, as found in direct imaging surveys, is $\sim$ 15 - 20% and including the results of spectroscopic binary studies, this frequency so far increases up to $\sim$ 25% (for extended discussions and the possibility of an even higher fraction, see Basri & Reiners (2006); Burgasser et al. (2007); Lodieu et al. (2007)). With a total sample of 13 brown dwarfs, the two confirmed binary systems yield a binary fraction of 15^{+18}_{-10} % (or 23^{+19}_{-13} % if 2MASSW 0337-1758 AB is confirmed as the third binary system) for this survey. Accordingly, both values fully correspond to what one could

have expected to find, at least within the meaning of brown dwarf binaries. In addition, a fraction of 23% would support the tendency to an overall higher binary frequency if surveys especially sensitive to very close orbits ($\leq 0.1''$) are included.

The discussion on the companion candidate to 2MASSW 0337-1758 can only be preliminary until second epoch observations confirm the companionship. Yet, it shows some very interesting properties. With a preliminary mass ratio of 0.28 - 0.31 (depending on its estimated age), this system would add to the very small number of brown dwarf binaries with $q \leq 0.5$. The only known and confirmed system with a brown dwarf primary and a similar mass ratio is 2M1207 AB ($q \approx 0.3$ if the most actual mass estimation of Mohanty et al. (2007) is taken into account). But even if its secondary has a mass estimation just below the deuterium burning limit and thus appears to correspond with the possible 2MASSW 0337-1758 AB system, the 2M1207 AB system has an unusual large separation and is much younger (~ 8 Myr). At these very young ages the surveys suggest a flatter mass ratio distribution than that for field or older cluster binaries (see shaded bins in Figure 2.7 on the left), thus the low q value might not be too unusual in the case of 2M1207 AB. Another interesting system in this account is SCR 1845 AB. Both components of this M8.5 - T6 field binary (where the secondary was discovered during a SDI survey as well) have mass estimations clearly in the brown dwarf mass regime, hence the mass ratio is also relatively low with $q \approx 0.41$ (Kasper et al. 2007b). Additionally, the system is, with a separation of ~ 4.5 AU, similar tightly bound as 2MASSW 0337-1758. Hence, both systems might be potential candidates for a dynamical mass determination on a reasonable time scale. This will further help to calibrate evolutionary models under a different aspect. Although very low mass binaries with low q values seem to be rare, such a ratio is not uncommon, at least for main-sequence star binaries (see Figure 2.7 on the right). Besides, a q value between 0.4 and 0.1 is, independent of age and separation, still much larger than the mass ratios known from general star - giant planet systems (determined with RV, transit etc. methods).

The minimum mass estimate of 10 - 15 $M_{\rm Jup}$ for the companion candidate of 2MASSW 0337-1758 does not allow to exclude a classification as a planet in principle. Nevertheless, a comparison of four of the ~ 600 K T dwarfs (all field dwarfs) in Leggett et al. (2009) shows, that at least three of them (so far single objects) have similar mass estimates, just right below or above 13 $M_{\rm Jup}$. Therefore, 2MASSW 0337-1758 is more likely a brown dwarf – brown dwarf binary system with a so far unusual very low mass secondary which possibly straddles the T/Y transition, rather than a system including an exoplanet. A definite classification will only be possible with further intensive ob-

servations of the system. Even more important, a larger number of further detections of objects in this mass and temperature regime are necessary to reliably calibrate the theoretical models.

2.7 Conclusions

High-resolution observations with HST/NICMOS of 12 L dwarfs within 30 pc to the sun were obtained, using the spectral differential imaging technique in the two narrow-band filters F108N and F113N. To this date, this is the only SDI survey for planetary mass companions around field brown dwarfs (not related to any young association or moving group) conducted from space or ground-based telescopes. Further, it is the solely one which used the water absorption spectroscopic feature instead of the methane feature.

The survey resolved two brown dwarf binaries (Kelu-1 AB and 2MASS 0310+1648AB) which could already be confirmed in follow-up observations. The overall binary fraction of 15.4%, as well as separations of the binaries smaller than 6 AU are consistent with previous brown dwarf binary statistics. The mass ratios of $q \geq 0.8$ confirm the preference for equal mass systems similar to a large number of other surveys.

Furthermore, tentative evidence was found for a very low mass companion close to the planetary mass regime around 2MASS 0337-1758. It has a very low $T_{\rm eff} \approx 600$ - 620 K and an unusual mass ratio ($q \approx 0.3$) compared to the vast majority of previously found brown dwarf binaries. Follow-up observations are strongly required to confirm common proper motion of the system and to derive more physical properties like colors for spectral type classification. In addition, these new observations will provide second epoch astrometry for the determination of orbital parameters and hence a dynamical mass estimation. If gravitationally bound and depending on the age, the 2MASSW 0337-1758 system will be one of the closest resolved brown dwarf binaries ($0.087'' \pm 0.015''$) with the so far coldest companion ever directly imaged and the least massive companion to any L or T dwarf. Therefore, including its multiplicity status, it will be an important testbed in the newly explored ≤ 700 K temperature regime and might imply new constraints on the existing formation scenarios.

3

THE L DWARF BINARY KELU-1 AB – A POSSIBLE TRIPLE SYSTEM

Stumpf et al. (2009) submitted to A&A

3.1 Motivation

KELU-1 was discovered as one of the first single free-floating brown dwarfs (BDs) in the solar neighborhood by Ruiz et al. (1997). Originally classified with a spectral type L3 in the near-IR (Knapp et al., 2004) at a distance of 18.7 ± 0.7 pc and with a large proper motion of 285.0 ± 1.0 mas/yr (Dahn et al., 2002), it has been intensively studied since. More than 100 refereed publications listed in the SIMBAD database made it a kind of a benchmark object for L dwarfs, especially in spectral classification schemes. Particular interest was devoted to its apparent overluminosity compared to objects of similar spectral type (Martín et al., 1999b; Leggett et al., 2001; Golimowski et al., 2004a), and to its photometric and spectroscopic variability with a 1.8 h period in H_α (Clarke et al., 2002, 2003). Since the presence of the Li I absorption feature at 6708 Å confirmed its brown dwarf nature (Ruiz et al., 1997; Kirkpatrick et al., 1999), the brightness could only be explained by a surprisingly young age ($\sim$10 Myr, Golimowski et al. 2004b) or unresolved binarity, as first proposed by Martín et al. (1999b). Due to the free-floating nature of Kelu-1, its age is difficult to assess. In a first estimate Basri et al. (1998) constrained the age on the basis of its Li I absorption strength to 0.3-1 Gyr, which was later slightly revised by Liu & Leggett (2005) to 0.3-0.8 Gyr. This meant that a very young age was unlikely the cause of the overluminosity. However, *Hubble Space Telescope* (HST) NICMOS observations of Martín, Brandner, & Basri (1999a) could not resolve any companion in a first attempt.

Six years later the mystery was solved. A binary companion was detected independently in March (Gelino et al., 2006) as well as in May 2005 (Liu & Leggett, 2005)

with the Keck *Laser Guide Star Adaptive Optics* (LGS AO) system. New (photometric) spectral types of L1.5-L3 for Kelu-1 A and L3-L4.5 for Kelu-1 B were determined, respectively. We were able to confirm the binary nature with our own HST/NICMOS data obtained in July 2005 and could already detect an orbital motion with an increase in separation by $0.015''$ and in position angle (PA) by 0.43° in five months. This made it a new promising L dwarf binary target for dynamical mass determination, due to the first predicted reasonably short period of ~ 35 years (Liu & Leggett, 2005).

Observational studies of brown dwarfs play a crucial role in the verification of evolutionary models and the theories of inner structure and atmospheres of substellar objects. As brown dwarfs never stabilize themselves on the hydrogen main sequence, there remains an ambiguity between the temperature or luminosity of a brown dwarf and its age or mass throughout its lifetime. However, spatially resolved binaries are expected to be coeval, thus removing part of the degeneracy in the mass-luminosity (age-temperature) relation which in turn can help to interpret their physical properties and test evolutionary models. In addition they provide the unique opportunity to determine the orbital motion and therefrom derive the dynamical mass of the binary and its components independently of any theoretical model. Although these dynamical mass measurements are strongly needed for very low mass stars (VLMS) and brown dwarfs, only few such measurements have been achieved up to now and large uncertainties remain (see Zapatero Osorio et al. 2004; Bouy et al. 2004; Brandner et al. 2004; Stassun et al. 2006; Ireland et al. 2008; Liu et al. 2008; Dupuy et al. 2008).

Therefore we started a detailed ground-based high-resolution adaptive optics photometric and spectroscopic observing campaign of the Kelu-1 AB system, including a long-term monitoring program to measure the orbital motion and derive a meaningful determination of the orbital parameters. In this chapter we present the first dynamical mass estimate for the binary system Kelu-1 AB independent of theoretical models. In addition we show the first resolved spectra for each component, leading to improved spectral types and evidence for a possible unresolved third component in the system.

3.2 Observations and data reduction

The results of this chapter are based on a variety of observations with different telescopes. For infrared photometry and astrometry we used our own HST/NICMOS and *Very Large Telescope* (VLT) NACO observations as well as archived SPITZER observations. The infrared spectroscopy was carried out by means of own NACO data. Each

observation will be consecutively described.

3.2.1 HST/NICMOS Photometry

KELU-1 AB was observed on July 31, 2005 as part of our HST spectral differential imaging program GO 10208 (PI: W. Brandner) described in Chapter 2. Kelu-1 AB was observed with the NICMOS1 (NIC1) camera, providing a high-resolution pixel scale of $0\farcs0432$ and a field of view (FoV) of $11'' \times 11''$, in the two narrowband filters F108N (1.08 μm) and F113N (1.13 μm). We received 4 different images for the object in each filter. Two images were obtained in the same orbit, but at different positions on the detector, to be able to optimize PSF sampling, reject bad pixel and gain redundancy against cosmic ray events. All data were acquired in MULTIACCUM mode and the total integration times per filters were 2560 s (F108N) and 2816 s (F113N), respectively.

The HST data analysis of the resolved binary is based on pipeline reduced frames as provided by the HST archive. To derive the magnitudes from the HST/NIC1 images we used aperture photometry with the IRAF *phot* routine in the *apphot* package. With a separation of $0.3''$ the distance between our components was less than the defined $0.5''$ (= 11.5 pixels) separation for well-isolated sources. Thus we used an aperture size of 3 pixels and corrected to 11.5 pixel photometry using an aperture scaling factor de-

Table 3.1: Observation log of high-angular resolution imaging of the resolved binary Kelu-1 AB

Date	Telescope/Instrument	Filter	Exp. time [sec]
31 / 07 / 2005	HST/NIC1	F108N	2560
		F113N	2816
28 / 04 / 2006	VLT/NACO	J	8 x 80
		H	8 x 60
		K_S	6 x 40
26 / 05 / 2006	VLT/NACO	L′	8 x 43.75
		NB4.05	8 x 60
12 / 08 / 2006	VLT/NACO	K_S	8 x 55
22 / 02 / 2007	VLT/NACO	K_S	8 x 22
15 / 05 / 2007	VLT/NACO	K_S	8 x 30
13 / 03 / 2008	VLT/NACO	K_S	8 x 30
09 / 05 / 2008	VLT/NACO	K_S	8 x 20
03 / 06 / 2008	VLT/NACO	K_S	8 x 30

rived from TinyTim[1] PSF measurements. Then we adjusted our results to a nominal infinite aperture and converted the count rates into flux using the most recent photometric keyword-value as provided by the STScI webpage[2]. For better comparison, we finally converted the flux into the Vega magnitude scale, using the flux zero points of 1937.0 and 1820.9 Jy for the F108N and F113N filters, respectively.

We also reexamined the first HST/NICMOS observation of Kelu-1 from 14 August 1998 (GO 7952, PI E.Martín). We retrieved 2 images from the HST archive which were acquired in MULTIACCUM mode with a total integration time of 448 s each.

3.2.2 VLT/NACO

Photometry

Follow-up imaging observations were obtained with the adaptive optics system NACO at the ESO VLT/UT4 (Yepun) in the *J* (1.25 μm), *H* (1.65 μm) and $K_{\rm S}$ (2.15 μm) broad-band filters on April 28, 2006 as well as in L (3.8 μm) and NB4.05 (4.051 μm) band filters on May 26, 2006. Between May 2006 and June 2008 we acquired 6 additional epochs of $K_{\rm S}$ broad-band images within the framework of our ongoing astrometric monitoring program, as listed in Table 3.1.

We used the CONICA S27 (for *J,H,*K_S) and L27 (*L, NB4.05*) camera, providing a FoV of 28″ x 28″ with a pixel scale of 0.″0271. Wavefront sensing was performed on Kelu-1 itself in the near-IR using the N90C10 dichroic for the observations in the *J,H,*K_S bands and the JHK dichroic for the *L, NB4.05* band observations. For sky computation and to optimize bad pixel/cosmic ray rejection the observations were executed in a jitter pattern with 6 - 8 points (see Table 3.1). To perform accurate photometry and astrometry, we chose the nearby point source 2MASS J13054388-25403805 from the GSC-II as PSF calibrator, which was observed in the same nights with the same instrumental settings as the binary. On average the observations were executed under good atmospheric conditions with a very good seeing of $\sim 0.6''$ FWHM leading to a Strehl ratio typically between 25 - 35 % in $K_{\rm S}$. Only the observation on August 12, 2006 had slightly worse conditions with a seeing of 0.8″ FWHM and a Strehl ratio of only 15 %, resulting in a larger error estimation for the astrometry.

[1] http://www.stsci.edu/software/tinytim/tinytim.html
[2] http://www.stsci.edu/hst/nicmos/performance/photometry/postncs_keywords.html

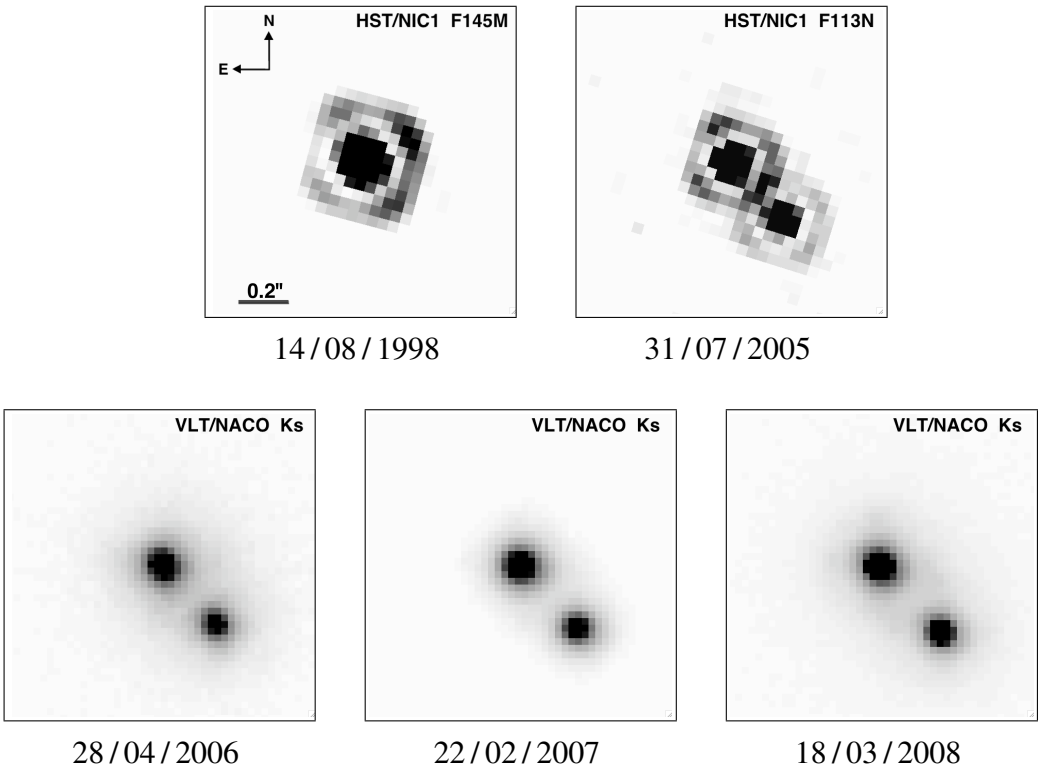

Figure 3.1: Images of Kelu-1 AB obtained with HST/NICMOS and VLT/NACO at different epochs. The orientation and scale are the same for all images. Kelu-1 A is the northern component while Kelu-1 B is the component to the south west.

For the NACO/VLT observations the standard image processing including flat-fielding, bad pixel cleaning, dark and sky correction as well as average combination, was accomplished using the recommended Eclipse *jitter* (Devillard, 1997) software package. We obtained very good final images in almost all filters with the exception of the images in the NB4.05 filter, where we could only barely detect the Kelu-1 AB system due to a very low S/N ratio. Thus no photometry was possible for this filter. Figure 3.1 shows the HST as well as the best final VLT/NACO images, clearly revealing the increasing separation of the binary components with time.

Spectroscopy

Our goal to obtain first spatially-resolved spectra of each component of the binary system was achieved by performing spectroscopy with NACO and its *H*- and *K*-filters (spectral range 1.37 - 1.72 μm and 2.02 - 2.53 μm) on April 26, 2006. We used the S27_3_SH and S27_3_SK modes, respectively, with a slit width of 0.086″ and a resolution of R $\sim$1500 and R $\sim$1400. A total of 20 spectra (in *H*-band) and 30 spectra

(in K_S -band) were obtained in an "abbaabb" nodding pattern along the slit with an exposure time of 60 s for each frame. The slit was oriented along the Kelu-1 AB axis, yielding simultaneous spectra of both components at each position. As a telluric calibrator the B4 IV standard HIP 067786 was observed immediately after Kelu-1 AB at a slightly lower airmass.

In a first step the raw, two-dimensional science spectra were pairwise subtracted to remove the sky and afterwards divided by the median-combined flat-field image. Due to the overlapping wings of the barely resolved spectra, we used a custom made IDL routine to perform an iterative fit to extract the individual spectra. This minimum least square fit method turned out to be more robust than standard IRAF reduction procedures leading to an improved S/N ratio. The wavelength calibration was determined based on argon lamp spectra.

To remove the telluric absorption lines and the instrument's relative spectral response function, we used the observed spectra of the B4 IV telluric standard. After correcting the standard star spectrum for its own hydrogen absorption lines, we divided it by a blackbody spectrum of $T_{\rm eff} = 17{,}050$ K in order to preserve the continuum shape of Kelu-1 A and B. However, the correction with the standard spectra did not sufficiently correct for all instrumental artifacts. Therefore we calculated an additional response function to correct the remaining slope. The added, individual spectra of Kelu-1 A and Kelu-1 B were first divided by the unresolved near-IR spectra of Kelu-1 from the NIRSPEC Brown Dwarf Spectroscopic Survey (BDSS) (McLean et al., 2003), which provided a similar resolution. Then the single Kelu-1 spectra were divided with this derived response function, receiving the finally reduced individual spectra of Kelu-1 A and B.

In general the achievable S/N ratio is biased by slit losses which are less in H- than in K-band (wavelength dependent since the FWHM of the AO PSF decreases with increasing wavelength). The K-band observation of Kelu-1 AB was in addition affected by an alignment error of the binary into the slit, which further decreased the S/N ratio. Thus our finally derived S/N ratio in the H-band is moderate, though in the K-band it is relatively low, especially for the B - component.

3.2.3 Astrometry

To obtain relative photometry and astrometry of the binary we used our custom-made IDL-based simultaneous PSF-fitting algorithm (Bouy et al., 2003), adapted to our HST/ NICMOS and VLT/NACO dataset.

In order to recover the binary parameters from the first epoch of HST/NICMOS observations in 1998, we tried to fit the observed light distribution with theoretical PSFs created with TinyTim, as well as with observed PSFs. A data base of observed NIC1 PSF stars was compiled by querying the HST archive for all observations with NIC1 in F110M obtained within a period of 3 months before or after the Kelu-1 observations. To select the best-matching PSFs, only observations with NICMOS focus setting "Camera 1" , i.e., a PAM (pupil alignment mechanism) focus value close to the value of the Kelu-1 observations were used. This led to a PSF library of 36 individual NIC1 exposures in F110M. Most of the PSFs resulted from the observations of very low mass stars and brown dwarfs in the Pleiades (GO 7952, Martín et al. 2000a), which were well exposed and represent relatively isolated stars.
As the photometry obtained from the spatially resolved NACO observations indicates that both components of Kelu-1 are not variable by more than a few millimagnitudes, we chose to keep the brightness ratio between the two components fixed at $q = 0.47$ for subsequent PSF - fitting, based on the values computed from the NIC1 observations in F108N and F113N obtained in the later epoch.

For the later obtained HST images of the clearly resolved binary, we used a library of 6 different PSFs for a better error estimate: two natural PSFs obtained during previous observations of similar objects of the same program and 4 theoretical PSFs considering different focus settings. The relative photometry and astrometry were measured separately for each of the 4 images per filter. Finally the results were averaged and the uncertainties were calculated from the standard deviation.
By contrast, for the VLT data only one reference PSF star was observed in the same night with the same instrumental settings. Therefore all VLT results were based on fitting one single PSF . For a better estimate of the accuracy of the results, we repeated the PSF fitting using also the previous PSF star observations. The derived differences are represented in the error calculations.

3.2.4 SPITZER Photometry

The imaging observations with the *Spitzer Space Telescope* (SPITZER) were retrieved from the SPITZER Science Archive. As part of the AOR ID 35 (PI G.Fazio) and AOR ID 3736 (PI B. Goldman) programs, unresolved Kelu-1 AB imaging data had been obtained on Jan 19, 2004 and Feb 05, 2006, respectively, using the Infrared Array Camera (IRAC). IRAC provides simultaneous broad band images at 3.6, 4.5, 5.8 and 8.0 μm (also referred to as *channels* 1 - 4 respectively) with a pixel scale of 1.2$''$ and a FoV of 5.2$'$ x 5.2$'$. Using a dichroic beam splitter, two adjacent fields are imaged in pairs (channels 1 and 3; channels 2 and 4). Then the telescope was nodded to image the target in all four channels.

The SPITZER/IRAC data analysis is based on Spitzer Science Center (SSC) pipeline-created mosaic images (with pipeline versions S13.2 and S14.0, respectively), the so-called post-BCD data (pbdc). The photometry was extracted using again the IRAF *phot* routine. As a first step we converted the physical unit of the images from surface brightness into counts by dividing with the conversion factor (found in the header of each image) and multiplying by the effective integration time of 26.8s. For the aperture photometry we chose an aperture size on source of 7 pixels and a sky-radius of 7 - 14 pixels. This guaranteed to receive all PSF flux and still have a sky area without any object or bad pixel in it. Since the absolute IRAC calibration is based on an aperture with a radius of 10 pixels we applied an aperture correction as listed in the IRAC Data Handbook 3.0. For re-transformation of the net source counts into flux we multiplied with the flux conversion factor and the solid angle for each pixel. Eventually, the instrumental magnitudes were converted into the Vega magnitude scale. The final results are based on the combination of the data sets of both programs and are listed in Table 3.4.

3.3 Results and Discussions

3.3.1 Orbital parameter determination and dynamical mass estimate

Being clearly resolved as a binary on March 04, 2005 for the first time with a separation of 284.3 ± 0.8 mas and a position angle of $220.9° \pm 0.3°$ (Gelino et al., 2006), the separation between the two components increased relatively steady to 366.0 ± 0.6 mas until June 03, 2008. But since the PA only changed by 1.84° during that time, a reliable new

orbit prediction would have been deficient.

Therefore, we also reexamined the HST/NICMOS observations obtained on Aug 14, 1998 (see Sect. 3.2.1 above) and derived a separation of 69.4 ± 5.1 mas and a PA = $22.7° \pm 8.2°$ as best fitting binary parameters. As a separation of 65 mas (or less) corresponds to 70% of the diffraction limit of HST at 1.1 μm, we did not attempt to fit the binary parameters at still longer wavelengths. At an observing wavelength of 1.5 μm, 65 mas are almost exactly half the diffraction limit of HST. Table 3.2 lists all astrometric results for the Kelu-1 AB system obtained so far.

Compared to the very first orbital predictions by Liu & Leggett (2005) and Gelino et al. (2006), our nine additional data points allow us to improve the determination of the orbital parameters substantially. Based on all astrometric measurements obtained so far, the best orbital solution was determined with our own IDL-based algorithm (see Köhler et al. (2008) for a detailed description of the method). The procedure consists of two steps: First, a grid search in period P, eccentricity e and time of periastron T_0 is carried out, while Singular Value Decomposition is used to solve the linear equation system for the four Thiele-Innes constants. From the Thiele-Innes constants, the remaining orbital elements (semi-major axis a, argument of periastron ω, position angle of the line of nodes Ω, and inclination i) are computed. The result of the grid search is χ^2 as function of P and e, which helps to assess the quality of the fit, and the confidence limits of the fit parameters.

In the second step, all 7 orbital elements are fit simultaneously by a Levenberg-Marquardt algorithm. This further improves the fit by interpolating between grid points and ensures that all 7 elements are treated equally in the final fit. To avoid that the algorithm converges on a local instead of the global minimum, we decided to use *all* orbits resulting from the grid-search as starting points and carried out 148×100 runs of the Levenberg-Marquardt algorithm (the grid spans 148 periods and 100 eccentricities).

To derive estimates of the confidence intervals for the parameters, we studied the χ^2 function around its minimum. To find the confidence interval for one parameter (for example T_0), we perturbed this parameter away from the minimum in χ^2 and optimized all the other parameters. Any perturbation of a parameter will of course lead to a larger χ^2. The range in T_0 within which $\chi^2(T_0) - \chi^2_{\rm min} < 1$ defines the 68 % confidence interval for T_0. This interval is usually not symmetric around the T_0 of the best fit, therefore we list in Table 3.3 separate limits for positive and negative perturbations.

Table 3.2: Relative astrometric results

Date	MJD	Telescope/Instrument	Filter	Sep. [mas]	PA [deg]	References
14 / 08 / 1998	51039.8	HST/NIC1	F110M	69.4 ± 5.1	22.7 ± 8.2	this work
04 / 03 / 2005	53434.0	Keck/NIRC2	K′	284.3 ± 0.8	220.90 ± 0.30	Gelino et al. (2006)
01 / 05 / 2005	53491.0	Keck/NIRC2	K′	291.0 ± 2.0	221.20 ± 0.60	Liu & Leggett (2005)
31 / 07 / 2005	53582.0	HST/NIC1	F108N	299.8 ± 0.2	221.33 ± 0.04	this work
28 / 04 / 2006	53853.1	VLT/NACO	K_S	320.3 ± 1.7	221.84 ± 0.1	this work
26 / 05 / 2006	53881.1	VLT/NACO	L′	322.7 ± 1.9	221.86 ± 0.1	this work
12 / 08 / 2006	53959.9	VLT/NACO	K_S	330.6 ± 5.0	222.24 ± 0.1	this work
22 / 02 / 2007	54153.4	VLT/NACO	K_S	341.5 ± 1.5	222.39 ± 0.1	this work
15 / 05 / 2007	54235.9	VLT/NACO	K_S	345.3 ± 1.6	222.48 ± 0.1	this work
13 / 03 / 2008	54538.8	VLT/NACO	K_S	362.8 ± 0.6	222.63 ± 0.1	this work
09 / 05 / 2008	54595.7	VLT/NACO	K_S	364.5 ± 0.5	222.67 ± 0.1	this work
03 / 06 / 2008	54621.5	VLT/NACO	K_S	366.0 ± 0.6	222.74 ± 0.1	this work

Finally, the total system mass is computed from the semi-major axis and orbital period through Kepler's third law. To convert the semi-major axis from arcsec into AU as well as to compute the mass in $M_{\rm Jup}$ we used a distance of 18.7 ± 0.7 pc as determined by Dahn et al. (2002).

We applied this IDL code to the relative astrometric data as given in Table 3.2 (hereafter data set N°1) and found a global minimum reduced χ^2 of 1.3. The best-fit results are summarized in Table 3.3, including the uncertainties of each fitted parameter, and the orbital solution is illustrated in Figure 3.2. The orbit is quite eccentric ($e = 0.82 \pm 0.10$) with an inclination of $84.9^\circ\ ^{+1.0}_{-2.0}$, i.e. seen almost edge-on. The period of 38^{+8}_{-6} years and the semi-major axis of $6.4^{+2.4}_{-1.3}$ AU yield a total system mass of $185^{+139}_{-57}\ M_{\rm Jup}$. This is the first purely dynamical mass estimate for the Kelu-1 AB system with no evolutionary models involved in the calculations.

This mass prediction reveals a slightly higher total system mass than one would expect for a BD–BD binary system, where an upper mass limit of 72 - 75 $M_{\rm Jup}$ for brown dwarfs (the substellar mass-boundary) would result in a maximum total system mass of $\sim 150\ M_{\rm Jup}$. Though, within the uncertainties of our estimate a pure BD–BD binary is still possible. The known presence of Li absorption in the unresolved optical spectrum (Ruiz et al., 1997; Kirkpatrick et al., 1999) indicates that at least one component must have a mass $\leq 65\ M_{\rm Jup}$ which is the lithium-burning limit (Rebolo et al., 1992; Basri,

Table 3.3: Parameters for the best orbital solution of Kelu-1 AB

Parameter	Value
System mass M_S [$M_{\rm Jup}$]	$185\ ^{+139}_{-57}$
Period P [years]	$38\ ^{+8}_{-6}$
Semi-major axis a [mas]	$339\ ^{+129}_{-66}$
[AU]	$6.4\ ^{+2.4}_{-1.3}$
Eccentricity e	$0.82\ ^{+0.10}_{-0.10}$
Argument of periastron ω [°]	$57.8\ ^{+15.0}_{-20.0}$
P.A. of ascending node Ω [°]	$39.4\ ^{+2.0}_{-2.0}$
Inclination i [°]	$84.9\ ^{+1.0}_{-2.0}$
Date of periastron T_0	$2452079\ ^{+200}_{-400}$ (Jun 18, 2001)
reduced χ^2	1.3

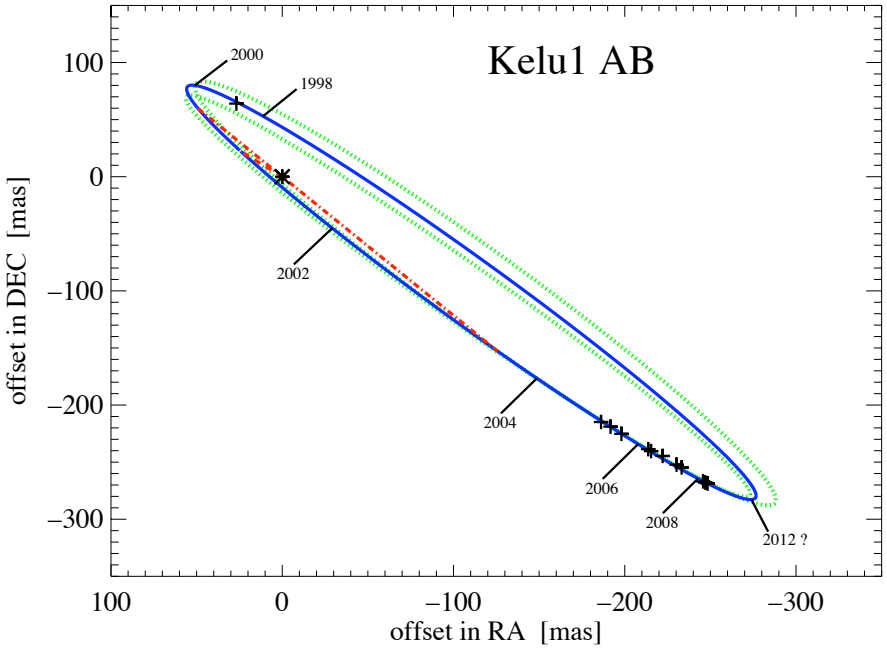

Figure 3.2: Orbit of the Kelu-1 AB system. The star indicates the position of Kelu-1 A while the measurements for the relative motion of Kelu-1 B around Kelu-1 A are indicated by crosses. Measurement errors are comparable to or smaller than the plotted symbols. The resulting best orbit fit is represented by the solid, blue curve and the green, dotted lines show the orbits at the 90% confidence limit (with periods of 32 and 46 years). The red, dash-dotted line marks the line of nodes and the dashed line indicates the position of the periastron. In addition the positions on January 1^{st} for the years 1998-2008, as well as the predicted position for 2012 are marked.

1998). If the system consists of two objects, this would imply that the primary has a mass of $\approx 110\ M_{\rm Jup}$, which in turn would correspond to a main-sequence spectral type of M8V. This is in contradiction to its early L spectral type as it has been determined both from integrated spectra (Kirkpatrick et al., 1999; Dahn et al., 2002) as well as in § 3.3.2 below from the spatially resolved spectroscopic observations of Kelu-1 A and B.

Comparison to previous orbit predictions

Since the HST/NICMOS observation from 1998 is obviously a key component to fit the orbit, we compared our binary parameters for this observation with those obtained by Gelino et al. (2006). They derived a separation of 45 ± 18 mas and a PA = 38.0° or $218.0° \pm 11.9°$ (due to their 180° ambiguity in position angle due to the unresolved objects). Within the uncertainties, these values are in good agreement with our measurements. In an additional check we analyzed what orbit solutions we would get with

their slightly different result. We applied our IDL code on two additional data sets which both contained the same values as data set N°1 except for the very first measurement. In data set N°2 we replaced the values of the August 1998 observation by a separation of 45 ± 18 mas and a PA of 38.0° while data set N°3 used a PA of 218.0° . The best-fitting orbital solution for data set N°3 results in a physically unacceptable total system mass of 108 *solar masses*. If we consider only orbital models with a total system mass $\leq$ 230 $M_{\rm Jup}$ (assuming a possible triple system), we find a minimum reduced χ^2 of 1.5, which is higher than that for data set N°1. Therefore we exclude the PA of 218° as a possible first data point. The result from the best-fit solution for set N°2 yields, without any constraints, a system mass of 101^{+110}_{-24} $M_{\rm Jup}$, period of 28^{+6}_{-10} years and semi-major axis of $4.3^{+0.5}_{-0.2}$ AU. These values are all slightly smaller, though within the uncertainties still consistent with the result for data set N°1. However, since its minimum reduced χ^2 of 1.4 is still higher than the one for set N°1 we stay with our own astrometric result for the first HST/NICMOS data point. In addition, this ensures a consistent data reduction method throughout the whole monitoring program.

Comparing the final results in Table 3.2 with the previously published orbit parameter predictions by Liu & Leggett and Gelino et al. we first exclude their assumed circular orbit, since with an eccentricity $\leq$ 0.01 this would result in unphysical parameters like a dynamical total system mass of 1.06 $M_\odot$ or a reduced $\chi^2 > 3$. Nevertheless, our derived inclination of $84.9^{\circ +1.0}_{-2.0}$ agrees well with the limiting values of $81 \leq i \leq 90^\circ$ reported by Gelino et al.. With a total system mass of 185 $M_{\rm Jup}$, our prediction is higher than the mass estimates of $\sim$120 $M_{\rm Jup}$ and $\sim$115 $M_{\rm Jup}$ by Liu & Leggett and Gelino et al. respectively. However, their calculations were purely based on photometric results compared with theoretical models and a still uncertain age estimation for the system.

Considering a possible third component in the system (as derived from the results in § 3.3.2 below), would allow all objects to have component masses $\leq$ 95 $M_{\rm Jup}$, and hence spectral types of L0 or later. This would resolve the above mentioned discrepancy between a system mass of $\sim$185 $M_{\rm Jup}$, spectral types of L0 and later, and the fact that at least one of the components must have a mass less than 65 $M_{\rm Jup}$ as indicated by the presence of Lithium in the combined spectra.

All together we showed a possible solution in reasonable agreement with the observations, but most likely not the final one, since the fraction of the orbit observed so far is too small for a reliable and consistent orbit determination. For a robust orbital solution, more observations are required, at least up to the turning point in the (projected)

orbit expected around the year 2012 (see Figure 3.2). Therefore further investigations, including the measurement of the radial velocities of the system components, will be done with our ongoing long-term monitoring program.

3.3.2 Spectral types

The extracted and reduced *HK*- spectra of Kelu-1 A and Kelu-1 B are shown in Figs. 3.3 and 3.4, respectively. To determine the spectral type of each component we compared them with low-resolution spectra of 5 late M dwarfs (M8 - M9.5) and 39 field L dwarfs (L0 - L9) from the SpeX prism data archive[3]. All spectra were normalized to the *H*-band. In addition the Kelu-1 spectra were smoothed to the template resolution and scaled by a factor of 0.95 to eliminate the normalization bias.

Kelu-1 A

The general *H*-band slope of Kelu-1 A best fits between the optically classified L0 2MASSI J2107316-030733 (hereafter 2M2107-0307, Burgasser et al. 2004) and the L1 optical standard 2MASSW J1439283+192915 (hereafter 2M1439+1929, Burgasser et al. 2004). In the *K*-band the overall shape is clearly very similar to that of 2M1439 +1929 with the same strong CO absorption band heads at 2.3 - 2.4 μm and, at the short - wavelength end of the *K*-band, a steeper slope than in the L0 spectrum, due to stronger H_2O absorption. This suggests a spectral type of L0.5 $\pm$ 0.5 which is slightly earlier than the derived spectral type of L1.5 - L3 from Liu & Leggett (2005) whose estimates were only based on *JHK* colors and absolute magnitudes. However, the *H*-band spectrum of Kelu-1 A shows a pronounced feature, a deep, broad depression from 1.6 - 1.65 μm. This feature is slightly offset from the 1.55 - 1.64 μm FeH absorption band heads which produce a flat plateau in this wavelength range and are usually present in early to mid type L dwarfs (Cushing et al., 2003). Instead, the 1.6 μm depression corresponds much more to the CH_4 absorption band which starts to appear at the L/T transition and strengthens through the T sequence and is therefore very unusual for an early L dwarf. In addition there is no indication of the 2.2 μm CH_4 absorption line, another defining feature for the T dwarfs.

Recently the same feature has been observed in 3 formerly classified single, early to mid-type L dwarfs (2MASS J05185995-2828372, Cruz et al. 2004; SDSS J080531.84

[3] http://www.browndwarfs.org/spexprism

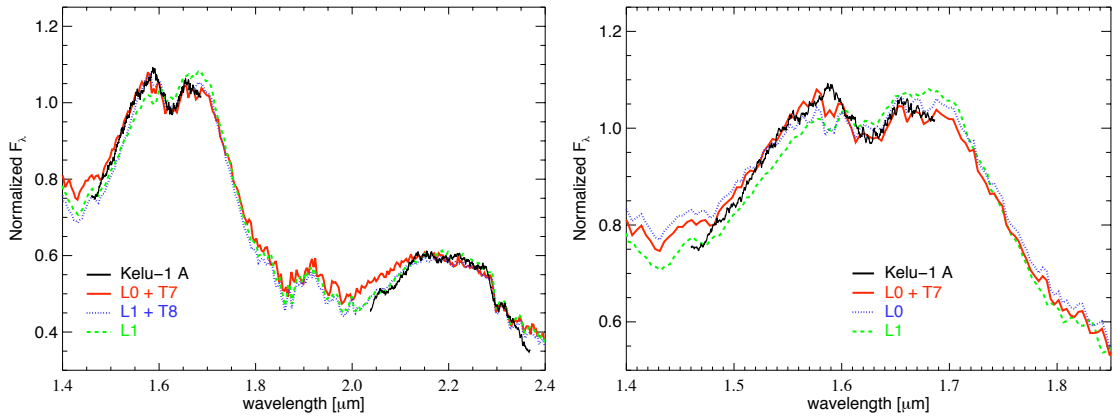

Figure 3.3: *Left*: *H*- and *K*-band spectrum of Kelu-1 A (smoothed to template resolution, solid line) compared to the best-fit binary composites of 2M2107-0307 (L0) combined with 2M0727-1710 (T7) (red, solid) and 2M1439-1929 (L1) with 2M0415-0935 (T8) (blue, dotted). In addition the single object spectrum of 2M2107-0307 (L0) (green, dashed) is plotted for comparison. *Right*: close-up of the *H*-band and the peculiar feature starting at 1.6 μm. While the single L0 (blue, dotted) and L1 (green, dashed) show a plateau shape from 1.55 – 1.64 μm due to the FeH absorption band heads, the L0 + T7 binary composite (red, solid) reproduces the deep depression to a much higher accuracy.

+481233.0, Burgasser 2007b; 2MASS J03202839-0446358, Burgasser et al. 2008a). By combining an early to mid L dwarf spectrum with an early to mid T dwarf spectrum, these objects were reinterpreted to be unresolved spectroscopic binaries, with the depression being very well reproduced by a combination of the FeH absorption in the L dwarf primary and the CH_4 absorption of the T dwarf secondary. For two of the targets multiplicity has been confirmed since then: 2MASS 0518-2828 with high-resolution imaging (Burgasser et al., 2006c) and 2MASS 0320-0446 with high-resolution spectroscopy to be a single-lined spectroscopic binary (SB1) (Blake et al., 2008).

To probe if we can also reproduce the depression in the Kelu-1 A spectrum including the overall shape of the *H*- and *K*-band, we created a large set of binary spectral templates by combining late M-dwarf / early L dwarf spectra (M8 - L4) with early to late T dwarf spectra (T2 - T8) from the SpeX prism data archive. We selected the SpeX data archive since it is the only archive which provides a continuous and large set of spectral types from late M-dwarfs to the latest T dwarfs in the *H*- and *K*-band and, therefore, provides the most homogenous set for assembling all the different binary templates. After normalization we calculated the RMS between the science spectrum and the binary templates to determine the best matches. The results with the least deviation are displayed in Figure 3.3 (left). The combination of 2M2107-0307 (L0) and 2MASS J07271824+1710012 (T7 standard) (2M0727+1710, Burgasser et al. 2006a) best fits the slope and depression in the *H*-band. Whereas the smallest RMS in the *K*-band is

achieved with the combined spectrum of 2M1439-1929 (L1) and 2MASS J04151954-0935066 (T8 standard) (2M0415-0935, Burgasser et al. 2004) with a better match of the steeper slope at the short-wavelength end of the *K*-band spectrum due to stronger H_2O absorption. On the right side of Figure 3.3 we show a close-up of the *H*-band and the peculiar feature starting at 1.59 μm. One can clearly see that neither the single best-fit L0 nor the L1 match the deep depression while the L0+T7 binary template reproduces the whole spectra to a much higher accuracy. Beside those best-fit comparisons there were several other matches with similar good results among the binary templates with secondaries of type T6.5 and later. Including the small difference between the best match with an L0 primary in *H*-band and an L1 primary in *K*-band we derive a component spectral type of L0.5 $\pm$ 0.5 for Kelu-1 Aa and T7.5 $\pm$ 1 for Kelu-1 Ab.

Kelu-1 B

A precise spectroscopic classification of Kelu-1 B is even more challenging. The object shows an *H*-band continuum notably different from the usual plateau-shape of "normal" early to mid-type L dwarfs (see Figure 3.4). Its sharply peaked, triangular-shaped continuum resembles much more that of the young, red L0pec 2MASS J01415823-4633574 (2M0141-4633, Kirkpatrick et al. 2006) and the red L6 2MASSI J0103320+193536 (2M0103+1935, Cruz et al. 2004). While the distinct dip around 1.58 μm in the Kelu-1 B spectrum (caused by two prominent FeH absorption bands) is not visible in the red spectrum of the L0pec and L6 dwarf, it is in turn present only slightly weaker in "normal" L dwarf spectra.

By contrast the *K*-band spectrum of Kelu-1 B does not fit any of the two red objects. While its overall flux distribution fits relatively well that of the L3 optical standard 2MASS J15065441+1321060 (2M1506+1321, Burgasser 2007a), it again reveals a triangular - shaped continuum with a slightly redward shifted *K*-band flux. In addition the CO absorption bands are somewhat weaker as in the L3 dwarf.

For comparison in the *H*-band, only the above mentioned two unusual red L dwarfs were available in the archive. Therefore, we used the surface gravity independent H_2O indices in the short - wavelength end of the *H*-band (1.49 - 1.56 μm) from Allers et al. (2007) for a better estimation of the spectral type. In a first attempt we applied this H_2O index to the L0pec 2M0104-4633 and obtained a spectral type of M9.7 $\pm$ 0.5, which is fully consistent with the L0 classification of Kirkpatrick et al. (2006). Using the same indices for Kelu-1 B we receive a spectral type of L2.6 $\pm$ 1.5 where the uncertainty

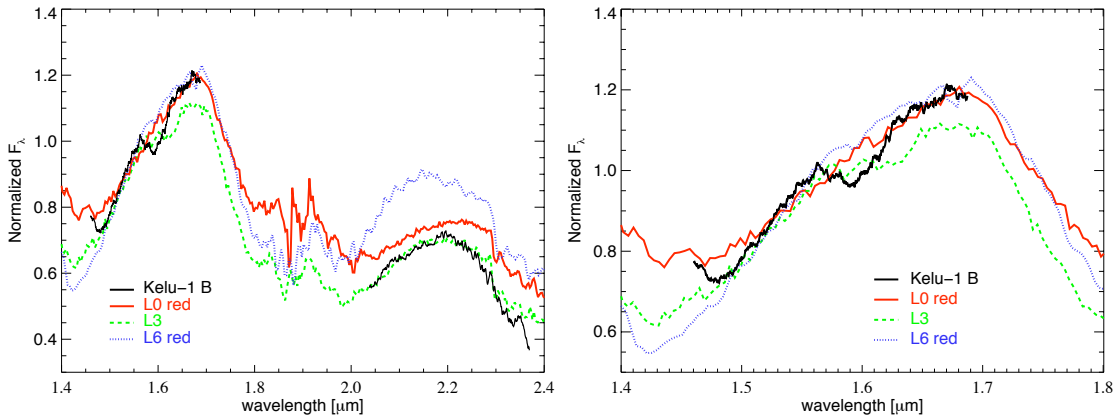

Figure 3.4: *Left*: *H*- and *K*-band spectrum of Kelu-1 B (smoothed to template resolution, solid line) compared to the best-fit spectra of the red L dwarfs 2M0141-4633 (L0 pec, red solid line) and 2M0103+1935 (L6, blue dotted line), as well as the field L dwarf 2M1506-1321 (L3, green dashed line). *Right*: close-up of the *H*-band with the same objects as on the left. The distinct FeH absorption dip around 1.58 μm is present in the L3 spectrum, but not in the L0 pec or L6 spectra, while the overall slope better fits the red objects.

includes the scatter of the index relation and the error of our index measurements. Using the results from our fits and calculations we thus adopt an overall spectral type of L3 pec $\pm$1.5 for Kelu-1 B.

Similar peaked *H*-band spectra and unusual red near-IR colors have been so far mainly detected as characteristics for young ultracool dwarfs (Luhman et al. 2004; Kirkpatrick et al. 2006; Allers et al. 2007; McElwain et al. 2007; Metchev et al. 2008). The effect can be explained by two possible scenarios which are both caused by lower gravity and lower atmospheric pressure: (i) a diminishing collision-induced absorption (CIA) of H_2 in the *H*- and *K*-band (Kirkpatrick et al., 2006), or (ii) increased water vapor absorption on each side of the *H*-band peak (Luhman et al. 2004; Allers et al. 2007). Another possible explanation for the peculiar shape is a higher metallicity which implies a higher opacity caused by greater dust production. This again results in an overall redder spectrum with weaker alkali (Na, K I) and molecular (FeH and H_2O) absorption lines and a red-shifted *K*-band peak.

While Kelu-1 B also shows slightly redder J-K_S colors (see § 3.3.3 below), the triangular-shaped *H*- and *K*-band spectra can not be explained by low gravity and thus implying a young age, since Kelu-1 A, the other member of the coeval binary system, shows (even with a possible companion) the "normal" behavior of an early L dwarf and no spectral evidence of a young ultracool object. Recently Looper et al. (2008b) identified two new peculiar L dwarfs which showed the same triangular-shaped *H*- and *K*-band spectra

as Kelu-1 B. For one of those objects, the L6.5 pec 2MASS J21481628+4003593 they suggest that the effect may arise from a metal rich atmosphere rather than from low gravity, since its large tangential velocity does not indicate an unusual young age.

Since low gravity as well as higher metallicity result in weaker alkali and FeH absorption, especially in the red-optical and *J*- band spectra, further investigations on resolved Kelu-1 B spectra in these wavelength ranges will be necessary for a better spectral characterization.

3.3.3 Magnitudes and Colors

We calculated the individual magnitudes of the components in the J, H, K_S and L' filters from the measured binary flux ratios (see § 3.2.3) and the integrated 2MASS (Cutri et al., 2003) and UKIRT (Leggett et al., 2002) magnitudes of the unresolved Kelu-1. Even if the 2MASS and VLT/NACO near-IR filters are not exactly identical we did not apply any correction factor, given that the spectral energy distributions (SEDs) of the Kelu-1 AB components are so similar that the flux ratio should not be noticeably affected by the difference in these two photometric systems. For the UKIRT L′ filter one has to consider that it cuts on slightly bluer wavelength than the VLT/NACO L' filter. However, Leggett et al. (2002) showed that a similar difference between the UKIRT and MKO filter in this particular wavelength regime is only significant for late L dwarfs and T dwarfs when the CH_4 absorption at 3.3 μm starts to play a role. For early L dwarfs they claim the effect to be less than the uncertainties in the published magnitudes. Thus we used no correction factors between the UKIRT L' and NACO L' filter system.

Table 3.4 summarizes the photometric results. For the determination of the absolute magnitudes we used a distance of 18.7 ± 0.7 pc from Dahn et al. (2002). Our error estimations include the uncertainties in the flux ratios, the corresponding uncertainties of the "unresolved" magnitudes, as well as the error of the distance. For comparisons with J, H and K magnitudes and spectral type relations derived in the MKO photometric system, we used the transformation equation for 2MASS into MKO of Stephens & Leggett (2004).

The photometric monitoring in the K_S - band over the past 2 years revealed no evidence of photometric variability within the errors for Kelu-1 A or Kelu-1 B. Compared to the values of Liu & Leggett (2005), our individual magnitudes in H and K_S - band are in good agreement within the errors, whereas our J- band magnitude for Kelu-1 B

Table 3.4: Apparent and absolute magnitudes of Kelu-1 AB

Telescope/Instrument	Filter	Kelu-1 AB m [mag]	Δ mag	Kelu-1 A m [mag]	Kelu-1 A M [mag]	Kelu-1 B m [mag]	Kelu-1 B M [mag]
HST/NIC1	F108N		0.83 ± 0.02	14.56 ± 0.02	13.20 ± 0.08	15.31 ± 0.02	13.95 ± 0.08
	F113N		0.82 ± 0.02	14.28 ± 0.02	12.92 ± 0.08	15.01 ± 0.03	13.65 ± 0.09
2MASS [a]	J	13.414 ± 0.026					
VLT/NACO	J		0.82 ± 0.09	13.83 ± 0.08	12.47 ± 0.11	14.65 ± 0.12	13.29 ± 0.14
2MASS [a]	H	12.392 ± 0.025					
VLT/NACO	H		0.51 ± 0.02	12.92 ± 0.03	11.56 ± 0.09	13.44 ± 0.04	12.08 ± 0.09
2MASS [a]	K_S	11.747 ± 0.023					
VLT/NACO	K_S		0.39 ± 0.01	12.32 ± 0.02	10.96 ± 0.08	12.72 ± 0.03	11.36 ± 0.09
UKIRT/IRCAM [b]	L′	10.78 ± 0.15					
VLT/NACO	L′		0.24 ± 0.01	11.42 ± 0.15	10.06 ± 0.17	11.66 ± 0.15	10.30 ± 0.17
Spitzer/IRAC	3.6 μm	10.90 ± 0.03					
	4.5 μm	10.85 ± 0.04					
	5.8 μm	10.68 ± 0.07					
	8.0 μm	10.55 ± 0.05					

[a] from Cutri et al. (2003)
[b] from Leggett et al. (2002)

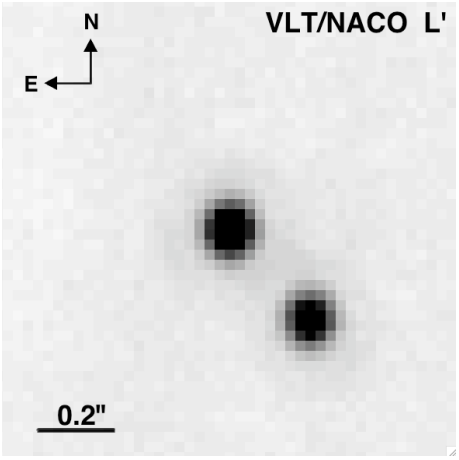

Figure 3.5: Kelu-1 AB image achieved with VLT/NACO on 26. May 2006. This is the first resolved L'- band image of a brown dwarf binary system.

is slightly fainter. This is likely due to in general lower AO performance in J-band, resulting in a considerably worse Strehl ratio and leading to broader PSF wings, which were hence not separated enough for an accurate flux ratio calculation. We took this into account by assuming a larger error. While the resulting J - $K_{\rm S}$ and J - H colors for both components are at the red end, both H - $K_{\rm S}$ colors fit very well into the color range for spectral types of L0 - L1 and L3 - L4 (see Cushing et al. 2008) respectively. The red colors of Kelu-1 B correspond to the redder H- and K- band spectra reported and discussed in § 3.3.2.

We note that our derived L'- band photometry with $L'_{\rm A} = 11.42 \pm 0.15$ mag and $L'_{\rm B} = 11.66 \pm 0.15$ mag are the first resolved L - band magnitudes for any L dwarf binary so far (see Figure 3.5). While the unresolved L' photometry was as overluminous as in the other near-IR bandpasses for a spectral type of L3 (Golimowski et al., 2004b), our resolved $(K_{\rm MKO} - L')_{\rm A} = 0.88 \pm 0.15$ and $(K_{\rm MKO} - L')_{\rm B} = 1.03 \pm 0.15$ colors, as well as the absolute L' magnitudes are consistent with a spectral type of L0.5 and L3, respectively (as in § 3.3.2), derived from the color - spectral type and magnitude - spectral type relations in Golimowski et al. (2004b).

To get an idea of the photometric values of the potential third component in the Kelu-1 AB system, we computed the J, H and $K_{\rm S}$ magnitudes from the Kelu-1 A magnitudes. We considered the allowed flux ratios of Aa and Ab in a filter, as well as the latest 2MASS color - spectral type relations in Cushing et al. (2008) under the assumption of spectral types $\sim$ L0.5 and $\sim$ T7 as derived in § 3.3.2. The primary Kelu-1 Aa would be only slightly fainter than the composite source with $J_{\rm Aa} = 13.89$, $H_{\rm Aa} = 12.95$

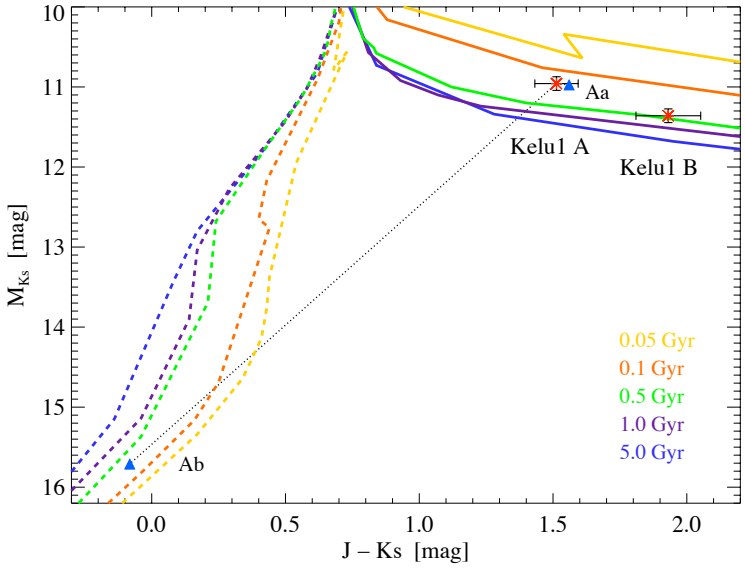

Figure 3.6: Color – Magnitude diagram: The red asterisks show the location of the resolved components Kelu-1 A and Kelu-1 B. The position of the components Kelu-1 Aa and Ab, if they were resolved, are indicated by the dotted lines and the triangles. While the DUSTY isochrones are displayed as solid lines in the upper right part, the COND isochrones are displayed by the dashed lines.

and $(K_S)_{Aa} = 12.33$ while Kelu-1 Ab is notably fainter: $J_{Ab} = 16.99$, $H_{Ab} = 16.95$ and $(K_S)_{Ab} = 17.07$mag. We do not assign any uncertainties to our magnitudes, since there was no direct photometric measurement and we just want to give a first prediction of possible photometric values. In addition the results are in a very good agreement to the absolute magnitude - spectral type relations of Liu et al. (2006).

3.3.4 Testing evolutionary tracks

Ages

Age estimates of field brown dwarfs without established cluster membership have to rely on theoretical isochrones, using the mass-luminosity-age relation for brown dwarfs. Figure 3.6 displays the color-magnitude diagram of Kelu-1 A and B compared to the widely used DUSTY models of Chabrier et al. (2000) for early to mid-type L dwarfs. For Kelu-1 A these models predict an age clearly between 0.1 and 0.5 Gyr taking into account the estimated photometric errors. For Kelu-1 B, however, they predict a slightly older age of 0.3 - 1 Gyr. Since binary components are believed to be coeval, we assess a minimum system age of 0.3 and a new upper age limit of 0.5 Gyr. In addition, the triangles in Figure 3.6 show the position of of the Kelu-1 Aa and Kelu-1 Ab compo-

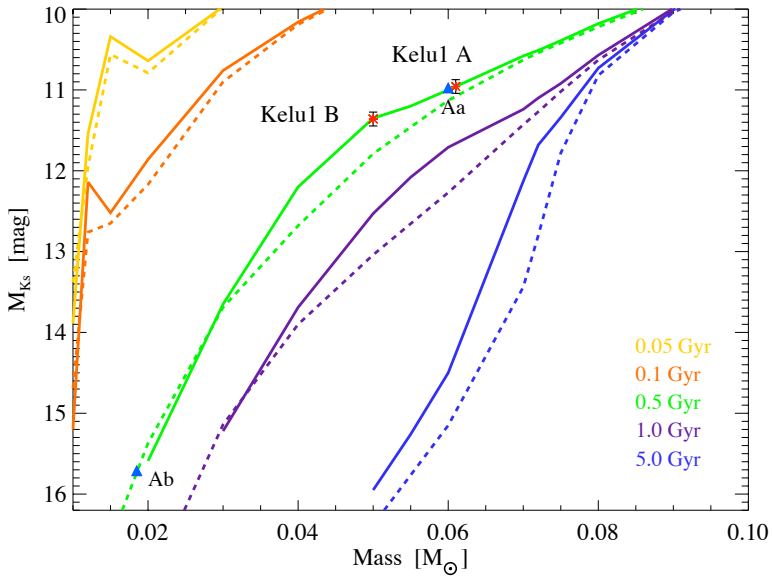

Figure 3.7: The absolute K_S magnitudes of the Kelu-1 system components compared to the DUSTY (solid lines) and COND (dashed lines) models at 0.05, 0.1, 0.5, 1 and 5 Gyr to derive maximum mass estimations for each component.

nents if they would be resolved. Therefore we included the COND models of Baraffe et al. (2003) which better consider the dust condensation of T dwarfs. The resulting age for both individual components is consistent with the above estimation. The here derived age estimate (0.3 - 0.5 Gyr) further decreases the upper age limit for Kelu-1 AB compared to previous estimates from Basri et al. (1998) (0.3 - 1Gyr) and Liu & Leggett (2005) (0.3 - 0.8 Gyr). The determination by Basri et al. (1998) was solely based on the strength of the unresolved Li I absorption feature, while Liu & Leggett (2005) relied on the mass evolutionary tracks of the same model. They took the presence of lithium and the substellar nature of both components into account, which restricts the maximum mass for each component.

Masses

In order to compare our dynamical mass determination of Kelu-1 AB with mass predictions from evolutionary models, we again utilize the DUSTY and COND models as a function of absolute K_S magnitude and age (see Figure 3.7). Using the upper limit for the system age of 0.5 Gyr as obtained in § 3.3.4, we derive maximum individual masses of $64 \pm 2\ M_{\rm Jup}$ for Kelu-1 A and $52 \pm 2\ M_{\rm Jup}$ for Kelu-1 B resulting in a maximum total system mass of $116 \pm 4\ M_{\rm Jup}$. Even if we include the possible third component Kelu-1 Ab, the additional mass of $19\ M_{\rm Jup}$ would only increase the total mass to $\sim 135\ M_{\rm Jup}$.

This mass is still about 50 $M_{\rm Jup}$ lower than the total system mass we derived in § 3.3.1 by dynamical mass determination. This discrepancy between luminosity, mass and age in the evolutionary tracks might result in an under-prediction of the masses. A similar finding has already been reported for other objects. Higher system masses were derived by dynamical mass determination, by Close et al. (2005) for AB Dor C, Ireland et al. (2008) for GJ 802 B or just recently Cardoso et al. (2008) for ϵ Ind Bab and Konopacky et al. (2009) for 2MASS 0746+2000 AB. They all claim as possible reasons the underestimation of the abundance of condensates in the atmospheres as well as the effect of magnetic fields hindering heat flow or even the unusual assumption of non-coevality in binary systems.

3.4 Conclusions

We presented new astrometric and photometric observations of Kelu-1 AB. For the first time we achieved resolved spectroscopy of the individual components of this brown dwarf binary system. The near-IR spectra display interesting peculiarities for each component. The spectrum of Kelu-1 A shows a distinct cup-shaped dip from 1.6 - 1.65 μm which did not fit any early, single L dwarf spectrum, but could be best reproduced by a combined spectrum of an early L and late T dwarf. Our spectral template matching algorithm leads to the result that Kelu-1 A itself is a close unresolved binary with spectral types of L0.5 $\pm$ 0.5 and T7.5 $\pm$ 1. In contrast, Kelu-1 B is characterized by a triangular-shaped continuum, similar to very young red L dwarfs and was classified as L3 pec $\pm$ 1.5 .

Nine epochs of high-resolution astrometry from 2005 - 2008 enabled us to compute the orbital parameters and derive the first dynamical mass measurement for the system. We found a quite eccentric orbit (e = 0.82 $\pm$ 0.10), seen almost edge-on. The period of 38^{+8}_{-6} years and a semi-major axis of $6.4^{+2.4}_{-1.3}$ AU yields a total system mass of 185^{+139}_{-57} $M_{\rm Jup}$ which is slightly higher than one would expect in a BD-BD binary system. If the system consists of only two objects, this would imply that the primary is more likely a very low mass star with a mass $\geq$ 85 $M_{\rm Jup}$. This is in contradiction to its defined early L - spectral type from spectroscopy which, along with its age estimation, indicates an affiliation to brown dwarfs. Including a possible third component in the system would solve this discrepancy with all component masses being below the substellar mass limit of 75 $M_{\rm Jup}$. The non-detection of this component in any previous high-resolution imaging observation (Keck, HST, NACO), indicates a maximum sepa-

ration of $\sim 0.22''$ (≈ 4.1 AU) related to the assumed brightness difference of Kelu-1 Aa and Ab.

The derived magnitudes of $L' = 11.42 \pm 0.15$ mag for Kelu-1 A and $L' = 11.66 \pm 0.15$ mag for Kelu-1 B provide the first resolved L - band photometry for any L dwarf binary. These values and the related near-IR colors support the spectral type determinations from spectroscopy. Comparing the derived near-IR photometry of the individual components with the widely used theoretical DUSTY models, led to a slightly younger age estimation of 0.3 - 0.5 Gyr compared to previous estimations of its age. Using this new upper age limit, the evolutionary tracks yield only a maximum total system mass of ~ 135 $M_{\rm Jup}$, even if a third companion is considered. This arising discrepancy to the dynamically determined mass shows the importance of further mass determinations independent of theoretical models.

With all the above conclusions, the hypothesis that Kelu-1 A itself is a binary system seems conclusive. If the third component in the Kelu-1 AB system can be confirmed in further observations, this would be the first pure brown dwarf triple system detected so far.

Future work includes resolved optical spectra of Kelu-1 AB. This will ascertain in which component Li absorption is present and thus help to better establish the age of the components. In addition, it will extend the individual spectral type determinations into the red optical. This might give further conclusions on mechanisms like low-gravity, high-metallicity and/or cloud condensation leading to the redder, triangular shaped near-IR spectra of Kelu-1 B. The continued monitoring of Kelu-1 AB will help to refine the orbital parameters and its dynamical mass. Further, upcoming spatially resolved high-resolution radial velocity observations will provide information on the spectroscopic orbit for the determination of individual masses and possibly resolve the third component. These results will help to improve and adjust the theory of brown dwarf evolution and improve the interpretation of the observations of these objects.

4

2MASS 0310+1648 AB – A NEW BINARY AT THE L/T TRANSITION

4.1 Motivation

THE TRANSITION from the L to the T spectral types of brown dwarfs is marked by a dramatic change in their near-IR spectral energy distribution (SED) and atmospheric properties. While this has already been an active area of inquiry, it still remains one of the most poorly understood phases of brown dwarf evolution. The late-type L dwarfs are characterized by very red near-IR colors, caused by condensate dust in their photospheres and metal hydrides, as well as CO absorption bands. In contrast, the T dwarfs are characterized by again bluer near-IR colors, due to the appearance of CH_4 absorption at 1.65 and 2.2 μm, stronger H_2O absorption and the increasing importance of collision-induced H_2 absorption (CIA), as well as relatively dust-free photospheres (Geballe et al., 2002). This change occurs over a comparatively narrow effective temperature range ($\Delta\,T_{\rm eff} \approx 200$ K) around 1500 - 1300 K for near-IR L7 - T3 dwarfs (Golimowski et al., 2004a), implying a very rapid transition phase. Including the interaction between temperature, gravity, metallicity and the physics of atmospheric dust clouds, this area remains a challenge to theoretical models (see also 5.3.2 and references therein for further discussion on atmospheric models).

Another very peculiar, yet unexplained observational feature is the remarkable brightening in the *Z*/*Y* ($\sim$ 0.9 - 1.1 μm) and *J* ($\sim$ 1.2 - 1.3 μm) bands of up to $\Delta\,M_J \sim 1$ mag for the early- to mid-type T dwarfs, the so-called *J* - band "bump" (Dahn et al. 2002; Tinney et al. 2003; Vrba et al. 2004), indicating a significant flux redistribution at almost constant luminosity. In the following, high-resolution imaging surveys revealed an almost twice as high binary frequency among the L / T transition objects relative

to earlier or later type brown dwarfs (Burgasser et al., 2006c). In a first attempt, it was suggested that the "bump" might be artificially enhanced by systems appearing overluminous due to binarity ("crypto-binarity") and where the integrated light of an L + T dwarf system could mimic the same spectral characteristics as an early - type T dwarf (Burrows et al. 2006; Liu et al. 2006; Burgasser et al. 2006c). However, recent discoveries suggest that at least a fraction of the observed *J* - band brightening is intrinsic to the atmospheres of early- to mid - type T dwarfs as they cool. Resolved high-resolution photometry revealed in four L / T dwarf binary systems a 1.0 - 1.3 μm flux reversal, with the T dwarf secondary being brighter than the late L or early T dwarf primary in this wavelength regime (2M172811+394859 AB, Gizis et al. 2003; SDSS J102109-030420 AB, Burgasser et al. 2006c; SDSS J153417+161546 AB, Liu et al. 2006; 2M140449-315932 AB, Looper et al. 2008a). In addition, a comparison with absolute *J* - band magnitudes of other resolved binary components having a spectral type of T1 - T5 (e. g. ϵ Indi Ba or SDSS0423-0414 B) shows, that they are still ~ 0.5 mag brighter than the latest L dwarfs (Burgasser et al. 2006c; Looper et al. 2008a). All this implies that the brightening across the L / T transition is a real effect, since it affects also binaries which are assumed to be coeval systems with common age and metallicity. Therefore, further discoveries and high-resolution observations of L / T transition binaries will play an important role. An extended sample of L + T dwarf binaries should provide independent crucial information on these issues and reveal the physical mechanism that drives the transition from dusty L dwarfs to dust-free T dwarfs.

One such important newly resolved binary is 2MASSW 031059 +164815 (hereafter 2M0310+1648), whose likely coeval components straddle the L / T transition. 2M0310 +1648 was originally discovered by Kirkpatrick et al. (2000) in the *Two Micron All Sky Survey* (2MASS) database. It was classified with a spectral type L8 in the optical and the presence of lithium implied a mass $M \leq 60\,M_{\rm Jup}$, confirming its brown dwarf nature. The first near-IR spectroscopic observations revealed some spectral discrepancy compared to other late-type L dwarfs in terms of a significantly depressed *K* - band spectrum starting around 2.2 μm, interpreted to be caused by collision-induced H_2 absorption (Reid et al., 2001a). By contrast, Nakajima et al. (2001) attributed this flux suppression to methane rather than H_2, which would explain also the very weak CO band head at 2.3 μm and indicate that much of the carbon is in CH_4. Finally, Geballe et al. (2002) slightly revised with their new classification scheme the spectral type of 2M0310+1648 to L9 in the near-IR. In September 2004, 2M0310+1648 was resolved as an almost equally bright binary system during our own *Hubble Space Telescope* (HST) NICMOS

survey. As an L / T transition binary it added up to the already apparently higher binary fraction in the transition regime and provides an important testbed to derive informations about the underlying physical and chemical processes in this transition regime. Therefore a monitoring program including resolved photometry and spectroscopy was started and the first results are presented in this chapter.

4.2 The new Laser Guide Star system PARSEC

For precise astrometry and resolved spectroscopy of brown dwarf binaries with small separations, diffraction limited observations are necessary. To achieve the essential sensitivity and very high spatial resolution, Adaptive Optics (AO) is essential for observations from the ground. In the past, observations with the near-IR wave front sensor (WFS) of NACO (and any other near-IR WFS system for observations on the southern hemisphere) were limited by the availability of a natural guide star (NGS) of $K \leq 13$ mag with a maximum distance of $55''$ to the target. For the WFS of the integral field spectrograph SINFONI the NGS was actually limited to $R \leq 14$ mag out to $30''$. Especially for field brown dwarfs it is hard to find such a bright NGS and the ultracool brown dwarfs themselves are usually too faint for NGS - AO. This severely restricted the fraction of brown dwarf targets for which AO observations could be obtained. The operation of an artificial Laser Guide Star (LGS) which is bright enough to serve as the wave front reference, can relax these restrictions a lot. In 2006, ESO added the new sodium LGS system PARSEC (Rabien et al., 2004; Bonaccini Calia et al., 2006) as supplement to the NGS - AO systems NACO and SINFONI. The only requirement for this facility is to provide a natural star brighter than $V \sim 17$ mag and within $60''$, to correct the tip-tilt motion for which the LGS is insensitive. Thus, the new LGS at the VLT provides the unique possibility to widely extend the sample of ground - based observable brown dwarf binaries.

The VLT/PARSEC monitoring program of binary brown dwarfs

As part of the MPIA guaranteed time observations (GTO) with PARSEC, a monitoring program of six brown dwarf binaries was started. The sample consisted of two L / L dwarf binaries, two binaries with both components having spectral types in the L / T transition regime and two T / T dwarf binaries. The targets were chosen considering predicted orbital periods between 3.5 and 15 years. This provides the possibility to monitor a sufficient part of the orbit on a reasonable timescale. In addition, three of the

binaries were just recently resolved systems. Beside multi-epoch orbital monitoring, another aim of the program was to derive multi-band (H, K_S) photometry with NACO and spatially resolved spectroscopy with SINFONI and its H + K grating. The results will enable to better constrain the physical properties like spectral types, effective temperature (T_{eff}), luminosity and colors of the individual components, for some of them for the first time.
Due to technical problems with the Laser Guide Star Facility during the first years of operation, only very few observations of this program have been conducted so far. The first results for 2M0310+1648 AB are discussed in the following, while the results for ϵ Indi Bab will be discussed in Chapter 5.

4.3 Observations and Data reduction

4.3.1 HST/NICMOS

The HST observations of 2M0310+1648 AB were obtained as part of the spectral differential imaging program described in Chapter 2. They were executed on September 24, 2004 with the NICMOS1 (NIC1) camera, providing a field of view (FoV) of 11″ x 11″ with a pixel scale of 0.0432″, in the two narrow band filters F108N and F113N. Four different images at two detector positions were acquired in MULTIACCUM mode for each filter, resulting in a total integration time of 2560 s and 2816 s, respectively (see Table 4.1).

The HST data analysis of 2M0310+1648 AB is based on pipeline reduced frames as provided by the HST archive. For the aperture photometry the IRAF *phot* routine in the *apphot* package was used to derive the magnitudes of the resolved components. Due to the small separation between the components an aperture size of 2 pixel was used.

Table 4.1: Observation log of high-angular resolution imaging of 2M 0310+1648 AB

Date	Telescope/Instrument	Filter	Exp. time [sec]	Seeing [a] [″]	Strehl ratio [%]
24 / 09 / 2004	HST/NIC1	F108N	2560		
		F113N	2816		
04 / 11 / 2007	VLT/NACO	H	14 x 60	1.02 - 1.19	21.9 - 43.8
		K_S	14 x 60	0.99 - 1.07	42.2 - 68.0

[a] Site seeing from the DIMM (measured in V- band)

Similar to the described procedure for Kelu-1 AB in §3.2.1, the results were thereafter corrected to a nominal infinite aperture, transformed into flux and finally converted into the Vega photomertic system. The individual magnitudes from the dithered exposures were then averaged to derive a single photometric measurement for each filter. For the astrometric measurements the same IDL - based simultaneous PSF - fitting algorithm from Bouy et al. (2003) as in §3.2.3 was used, adapted for HST/NIC1 data. The PSF library consisted of the same four theoretical PSFs but two different natural PSFs (this time 2MASSI 082519+211552 and 2MASSW 152322+301456, with spectral types of L7.5 and L8, respectively), according to the later spectral type of 2M0310+1648 AB. The precise separation, position angle (PA) and flux ratio were measured separately for each of the 4 images per filter. Finally the results were averaged and the uncertainties were calculated from the standard deviation.

4.3.2 VLT/NACO with PARSEC

Follow-up imaging observations were obtained with PARSEC and the AO system NACO at the VLT in the H (1.65 μm) and K_S (2.15 μm) broad-band filters, as part of the GTO monitoring program described in § 4.2. The observations were carried out in service mode on November 4, 2007 with the CONICA S27 camera, providing a FoV of $28''$ x $28''$ and a pixel scale of $0.0271''$. While the wavefront sensing was performed on the LGS, using the VIS dichroic for the observation, the necessary reference star for Tip/Tilt correction was chosen from the GSC-II (V 2.2.01). The star N33133125783 has $V = 17.21$ mag and a distance of $46.14''$ to 2M0310+1648 AB. Altogether 14 images were obtained in each filter, executed in a 7 point dither pattern to allow for cosmic ray and bad pixel correction, resulting in 840 s of total integration time. The observations were performed during clear sky conditions, but wind shake of the telescope and highly variable seeing conditions (between $0.99''$ and $1.19''$ FWHM), which were far above the requested constraints of $0.6''$ FWHM, significantly degraded the AO performance especially in H -band.

The standard image processing included flat-fielding, dark and sky subtraction and bad pixel correction. The final average combination was accomplished using the recommended Eclipse *jitter* (Devillard, 1997) software package. Since no separate reference PSF star was observed, the previously used simultaneous PSF-fitting algorithm from Bouy et al. (2003) could not be applied. Therefore, a new IDL fitting algorithm was implemented that fits a system created of two asymetric Moffat PSFs and provides the

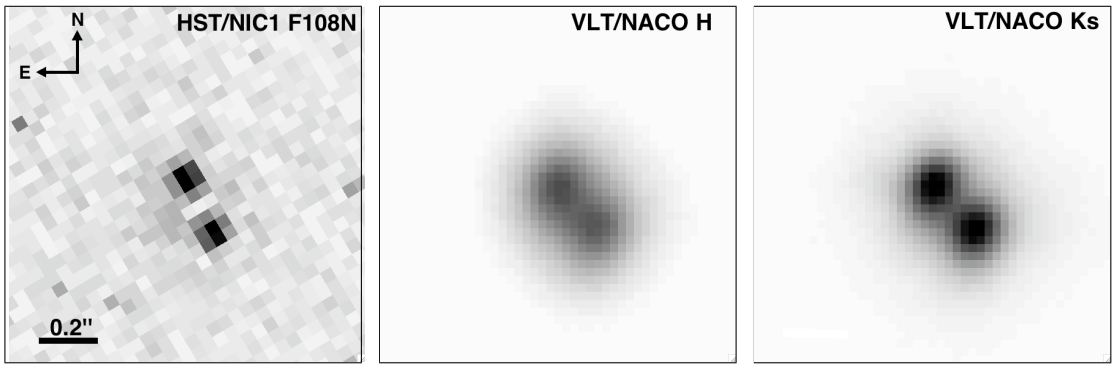

Figure 4.1: Images of 2MASS 0310+1648 AB obtained with HST/NICMOS and VLT/NACO including PARSEC. The orientation and scale are the same for all images. 2MASS 0310+1648 A is the northern component while 2MASS 0310+1648 B is the component to the south west.

separation, PA and flux ratio of the two components. The only constraint for this procedure is a similar shape of the observed component PSFs which worked very well for 2M0310+1648 AB due to the small separation of the binary components. To determine the statistical error of this fit, the algorithm was also applied to each single reduced image. All results per filter were averaged and the error calculated from the standard deviation. Figure 4.1 displays the HST data, as well as the final reduced VLT/NACO + PARSEC images in the H- and K_S - band.

4.4 Results

4.4.1 Resolved Photometry and Spectral Types

The magnitudes of the components in the HST F108N and F113N filters were determined by aperture photometry and are listed in Table 4.2. A comparison of the calculated flux ratios from these results with the flux ratios directly derived during the PSF fitting shows a very good agreement within the uncertainties. The slightly fainter magnitudes of both components in the F113N filter compared to those in the F108N filter are real and caused by the increasing water absorption in late L spectral types at this narrow wavelength band. This result is also a very good verification of the spectral differential imaging observing strategy in § 2.2.

The individual component H and K_S magnitudes were determined from the measured flux ratios in these filters and the published photometry of the unresolved 2M0310+1648 on the 2MASS system (Cutri et al., 2003). Similar to the case of Kelu-1 AB in § 3.3.3,

Table 4.2: Resolved component properties of 2MASS 0310+1648 AB

Property	flux ratio	Δ mag	2M0310+1648 A	2M0310+1648 B
F108N	0.892 ± 0.008	0.12 ± 0.02	17.42 ± 0.07	17.54 ± 0.08
F113N	0.891 ± 0.008	0.12 ± 0.02	17.51 ± 0.06	17.63 ± 0.05
J^*	0.908 ± 0.020	0.10 ± 0.06	16.73 ± 0.11	16.83 ± 0.13
H	0.947 ± 0.012	0.06 ± 0.04	15.66 ± 0.09	15.71 ± 0.10
K_S	1.008 ± 0.005	-0.01 ± 0.02	15.07 ± 0.07	15.06 ± 0.07
$J-H$			1.07 ± 0.14	1.12 ± 0.16
$H-K_S$			0.59 ± 0.11	0.65 ± 0.12
$J-K_S$			1.66 ± 0.13	1.77 ± 0.15

* the resolved J- band magnitudes are based on an estimated flux ratio due to the lack of observations (see description in the text).

it was assumed that the flux ratio of the components should not be significantly affected by the difference between the VLT/NACO and 2MASS photometric systems, thus no correction was applied. The final errors in the photometry include the uncertainties of the unresolved 2MASS magnitudes and the determined flux ratios. Due to the lack of J - band observations, the magnitude difference between the two components in this wavelength regime had to be estimated. As discussed in § 2.2 the SED of L dwarfs is comparatively flat between 1.06 μm and 1.15 μm which is continued through the whole J - band (see McLean et al., 2003). Thus, the flux ratios between different L spectral types show no significant trend. In addition, both components are almost equally bright, suggesting a very similar flux ratio in the F108N and J filter. A more quantitative determination was achieved by the convolution of the SED of late L dwarf synthetic spectra with the corresponding filter curves. The result yielded a Δ mag correction of 0.02 mag between these two filters.

Table 4.2 lists all the derived individual magnitudes and the resulting colors. Within the errors, the two components are equal in magnitude, implying that 2M0310+1648 AB is likely to be a near equal mass binary ($q \sim 1$). However, a closer look at the flux ratios[1] (f_B / f_A) reveals a steadily decreasing brightness difference between the A and B component from the Y (F108N and F113N) to the K_S - band. In the K_S - band there even occurs a flux reversal between the components. This is puzzling, since one would not expect the inversion of the brightness ratio if both dwarfs were equal. Yet, it is not a completely

[1] The flux ratios have smaller and more accurate errors, since the values were derived during direct measurement of the ratio.

new effect, as it reminds of the J - band flux reversal detected in the four other L / T transition binaries described in § 4.1. Three of these previously detected reversal binaries (SDSS 1021-0304 AB, SDSS 1534+1615 AB, 2M1404-3159 AB) are composed of a T1 - T1.5 primary and a T5 - T5.5 secondary, where the secondary is brighter in J ($\Delta J \sim 0.04$ - 0.54 mag in the MKO system) but significantly fainter in H and K_S. First, 2M0310+1648 AB seems to be different, since the flux reversal appears in the K_S - band. However, if one would consider that the so far assumed primary 2M0310+1648 A[2] is actually of slightly later spectral type than the so far secondary 2M0310+1648 B, the later-type (A) component would be also notably brighter in Y and J - band and fainter in K_S. A possible explanation for the still slightly brighter flux in H - band could be that both components have much closer spectral types, thus very similar SEDs with similar strong H_2O and CH_4 absorption, in contrast to the above mentioned T1 + T5 binaries. Therefore, the inversion might take place in a more continuous way.

To derive more information on the individual spectral types, they are assumed to be identical in a first approach, since both components are almost equally bright and thus should not have significantly different spectra compared to the unresolved 2M0310+1648 spectrum which has an assigned spectral type of L9. Additionally, while the flux of both components drops in the F113N filter due to water absorption, their flux ratio remains the same as in F108N, indicating the same strength of absorption in each component and thus same spectral type. To check these estimates, the resolved *JHKs* colors of 2M0310+1648 AB are compared to those of 61 known L7 - T4.5 dwarfs from the *Dwarf Archive*[3] (provided in the 2MASS photometric system), excluding any known binaries. The color - color diagram in Figure 4.2 shows that both components have colors coincident with a cluster of late L dwarfs (L7 - L9) and very early T dwarfs (T0 - T1), supporting the assumption that 2M0310+1648 A and B have a spectral type $\sim$ L9. At the same time, the color composition illustrates very well the peculiar redder colors of component B compared to component A, indicating the possibility that 2M0310+1648 A is of slightly later spectral type, possibly T0. In fact, a comparison of 2M0310+1648 A with the T0 standard SDSS 120747+024424 (Tinney et al., 2005; Burgasser et al., 2006b) reveals a very good agreement of the colors within the uncertainties (SDSS 1207: $J-H = 1.02 \pm 0.09$, $H-K_S = 0.57 \pm 0.09$, $J-K_S = 1.59 \pm 0.09$). However, a wider spread of colors for the same spectral type is not uncommon for dwarfs in the L / T transition (see, e. g. Knapp et al., 2004).

[2] The history of naming the actual A component as the primary, arose from the first resolved photometry derived with HST, where "A" was the brighter object.

[3] http://www.DwarfArchive.org

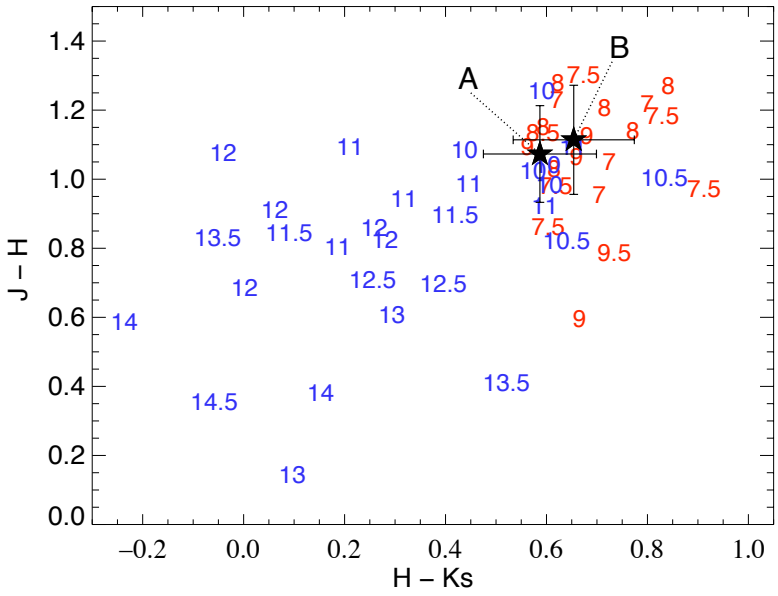

Figure 4.2: Near-IR color - color diagram of 61 known L7 - T4.5 dwarfs from the *DwarfArchive* with a near-IR spectral type uncertainty $\leq$1 subtype and known binary systems excluded. The L dwarfs are shown in red while the T dwarfs are shown in blue. The numbers indicate the individual spectral types from 7 = L7 to 14.5 = T4.5. The resolved colors of 2M0310+1648 A and B are plotted as stars with corresponding error bars.

Hence, only resolved spectroscopy can provide unambiguous spectral type determinations, which will further help to explain the physical mechanisms in the L/T transition. For the present, the assumption that both components have the same spectral type of L9 $\pm$ 1 in the near-IR will be retained until spectroscopic results are obtained.

4.4.2 New photometric distance

Since 2M0310+1648 has no trigonometric parallax determination so far, an assigned photometric distance of 20 pc (Kirkpatrick et al. 2000) was commonly used for the unresolved system. To correct this value for the bias introduced by the multiplicity of the system, the individual component magnitudes were compared to the absolute magnitude vs. Spectral Type (SpT) relation from Looper et al. (2008a)[4]. With an assumed near-IR spectral type of L9 for each component this $M_{\mathrm{JHK_S}}$ – SpT relation gives $M_H = 13.67 \pm 0.29$ mag and $M_{K_S} = 13.04 \pm 0.33$ mag. This yields distances of $\sim$24.9 and $\sim$25.4 pc, respectively, for component A and $\sim$25.6 and $\sim$25.3 pc, respectively, for component B. With these results a mean distance of 25.3 ± 3.7 pc is assigned, in-

[4] In contrast to the Burgasser (2007a) relation, this relation is based on 2MASS photometry, thus not introducing additional errors due to the conversion from one photometric system into another.

cluding the uncertainties in the photometric magnitudes and the rms error in the spectral type relation.

4.4.3 Orbit estimates

Table 4.3 lists the measured separations and position angles for the 2M0310+1648 AB system obtained over a time of $\sim$ 3 years. During that time the position angle changed by 15.5° while the separation increased only slightly from 204.3 ± 0.4 mas to 210.8 ± 1.8 mas. For a first estimation of the orbital parameters, a face-on circular orbit was assumed, since the separation between the components did not change significantly. This resulted in the approximation that the semi-major axis corresponds to the projected separation of 5.33 ± 0.2 AU (at a distance of 25.31 pc). With an orbital period of $72.2^{+4.0}_{-3.6}$ years, calculated from the fractional change in PA, and using Kepler's third law, this finally yields a first rough total system mass of $\approx 31\ M_{\rm Jup}$. This implies a relatively low mass binary brown dwarf system with both components having masses close to the brown dwarf/planetary mass boundary.

However, as the projected separation was assumed to be equal with the true semi-major axis, the mass prediction can only be a lower limit. Depending on the orientation in space (different perspectives on inclination *i* and eccentricity *e*), the true separation might be larger and / or the observations were obtained very close to the apastron passage, resulting in an increase of the total system mass. Fischer & Marcy (1992) showed that on average the true semi-major axis for binaries is about 1.26 times larger than the observed separation. Correcting with this statistical factor, the true semi-major axis for 2M0310+1648 AB can be estimated as a = 1.26 x ρ $\approx$ 6.72 AU. Using the same

Table 4.3: Orbital parameters for the 2MASS0310+1648 AB system

Parameter		HST/NIC1 (24 / 09 / 2004)	VLT/NACO (04 / 11 / 2007)
Separation	ρ [mas]	204.3 ± 0.4	210.8 ± 1.8
Position Angle	θ [deg]	206.35 ± 0.1	221.88 ± 0.8
estimated distance	d [pc]	25.3 ± 3.7	
Semi-major axis	a [AU]	$\geq 5.33 \pm 0.2$	
Orbital period	P [years]	$72.2\ ^{+4.0}_{-3.6}$	
System mass	M_{tot} [$M_{\rm Jup}$]	≥ 31	

orbital period as before implies an almost doubled total system mass approximation of $\approx 61\,M_{\rm Jup}$. This discrepancy shows the need for further astrometric observations to better determine the orbital parameters.

4.5 Conclusions

Own HST/NICMOS imaging in the F108N and F113N filters revealed the binary nature of another very interesting L/T transition brown dwarf: 2M0310+1648 AB. In the following, second epoch astrometry and first resolved high-resolution photometry in the H - and $K_{\rm S}$ - bands were obtained with VLT/NACO and its new LGS AO system PARSEC.

The two epochs of astrometric measurements spanning $\sim$ 3 years, allowed for first rough orbital parameter estimations. Due to a non-significant change in the separation, a face-on circular orbit was assumed, yielding an orbital period of 72.2 $^{+4.0}_{-3.6}$ years. Depending on the assumed semi-major axis, Kepler's third law yielded a first total system mass estimate of $\sim$ 31 - 61 $M_{\rm Jup}$, placing the individual component masses at the lower end for brown dwarfs. Even if the orbit period estimate of $\sim$ 72 years does not suggest a dynamical orbit determination in a reasonable time scale, follow-up observations in the next years will still enable more information on the orbital elements and therefore provide a more precise mass determination.

The derived photometry revealed a very intriguing nature of 2M0310+1648 AB. The component fluxes show a stunning decrease in brightness difference, resulting in a flux reversal in the $K_{\rm S}$ - band. An additional comparison of the obtained component colors reveals a redder nature of the B component. These results indicate that the so far primary component 2M0310+1648 A might actually be of slightly later spectral type than 2M0310+1648 B. This could at least partly explain the observed flux reversal as part of the J - band brightening of early- to mid-type T dwarfs, but a full explanation for the true nature of the reversal is still owing. Upcoming spatially resolved spectroscopic observations with VLT/SINFONI and the PARSEC AO system will allow a precise spectral type determination and an investigation of the underlying spectral morphologies. If it turns out that 2M0310+1648 A is really of later spectral type than 2M0310+1648 B, the system would not only add up to the yet small sample of flux reversal binaries. Additionally, 2M0310+1648 AB would be the first binary with a secondary showing the J - band brightening already at the very late - L (L9) or very early-T (T0) dwarf stage rather than at a T1.5 spectral type or later. This would even more challenge the existing

theoretical models.

In future work the likely coeval system 2M0310+1648 AB will serve as a very important benchmark object in the L / T transition. Further high-resolution observations will provide an improved understanding of and new insights into the challenging picture of this still poorly understood, yet remarkable evolutionary phase of brown dwarfs.

5

EPSILON INDI BAB – A BENCHMARK T DWARF BINARY

5.1 Motivation

IN THE previous chapters the importance of brown dwarf binaries to study the physical properties of brown dwarfs was shown. These systems facilitate a dynamical mass determination independent from theoretical models and constitute of a coeval system at the same age and metallicity. However, the absolute values of age and metallicity of field population objects are still unknown. In this regard, resolved brown dwarf companions to more massive main-sequence primaries are very valuable. Under the assumption that they are formed of the same chemical composition, their ages, metallicities and distances can be inferred from these quantities of the primary star. This allows to overcome the mass-age degeneracy of the brown dwarfs. Beside the important detections of single brown dwarf companions to main-sequence stars (e.g. Gl 229 B, Gl 570 D, HD 3651 B, SCR 1845 B, HN Peg B), especially gravitationally bound brown dwarf binaries to such stars can be used as benchmark objects, providing powerful empirical tests of the evolutionary models. But only a few such objects have been resolved so far: Gl 569 Bab (Martín et al., 2000b); HD 130948 BC (Potter et al., 2002); Gl 417 BC (Bouy et al., 2003); GJ 1001 BC (Golimowski et al., 2004a); Gl 337 CD (Burgasser et al., 2005).

Another very important brown dwarf binary system is ϵ Indi Bab. It was discovered as a widely separated companion ($402.3'' \approx 1459$ AU) to the high proper motion ($4.7\,''$/yr) K4 V star ϵ Indi A by Scholz et al. (2003), and resolved into a T1/T6 dwarf binary system itself by McCaughrean et al. (2004) with a separation of $0.73\,''$ (≈ 2.65 AU) and a nominal orbital period of ~ 15 years. An accurately measured *HIPPARCOS* dis-

tance of only 3.623 ± 0.009 pc to our Sun, makes ϵ Indi Ba and Bb the most nearby known brown dwarfs. Thus, they are very bright for T dwarfs with $K_{\rm A} = 11.35$ mag and $K_{\rm B} = 13.53$ mag, respectively, and allow to obtain high signal-to-noise photometry and spectroscopy, even in the far red optical wavelength regime. In addition, ϵ Indi A has a relatively well constrained age of ~ 1.3 Gyr (range 0.8 - 2.0 Gyr, Lachaume et al. 1999) and a metallicity similar to the sun of [M/H] = - 0.05 ± 0.02 (Beirão et al., 2005).

These well constrained physical properties make ϵ Indi Ba and Bb certainly two of the best studied T dwarfs and an unique system to test the brown dwarf models. Based on the most likely age of ϵ Indi A, the resolved NACO photometry of the components, their determined spectral type, and the evolutionary models from Baraffe et al. (2003), McCaughrean et al. (2004) obtained effective temperatures of $1276\,^{+30}_{-40}$ K and 854 ± 20 K for ϵ Indi Ba and Bb, respectively, corresponding to masses of $47 \pm 10\,{\rm M_{Jup}}$ and $28 \pm 7\,{\rm M_{Jup}}$.

As part of the VLT/PARSEC GTO program described in § 4.2, *H*-band and, for the first time, resolved *K*-band spectra of the binary components were obtained. These near-IR spectra allow the most precise determination of the spectral types so far. They are not only based on spectral indices, but also on comparison with template and model spectra. This allows to verify the above physical parameters with the new parameters for ϵ Indi Bab, where especially the effective temperatures and surface gravities are derived independently of evolutionary models.

5.2 Observation and Data reduction

For the spectroscopic observations of ϵ Indi Ba and Bb we used the SINFONI instrument with the H+K grating (covering a spectral range of 1.45 - 2.45 μm) and the smallest available FoV of $0.8'' \times 0.8''$, resulting in an effective image scale of 12.5 x 25 mas/pix, to achieve the best spatial sampling and a spectral resolution of R $\sim$ 2000. The observations were carried out in service mode on July 18, 2007 with S3113321698 as the reference Tip/Tilt star for the LGS system, chosen from the GSC-II (V 2.2.01) with $R = 16.85$ mag at a distance of $47.04''$ to ϵ Indi Bab. The weather conditions at the start of the observation were excellent with clear sky and a seeing of $0.4''$, but slightly degraded to $0.66''$ (measured by the seeing monitor in *V*-band) and some thin cirrus clouds at the end. A total of eight on-source and two sky exposures of 150 s each followed a dither pattern to allow for cosmic ray and bad pixel correction and yielded in a total integration time of 20 minutes on the target. The star HIP 8352 (B8V) was observed as

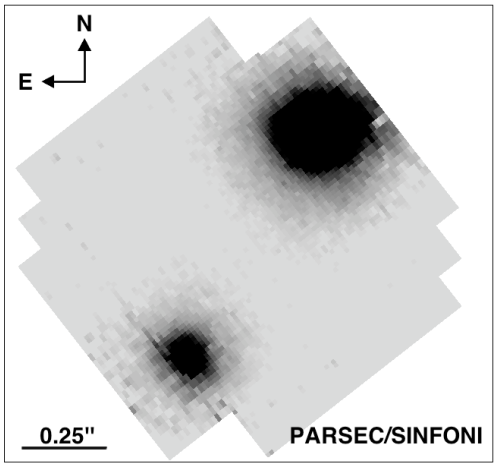

Figure 5.1: ϵ Indi Bab image from the SINFONI data cube of a single image slice at 1.586 μm, obtained with the Laser Guide Star AO system.

telluric standard immediately after ϵ Indi Bab at similar airmass.

For data extraction and reduction we used the data cubes for ϵ Indi Ba, Bb and the telluric standard star, as provided by ESO. They were generated with the Gasgano GUI of the ESO standard data reduction pipeline, which already includes the basic reductions like flat fielding, bad pixel and cosmic ray removal, sky subtraction, as well as wavelength calibration and combination of the dithered frames. As an advantage of the integral field spectroscopy (IFS), these data cubes still contain the full three-dimensional information (one spectral and two spatial axes) of the original data. Figure 5.1 displays an image of ϵ Indi Bab in a single slice of this data cube at 1.586 μm at the flux peak of the H-band.

To optimally extract the individual spectra of ϵ Indi Ba and Bb out of the data cube we used a dedicated IDL pipeline developed by Markus Janson at the MPIA. This algorithm consists of the following major steps: First, a preliminary median-collapsed frame of the cube is created to achieve a preliminary PSF reference. To compensate for spatial drifts of the PSF as a function of wavelength, cross-correlation between the PSF image and each individual image slice in the cube is performed to get the relative shifts. Then each slice is re-shifted to a common center including bilinear interpolation for sub-pixel shifts. Finally a new median-collapsed frame for this new data cube is created. In the last step, amplitude fitting of the PSF to each image slice in a $\sim 20 \times 20$ pixel box centered on each object in the cube results in the individual spectra of ϵ Indi Ba and Bb.

The same algorithm was used for the extraction of the telluric standard spectrum which was then corrected for its own hydrogen absorption lines. To keep the local

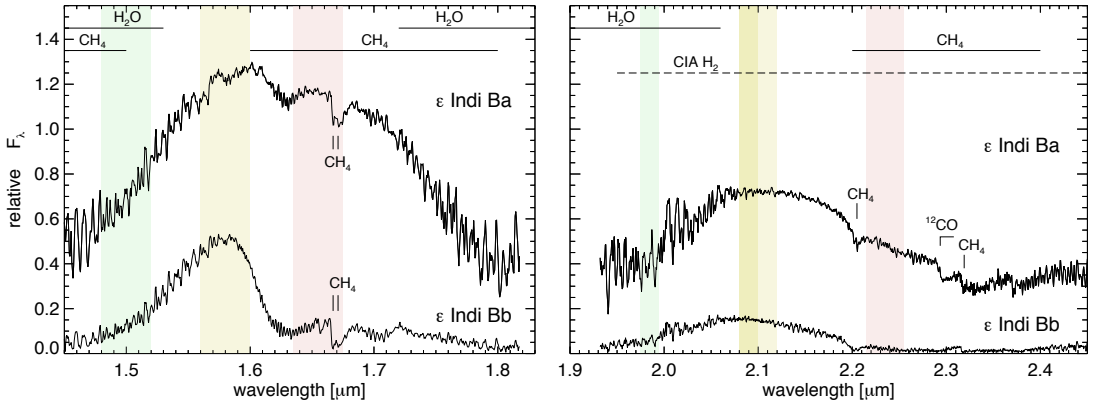

Figure 5.2: The reduced spectra of ϵ Indi Ba and Bb in *H*- and *K*-band obtained with SINFONI. The major H_2O and CH_4 absorption bands are indicated, as well as prominent lines of CH_4 and ^{12}CO and the region of strongest CIA H_2 absorption. The green (H_2O), yellow (flux peak in the corresponding near-IR band) and red (CH_4) shaded areas indicate the wavelength areas used for the calculation of the spectral indices in 5.3.1.

telluric information included in these absorption lines, the standard spectrum was first divided with a telluric spectrum of the Earth's atmosphere as provided on the ESO web-page and interpolated to the same wavelength grid as the telluric standard. For this pre-reduced standard spectrum we calculated the pure hydrogen absorption profile of HIP 8352 by fitting a Lorentz function to each absorption line. Afterwards the original standard spectrum was divided by this hydrogen absorption profile which resulted in the correct telluric spectrum at the time of observation.

To preserve the continuum shape of ϵ Indi Ba and Bb, the corrected telluric spectrum was divided by a blackbody spectrum of $T_{\rm eff} = 11{,}900$ K, corresponding to the spectral type of HIP 8352. In the final step, the science spectra were divided by the reduced standard spectrum. This ensures the elimination of the instrumental response function, the PSF effects from the wavelength dependent Strehl ratio, and the telluric impact on the ϵ Indi Ba and Bb spectra.

5.3 Results

5.3.1 Spectral type determination

The spectral appearance of T dwarfs in the near-IR is dominated by the H_2O absorption bands at 1.4 and 1.8 μm and the CH_4 absorption bands at 1.6 and 2.2 μm. These are the most defining features of this spectral class and are generally correlated: strong H_2O

absorption is associated with strong CH_4 absorption. This forces the *H*- and *K*- band flux to get a steeper and much narrower peak with later spectral types. In addition the overall *K*-band flux distribution is suppressed by collision-induced H_2 absorption (CIA). These effects are clearly revealed in Figure 5.2 by comparing the finally reduced spectra of the early T dwarf ϵ Indi Ba and the late T dwarf ϵ Indi Bb. The figure also indicates the main individual CH_4 absorption lines in both spectra, as well as the only remaining ^{12}CO band head in the ϵ Indi Ba spectrum at 2.29 μm which is visible until spectral types T2. The region of strong telluric absorption between 1.82 μm and 1.93 μm is not displayed for clearity. The distinct ripples visible in the *H*- and *K*- band are real features mainly caused by water and methane and will be further discussed in § 5.3.2. The only exceptions are the two larger ripples around 2.01 μm which are remnants of not fully corrected telluric absorption.

In the following, the SINFONI spectra are used to verify the near-IR spectral types derived by McCaughrean et al. (2004), whose spectral analysis was only based on the NACO *H*-band spectra with slightly lower resolution. In addition the analysis is complemented with the first resolved, mid-resolution *K*- band spectra of ϵ Indi Ba and Bb.

Direct comparison

There are several possibilities for spectral classification of a brown dwarf. The first and most straightforward way is usually the direct comparison of the observed overall spectral morphologies to near-IR spectral standards. For the comparison of the ϵ Indi Ba and Bb spectra we used the T dwarf spectral standards T0 - T2 and T5 - T7, respectively, as defined by Burgasser et al. (2006b). Beside the T5 standard all other spectra were derived from S. Leggett's L and T dwarf online archive[1]. The spectra are normalized to the *H*-band peak and the standard spectra T0 - T3 were additionally scaled by a factor of 1.075 in *K*-band, to compensate flux losses due to slit spectroscopy compared to our IFS . The results are shown in Figure 5.3 . For ϵ Indi Ba the T1 standard SDSS 083717-000018 provides a very good agreement in the band strengths and overall spectral shape in the *H*- and *K*- band. However, the observed CH_4 absorption in *H* - band between 1.6 and 1.7 μm is slightly stronger than the one for the T1 standard and lies in-between the T1 and T2 standard spectra. A similar trend is visible in the spectrum of ϵ Indi Bb. The T6 standard SDSS 162414+002915 shows an excellent match to the *K*- band morphology and corresponds very well to the *H*-band slope caused by the H_2O absorption.

[1] http://www.jach.hawaii.edu/∼skl/LTdata.html

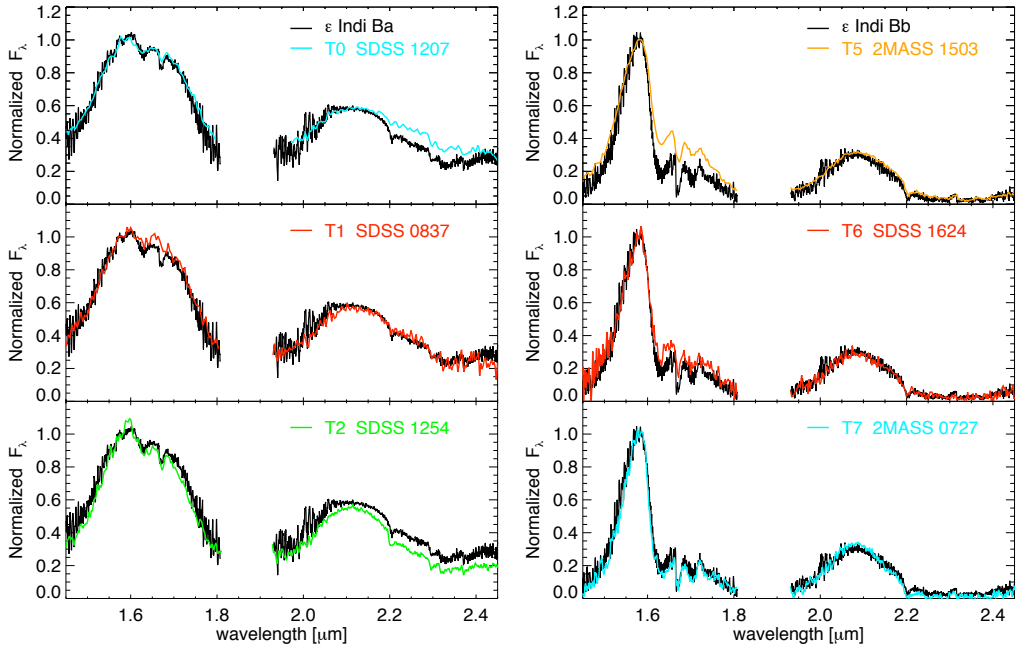

Figure 5.3: *Left*: Spectrum of ϵ Indi Ba (black line) overplotted with the three spectral standards T0 SDSS 120747+024424 (blue), T1 SDSS 083717-000018 (red) and T2 SDSS 125453-012247 (green). *Right*: the same for ϵ Indi Bb (black line), compared to T5 2MASS 150319+252519 (orange), T6 SDSS 162414+002915 (red) and T7 2MASS 072718+171001 (blue). In both panels, the target spectrum and standard spectra are normalized to the *H*-band peak.

Nevertheless, longward of 1.6 μm ϵ Indi Bb reveals the same stronger CH_4 absorption as ϵ Indi Ba and places it clearly between T6 and T7.

Spectral Indices

A more quantitative way to determine the spectral type is the calculation of predefined spectral indices. These indices are calculated ratios of the integrated flux in *i)* a spectral region of strong and defining molecular features like H_2O and CH_4 and *ii)* a nearby pseudocontinuum region, which is usually the flux peak of the corresponding wavelength band. From the five primary indices for T dwarf classification (H_2O-*J*, CH_4-*J*, H_2O-*H*, CH_4-*H* and CH_4-*K*) defined in Burgasser et al. (2006b), the last three were computed, since *J*-band spectroscopy data was missing for the first two. In Figure 5.2 the color shaded areas on top of the ϵ Indi Ba and Bb spectra highlight the wavelength ranges used for the calculations.

To determine the spectral types for each individual index value, three different indirect methods were used:

1. Comparison of each measured index to the corresponding index values of the spectral standards and assignment of the spectral type based on the closest match.

2. Comparison to a predefined subtype range, which is specified by the typical values for each spectral type, to find the best subtype or half-subtype (if the value is close to the range border).

3. The spectral type is calculated from the fourth-order polynomial fits to spectral index relations listed in Burgasser (2007a).

The results for the different classification methods are summarized in Table 5.1. The final spectral type was assigned by averaging the index subtypes. The fourth index ($H_2O - K$) was not included in the final assignment, since this index is likely affected by increasing noise due to telluric absorption around 1.9 μm. While it is mentioned by Burgasser et al. (2006b), it is usually not used as a primary index, since the comparison with different data sets revealed a large scatter as a function of spectral type. The values for ϵ Indi Ba and Bb for this index are nevertheless listed for completeness in Table 5.1. They correspond to spectral types of T1.5 - T2 and T5.5 - T6.5, respectively.

The spectral classifications obtained with the two different methods, direct comparison and spectral indices, are then combined. For ϵ Indi Ba, the indices support the result based on direct classification, yielding a spectral type of T1 $\pm$ 0.5. This result confirms the previously derived spectral type by McCaughrean et al. (2004). For ϵ Indi Bb the spectral type is revised to T6.5 $\pm$ 0.5, since both classification schemes indicate much stronger methane absorption at 1.6 μm and slightly stronger water absorption in *H* - band than for standard T6 dwarfs, even if the *K*- band slope provides a perfect fit to the available T6 dwarf spectra. The same anomalous high methane absorption has previously been reported for the peculiar T6 dwarf Gl 229 B (Geballe et al., 2002; Burgasser

Table 5.1: Near-IR spectral indices and classification for ϵ Indi Ba and Bb

	ϵ Indi Ba				ϵ Indi Bb			
Index	Value	Ind 1	Ind 2	Ind 3	Value	Ind 1	Ind 2	Ind 3
H_2O - *H*	0.571	T1	T1	T0.8	0.261	T6.5	T6.5	T6.2
CH_4 - *H*	0.924	T1.5	T1.5	T1.4	0.209	T6.5	T7	T6.8
CH_4 - *K*	0.667	T1	T1	T1.2	0.149	T6	T6	T6.1
H_2O - *K*	0.557				0.376			
averaged SpT		T1	T1	T1		T6.5	T6.5	T6.5

et al., 2006b) and the also very nearby T6 dwarf SCR 1845B (Biller et al., 2006). For the latter one Kasper et al. (2007b) found very similar absolute *J*, *H* and *Ks* magnitudes with differences less than 0.1 mag. In contrast, while a comparison of our ϵ Indi Bb SINFONI spectrum with the SCR 1845B VLT/NACO spectrum reveals an almost identical *H* - band spectrum (with an only somewhat stronger methane absorption for ϵ Indi Bb), it does not show the same suppressed *K* - band flux as for SCR 1845B. Hence, it is interesting to investigate which physical and chemical peculiarities might cause the deviations in the spectral morphologies of these similarly classified objects.

5.3.2 Physical properties of ϵ Indi Ba and Bb

Temperature and Surface Gravities

The near-IR spectral energy distributions (SED) of brown dwarfs are strongly influenced by their temperature, surface gravity and metallicity. The largest effects occur in the wings of the *H* - band flux peak and at the peak of the *K* - band. As mentioned above, the spectral types are based on the strengths of the molecular H_2O and CH_4 bands. While those bands are almost not affected by surface gravity or metallicity, the additionally observed correlation between $T_{\rm eff}$ and spectral type links H_2O and CH_4 directly with temperature. In contrast, the morphology of the *K* - band is not only shaped by the H_2O and CH_4 bands, but heavily influenced by the broad, featureless collision-induced H_2 absorption. This absorption emerges from kinematic perturbations and is facilitated in higher density and higher pressure atmospheres. In brown dwarfs these higher pressure photospheres are achieved with higher surface gravity and/or lower metallicity (Burrows et al., 2002; Knapp et al., 2004; Burrows et al., 2006). Nevertheless, since pressure regulates the atmospheric abundance of H_2O and CH_4 with:

$$\mathrm{CO} + 3\mathrm{H_2} \rightleftharpoons \mathrm{H_2O} + \mathrm{CH_4} \tag{5.1}$$

(Burrows & Sharp, 1999) and these abundances are also modulated by metallicity, nearly all major absorption features in T dwarf spectra are affected either way by $T_{\rm eff}$, g and $[\mathrm{M/H}]$.

Furthermore, condensate clouds in the atmospheres of brown dwarfs have a high impact factor on their SEDs. The thickness of these clouds increases from early to late L dwarfs and defines the L dwarfs spectral range. With even lower temperature (cooler atmospheres) and thus later spectral types, clouds are expected to play a decreasing role

in shaping these spectra. The photospheres of late-type T dwarfs then appear to be relatively cloud-free. Nevertheless, it seems that they play a major role in the spectral range of the L / T transition and might therefore be responsible for the transition effects described in 4.1 (Tsuji et al., 1999; Marley et al., 2002; Burrows et al., 2006). Possible explanations include the breakup of the condensate cloud deck due to the formation of holes (Ackerman & Marley, 2001; Burgasser et al., 2002b; Folkes et al., 2007), a global collapse of the condensate cloud layer (Tsuji, 2005), or a rapid change in the efficiency of condensate sedimentation, resulting in increasing transparency in some spectral regions due to the settling of the dust cloud layers below the photosphere (Ackerman & Marley, 2001; Knapp et al., 2004).

Atmospheric models of brown dwarfs have substantially improved over the past years and are now capable to reproduce the spectral characteristics of early to mid-L dwarfs and mid- to late T dwarfs very well. However, they still fail to reproduce some of the observational results, particular at the L / T transition. By now, self-consistent models that include the breakup of the condensate clouds are not available, so only models with changes in the cloud sedimentation efficiency $f_{\rm sed}$ can be compared.

To further investigate the physical properties of the ϵ Indi Bab binary system and to constrain the individual effective temperatures and surface gravities, we adopted the determined near-solar metallicity of the primary star ϵ Indi A and used the most recent atmosphere models from M. Marley and D. Saumon (2008, private communication). These models assume chemical equilibrium and solar metallicity. They are calculated for various combinations of the three parameters $T_{\rm eff}$, g and $f_{\rm sed}$: For $T_{\rm eff}$ the range is considered in steps of 100 K, for $\log g$ the values of 4.5, 5.0 and 5.5 are used, and a $f_{\rm sed}$ with 1,2,3,4 and nc can be chosen. Here, larger $f_{\rm sed}$ values imply larger particle sizes and thus stronger cloud sedimentation, resulting in less total opacity, whereas $f_{\rm sed} = {\rm nc}$ marks the "no cloud" opacity = "clear" models. A more detailed description of these models and their calculation is given in Cushing et al. (2008). With a spectral type of T1, ϵ Indi Ba belongs to the L/T transition objects and one has to consider the effects of the condensate clouds. Hence, we used $f_{\rm sed} = 2,3,4$, all three available $\log g$ values and a temperature range of 1200 - 1500 K for the comparison. For the T6.5 dwarf ϵ Indi Bb we employed the "no cloud" opacity models and a possible temperature range of 800 - 1100 K. Figure 5.4 shows the best-fit results for the comparison of the ϵ Indi Ba spectrum (left) and ϵ Indi Bb spectrum (right) to these model spectra.

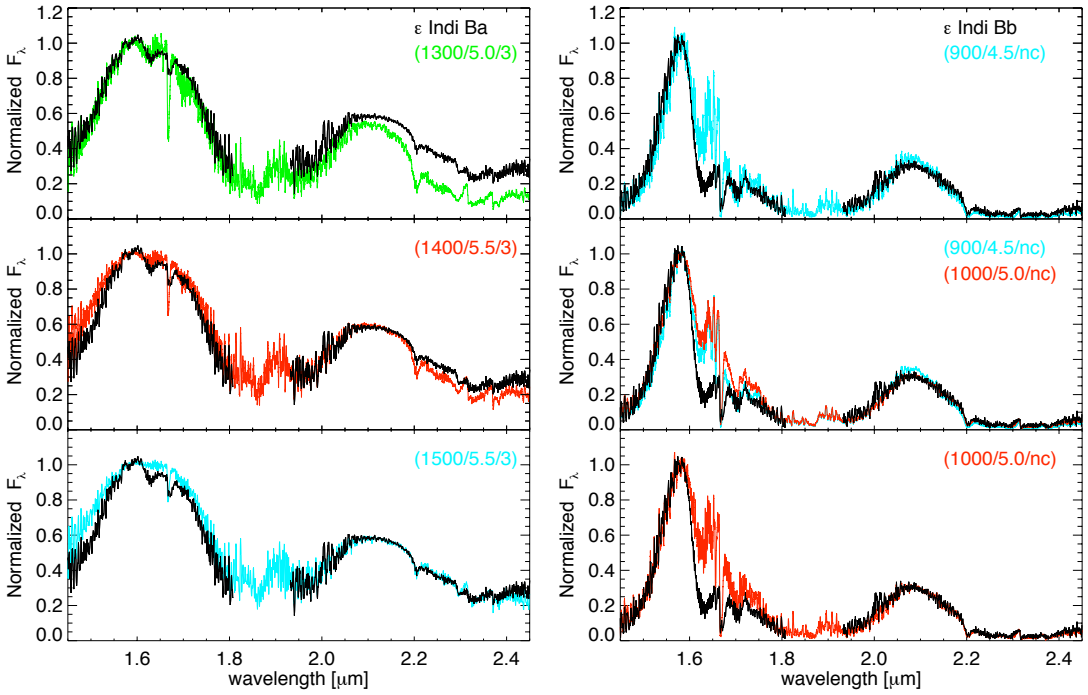

Figure 5.4: *Left*: Spectrum of ϵ Indi Ba (black line) overplotted with the best-fitting models ($T_{\rm eff}$, log g, f_{sed}) in H-band (top), overall (middle) and K-band (bottom). *Right*: the same for ϵ Indi Bb. All spectra are normalized to the H-band peak and the model spectra are smoothed and resampled to match the science spectra resolution and wavelength grid.

The fits to the spectrum of ϵ Indi Ba did not yield an unambiguous model result. This is likely due to the remaining short-comings of current models in the L / T transition as described above. While the slope in H-band was best fitted with a $T_{\rm eff}$ of 1300 K and log g of 5.0 (top panel), this model poorly fits the K-band morphology by underestimating the flux distribution and overestimating the 2.2 μm CH_4 absorption. By contrast, an almost perfect K-band fit was achieved with a higher $T_{\rm eff}$ of 1500 K and the correlated higher log g of 5.5 (bottom panel). The same higher temperature was derived by Smith et al. (2003), who compared a high-resolution spectrum of ϵ Indi Ba at 2.314 μm with synthetic atmosphere spectra of Tsuji (2002). This discrepancy in $T_{\rm eff}$ between different single photometric band comparison results has also been reported by Cushing et al. (2008). They showed that this method can add up to a scatter of $\sim$ 300 K, especially in K- band and thus a $T_{\rm eff}$ determination based only on the analysis of a narrow spectral range is not as reliable as the fitting of a wide-range SED. The lowest overall residuals in our comparison were accomplished for a model with $T_{\rm eff} = 1400$ K and log $g = 5.5$. This is displayed in the middle panel of Figure 5.4. For the sedimentation efficiency we could very well establish a value of $f_{\rm sed} = 3$, since none of the higher or lower $f_{\rm sed}$ value

models provided similar good results. Taking the average of the derived temperature range as being the best estimate, we find an T_{eff} of 1400 ± 100 K and a surface gravity of $\log g = 5.25 \pm 0.25$ for ϵ Indi Ba.

For the ϵ Indi Bb spectrum the models show equally good best-fit results for $T_{eff} = 900$ K and a $\log g$ of 4.5 (top panel) and $T_{eff} = 1000$ K with $\log g$ of 5.0 (bottom panel). While the 900 K model fits slightly better in *H*-band, the 1000 K model fits again almost perfectly the *K*-band. Consequentially, we assign a T_{eff} of 950 ± 50 K and a surface gravity $\log g$ of 4.75 ± 0.25 for ϵ Indi Bb. The increasingly poor match of the models to the observations between 1.60 - 1.75 μm with decreasing temperature is caused by an incomplete line list of CH_4 in the *H*-band that can hardly be determined from laboratory measurements alone (Freedman et al., 2008). This results in a too high flux distribution for the latest T dwarf models in this wavelength regime and is already visible in a too strong CH_4 absorption line at 1.67 μm for the L / T transition dwarfs.

Figure 5.5 and 5.6 show an enlarged cutout of the *H* - band (top) and *K*- band (bottom) spectra of ϵ Indi Ba and Bb, overplotted with the corresponding best-fit model for the appropriate wavelength regime. In both wavelength bands the observed ripples are extremely well reproduced by the models and are thus all intrinsic features. In the *H*-band, even most of the 19 individual CH_4 absorption lines stated in Cushing et al. (2005) can be identified. Extending the enlarged view to the short- and longer - wavelength ends of this band would reveal a similar good match between the detailed structure in the observed spectra and the models, this time caused by H_2O absorption. This indicates that at least the H_2O opacity tables are relatively good in the *H*-band (Cushing et al., 2008), in spite of all the shortcomings the existing models still comprise.

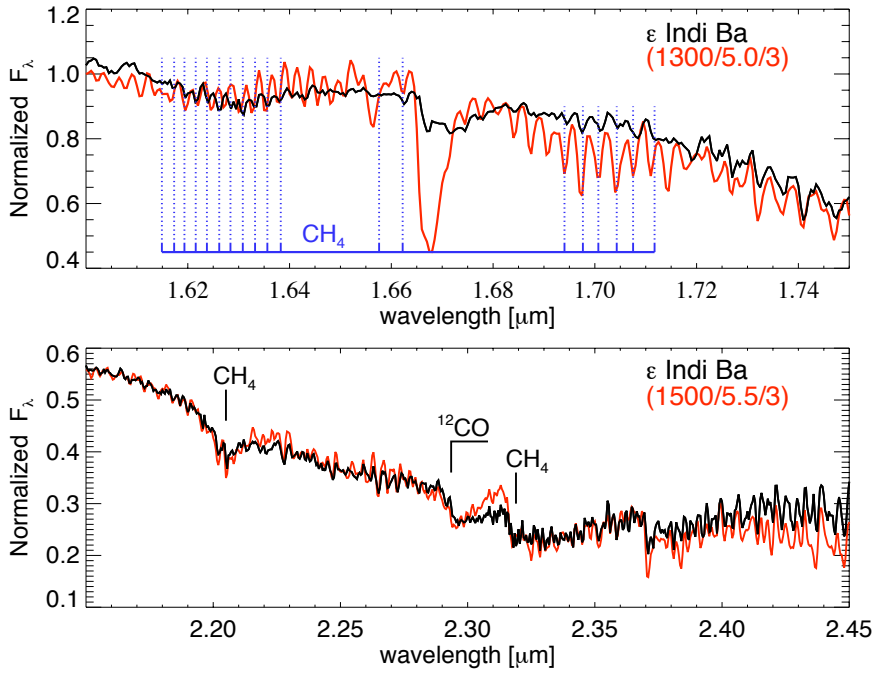

Figure 5.5: *Top*: Spectrum of ϵ Indi Ba centered on the CH_4 $2\nu_3$ absorption band and overplotted with the best-fitting model spectrum for this wavelength regime. In addition the 19 individual CH_4 absorption features identified by Cushing et al. (2005) are indicated by dotted lines. *Bottom*: the same for the specific absorption features in the *K*-band.

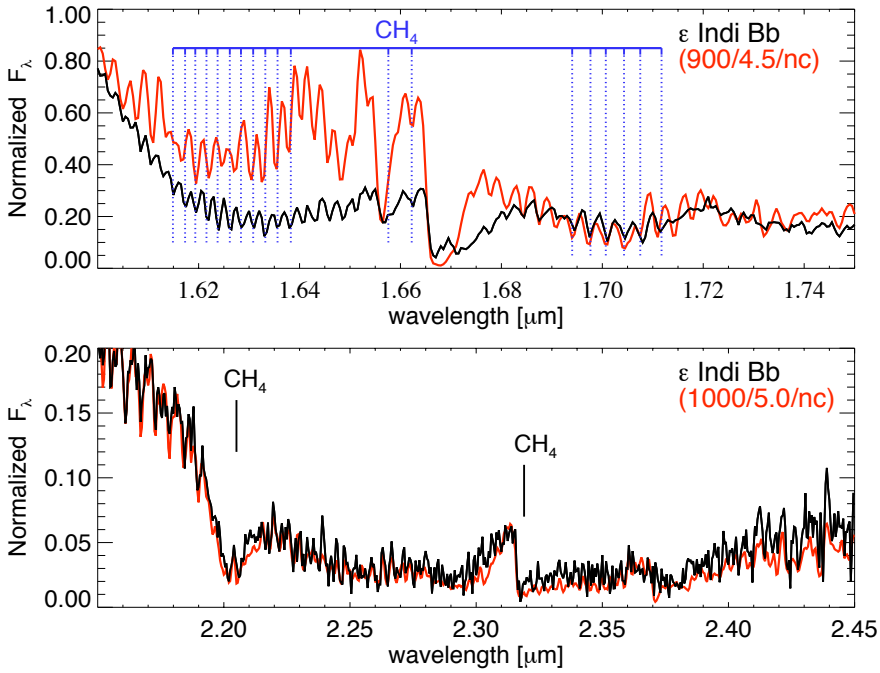

Figure 5.6: same as Figure 5.5, but for the ϵ Indi Bb spectrum.

Masses and Age

Brown dwarf evolutionary theory predicts, how effective temperature and surface gravity of a brown dwarf are directly related to its age and mass. Therefore, we combined our derived T_{eff} and $\log g$ ranges with the most recent evolutionary models of Saumon & Marley (2008), to derive the first pure spectroscopic mass estimates for ϵ Indi Ba and Bb. The only cloud-related evolution sequence available, is for $f_{sed} = 2$, but can be used for all cloudy cases according to Saumon & Marley (2008). The solid black lines displayed in Figure 5.7 represent these iso-mass tracks and were used in the case of ϵ Indi Ba, whereas the grey lines are the tracks for the cloudless atmospheres applied to ϵ Indi Bb. Showing the tracks for both, the cloudy model and the "cloud-free" model in the same figure, allows to understand the relation between clouds and the surface gravity for a given mass. In general, the observation of "cloud-free" brown dwarfs enables a deeper look into their atmospheres and thus one obtains higher T_{eff} and $\log g$ values compared to brown dwarfs with clouds. Especially at intermediate temperatures, this cloud effect is maximal, visible in the significant difference in surface gravity for cloudy and cloud-free models at a given mass and age.

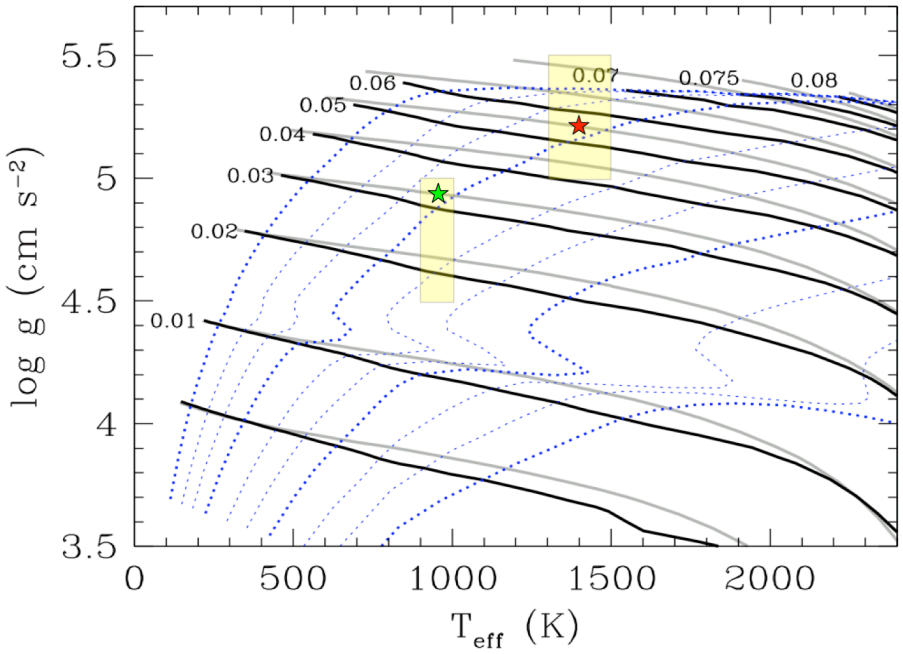

Figure 5.7: The derived best-fit T_{eff} and $\log g$ values (shaded yellow areas) compared to the evolutionary tracks from Saumon & Marley (2008). The iso-mass tracks for the cloudless atmospheres are in gray and those for a cloudy atmosphere with $f_{sed} = 2$ in black. Masses are given in units of $M_{\odot}$. The Isochrones are indicated by the blue dotted lines (**10**, 4, 2, **1**, 0.4, 0.2, **0.1**, 0.04, 0.02 and **0.01** Gyr, from left to right). The stars denote the masses for ϵ Indi Ba (red) and Bb (green), inferred for an estimated age of 1.3 Gyr, if coeval to ϵ Indi A.

To estimate the masses of ϵ Indi Bab the yellow shaded regions indicate the allowed range of the $T_{\rm eff}$, $\log g$ values for ϵ Indi Ba and Bb as given by the comparison of the observed spectra with the atmospheric models. At the lower temperature level with the lower gravity we get a mass of $\sim 40\,M_{\rm Jup}$, corresponding to an age of ~ 0.7 Gyr for ϵ Indi Ba. In contrast, looking at the highest derived gravities from the atmospheric models, reveals a discrepancy to the highest possible gravities in the evolutionary tracks. This maximum gravity boundary is caused by the mass-radius relation of the old, degenerate brown dwarfs and slightly varies with the sedimentation efficiency. Therefore, we assign a new maximum $\log g \approx 5.35$ for $T_{\rm eff} = 1500$ K with a mass of $\sim 70\,M_{\rm Jup}$ and an age of 4 - 10 Gyr. Performing the same method on ϵ Indi Bb, we find $\sim 16\,M_{\rm Jup}$ with a corresponding age of 0.35 Gyr for the lower $T_{\rm eff}$, $\log g$ values and $\sim 34\,M_{\rm Jup}$, being 1.5 Gyr old, at the highest $T_{\rm eff}$ and $\log g$ values. Since ϵ Indi Ba and Bb are assumed to constitute a coeval system together with the primary star ϵ Indi A, we adopt its mean age of 1.3 Gyr to constrain our results. Together with the previously established temperature ranges, we finally obtain masses of $56\,^{+4}_{-6}\,M_{\rm Jup}$ and $30\,^{+3}_{-3}\,M_{\rm Jup}$ for ϵ Indi Ba and Bb, respectively, with corresponding $\log g = 5.22\,^{+0.03}_{-0.07}$ and $\log g = 4.92\,^{+0.07}_{-0.04}$. In Table 5.2 we summarize all our derived results.

Considering the apparent discrepancy in the *K*-band spectra between ϵ Indi Bb and SCR1845 B (see § 5.3.1), the newly derived temperature and gravity values for ϵ Indi Bb might provide a good explanation. As previously described, the spectral type and the *H*-band morphologies are a function of temperature. Thus, it is not a surprise that both objects have the same spectral type and an almost identical *H*- band spectrum due to their same estimated $T_{\rm eff}$ of ~ 950 K. In contrast, we assigned a lower surface gravity of $\log g = 4.92\,^{+0.07}_{-0.04}$ for ϵ Indi Bb, which has therefore a less suppressed *K*-band flux due to the gravity sensitive collision-induced H_2 absorption, compared to the higher $\log g = 5.1$ object SCR1845 B.

Table 5.2: Summary of the derived physical parameters for ϵ Indi Ba and Bb at an age of 1.3 Gyr

	SpT	$T_{\rm eff}$ [K]	$\log g$	Mass [$M_{\rm Jup}$]
ϵ Indi Ba	T1 $\pm$ 0.5	1400 $\pm$ 100	$5.22\,^{+0.03}_{-0.07}$	$56\,^{+4}_{-6}$
ϵ Indi Bb	T6.5 $\pm$ 0.5	950 $\pm$ 50	$4.92\,^{+0.07}_{-0.04}$	$30\,^{+3}_{-3}$

Consistency with previous results ?

The comparison of the determined temperatures: 1400 ± 100 K and 950 ± 50 K, with the photometrical results from McCaughrean et al. (2004): $1276\,^{+30}_{-40}$ K and 854 ± 20 K, reveals an overall higher T_{eff} estimate from our spectroscopic analysis, which is, however, within 1σ for ϵ Indi Ba and $1.5\,\sigma$ for ϵ Indi Bb. One possible explanation for this discrepancy is the inclusion of the *K*- band spectra. Only considering the *H* - band, we also would have derived slightly lower effective temperatures for ϵ Indi Ba, Bb. Another explanation might be the difference in the temperature determination technique. In evolutionary models the T_{eff} is a pure theoretical parameter dependent on the theoretical size (= radius) of the brown dwarf and its measured luminosity, thus more affected by systematic errors. While the luminosity is also dependent on a bolometric correction factor related to a pre-determined spectral type and the distance of the object, the used photometry can be additionally biased. In the beginning we already discussed the strong influence of the CO, H_2O and CH_4 absorption features on the individual near-IR bandpasses and thus the measured flux. Therefore, a small change in the width of the filters (here between NACO and SINFONI) can lead to significant differences in the calculated flux levels and thus luminosity. Nevertheless, the masses assigned for ϵ Indi Ba and Bb agree well within the errors, with only a slightly higher trend on our values, mainly caused by the higher temperatures.

Even if our derived total system mass of $86\,^{+5}_{-7}\,M_{\rm Jup}$ at 1.3 Gyr is somewhat higher than the $75\,M_{\rm Jup}$ from McCaughrean et al. (2004) at the same age, it still shows the same disagreement with the dynamical mass estimation for the system ($\sim 120\,M_{\rm Jup}$) derived by Cardoso et al. (2008). This conclusion is similar to the one obtained for Kelu-1 AB in 3.3.4 and supports the hypothesis that current evolutionary models under-predict the masses.

5.4 Conclusions

The binary T dwarf system ϵ Indi Bab is not only an important, general test bed for dynamical mass determination in a reasonable time scale and acts as a calibrator for theoretical evolutionary models with well-determined age and metallicity due to its host star ϵ Indi A. Its individual components additionally provide a powerful insight into the particularly interesting L / T transition region and the lower, thus colder end of the T spectral types, all in one system. IFU spectroscopy was performed in *H* - and *K*- band

to verify previous spectral type determinations and to derive temperature, gravity and mass estimates from spectroscopy for the first time.

A combination of the results from direct spectral template comparison and calculated spectral indices yields a spectral type of T1 $\pm$ 0.5 for ϵ Indi Ba and T6.5 $\pm$ 0.5 for ϵ Indi Bb. For ϵ Indi Ba this result is in agreement with its previously assigned spectral type, whereas the spectral classification for ϵ Indi Bb was slightly revised due to the strong methane absorption in *H* - band.

To achieve a deeper insight into the physical properties of the components, we performed a comparison of the observed and the synthetic spectra. For ϵ Indi Ba we derived a relatively broad effective temperature range of $\sim$ 200 K and assigned an average $T_{\rm eff}$ of 1400 $\pm$ 100 K. The combination of the derived $T_{\rm eff}$ and $\log g$ with evolutionary models linked to an estimated age of 1.3 Gyr, allowed to constrain $\log g$ value to $5.22^{+0.03}_{-0.07}$ and obtain a mass of $56^{+4}_{-6}\,M_{\rm Jup}$. The sedimentation efficiency could be very well established to $f_{sed} = 3$, indicating a relatively thin, but still existing cloud deck in the photosphere of ϵ Indi Ba. In a similar way we derived $T_{\rm eff} = 950 \pm 50$ K, $\log g = 4.92^{+0.07}_{-0.04}$ and a mass of $30^{+3}_{-3}\,M_{\rm Jup}$ for ϵ Indi Bb. The somewhat different/higher temperature estimates compared to previous results show that not only the spectral type (used with the photometric method) defines the properties of a brown dwarf, but it is even more important to consider and understand their inner structure (as with the spectroscopic method).

As a next step, a more constrained conclusion on the physical properties of ϵ Indi Ba and Bb might be achieved using synthetic spectra with a higher resolution in the effective temperature and surface gravity grid. This would better reflect the sensitive relation between these two parameters. In addition, different metallicity values should be considered, since Burgasser et al. (2006a) and Liebert & Burgasser (2007) showed that slightly subsolar metallicity can lead to significantly different $T_{\rm eff}$ and $\log g$ values.

6

SUMMARY AND OUTLOOK

BASED ON A COMPREHENSIVE set of high - spatial resolution observations in the near-IR, this thesis investigated the physical properties of brown dwarfs. The aim was to obtain a deeper understanding of their origin, the formation of substellar bodies in general and binarity in the brown dwarf domain in particular. Special emphasis was put on the test and calibrate of theoretical models for substellar objects, which bridge the gap between VLM stars and giant planets. The content of this thesis can be divided in two main topics: the search for planetary mass companions to relatively young brown dwarfs and the analysis of three different brown dwarf binary systems, whose components represent the entire early - L to late - T spectral type regime. All objects were situated in the solar neighborhood within 30 pc from the Sun.

In the past years, the effort to directly image an extrasolar planet became an area of intensive research, since a successful detection would provide direct access to their physical properties such as brightness, color, effective temperature and composition. While previous direct imaging surveys focused especially on searches for exoplanets around young stars in nearby associations, the differential imaging survey with HST conducted as part of this thesis focused for the first time on nearby, relatively young (≤ 1 Gyr) field brown dwarfs in an effort to optimize the brightness contrast and to be able to find planetary mass objects at small physical separations from their host. Further, it is so far the sole one which used the water absorption spectroscopic feature instead of the methane feature. The high-resolution observations clearly resolved two brown dwarf binaries which were confirmed in follow-up observations. Their derived separations as well as the overall binary fraction of this survey are in full agreement with previous findings and add up important values to the brown dwarf binary statistics. Moreover, the preference of brown dwarfs to form equal mass systems, in contrast to the lower mass ratio main-sequence star binaries, could be confirmed.

Another very interesting finding in this context was the identification of a tentative companion to the brown dwarf 2MASSW 0337-1758, straddling the brown dwarf / planetary mass boundary and revealing an uncommonly low mass ratio system. A planetary nature of the secondary cannot be ruled out yet. However, it seems to be most likely a very low mass brown dwarf secondary at the border of the spectral T/Y transition regime because of its similarities to recently found very cool T dwarfs. This makes it one of the closest resolved brown dwarf binaries with the coolest and least massive companion to any L or T dwarf. However, the physical nature of this binary has yet to be confirmed.

In the second part of this thesis, the properties of three different brown dwarf binaries were studied. The degeneracy in the mass-luminosity (age-temperture) relation of substellar objects makes it hard to establish the physical properties of isolated, single brown dwarfs in order to improve and calibrate the evolutionary models and to guide the interpration of the observations. These issues were directly addressed with a detailed study of three brown dwarf binaries and their properties, benefitting from the fact that the system components are expected to be coeval, removing part of the mentioned degeneracy.

Continuous high-spatial resolution astrometric and photometric monitoring over three years and an overall observational period of ~ 10 years allowed for the first dynamical mass estimation of the benchmark L dwarf binary Kelu-1 AB in its very eccentric and almost edge-on tilted orbit. Furthermore, for the first time spatially resolved spectra of the system components were achieved and spectral types of L0.5 $\pm$ 0.5 for Kelu-1 A and L3 pec $\pm$ 1.5 for Kelu-1 B were determined. The first derived resolved *L* - band photometry for any L dwarf binary and the resulting near-IR colors supported these spectral type determinations. However, a comparison of the total system mass established from evolutionary models ($116 \pm 4\ M_{\rm Jup}$) for an upper limit of the system age of 0.5 Gyr, with the dynamical mass estimations ($185^{+139}_{-57}\ M_{\rm Jup}$) revealed a discrepancy of $\sim 1.5\,\sigma$. Interestingly, while for several very low mass (VLM) binary systems the so far derived dynamical mass determinations are in agreement with model predictions, similar discrepancies to the models, like for Kelu-1 AB, have been recently reported also for other brown dwarf binary systems. There have been different approaches to interpret these disagreements. In the case of Kelu-1 AB, the explanation for the discrepancy of dynamical masses with model predictions might be completely different: Spectroscopic evidence was found for a third, yet unresolved, system component, which would account for the "missing mass".

The very peculiar and still poorly understood transition between the L and T spectral types was covered by first observational results on the recently resolved binary system 2MASSW 0310+1648 AB. A rough first estimation of the orbital period and the dynamical mass was possible based on two epochs of astrometric data. A minimum semi-major axis of 5.33 ± 0.2 AU and the assumption of a face-on circular orbit yielded an orbital period of $72.2\ ^{+4.0}_{-3.6}$ and a total system mass estimate of ~ 31 - $61\ M_{\rm Jup}$. This places the individual component masses at the lower end for brown dwarfs. A comparison of the dynamical mass with the evolutionary models would have not been significant enough and has to be postponed until future observations. Nonetheless, the achieved photometry revealed a very puzzling nature of the system, resulting most likely in the detection of the fifth resolved L/T transition binary with a flux reversal. While ultimate explanations for this effect are still owing, the 2M0310+1648 system adds an important testbed in future observations to improve our understanding of this remarkable evolutionary phase of brown dwarfs. Additionally, the observational results of 2M0310+1648 AB derived with the new PARSEC AO system at the VLT show the importance of this technical improvement, which allows to significantly extend the sample of brown dwarfs observable with high-resolution from the ground and to reveal more of their physical properties.

The T dwarf binary ϵ Indi Bab is one of only few known brown dwarf binary systems gravitationally bound to a star, although these systems are important to overcome the mass - age degeneracy of brown dwarfs. A high-spatial resolution spectroscopic study with SINFONI / PARSEC in the *H* - and for the first time *K* - band, allowed spectral type classification by direct comparison and spectral indices calculation. This resulted in a confirmation of the previously assigned type for ϵ Indi Ba (T1 $\pm$ 0.5) and a slight revision for ϵ Indi Bb (T6.5 $\pm$ 0.5) due to a detection of stronger methane absorption than what had previously been reported. While disentangling the physical properties, like effective temperature, surface gravity and metallicity is a principle goal of substellar astrophysics, their measurement for brown dwarf companions enable another test of evolutionary models. By comparison with synthetic atmospheric spectra conclusive evidence was found that the L / T transition straddling primary ϵ Indi Ba has a relatively thin but still existing dust cloud deck (mainly consisting of silicates) in its photosphere, whereas the late T dwarf ϵ Indi Bb is cloud-free. This is consistent with existing model predictions for these spectral types.

The differences found between the SEDs of the two T6 dwarfs ϵ Indi Bb and SCR 1845 B could be very well explained by the slightly lower surface gravity of $\log g = 4.92\ ^{+0.07}_{-0.04}$ for ϵ Indi Bb. This is conclusive with the older age estimate for the SCR1845

system (1.8 - 3.1 Gyr) compared to that of ϵ Indi Bab ($\sim$ 1.3 Gyr). On the other hand, the temperature estimates of $T_{eff} = 1400 \pm 100$ K and $T_{eff} = 950 \pm 50$ K for ϵ Indi B and ϵ Indi Bb, respectively, are somewhat higher compared to previous results. This shows the importance to determine the physical properties on a broader wavelength range, since their influence on the SEDs strongly depends on the wavelength. Not only the spectral type (used with the photometric method) defines the properties of a brown dwarf, but its even more important to consider and understand their inner structure (as with the spectroscopic method). Atmospheric models substantially improved over the past years to reproduce the overall spectral characteristics of L and T dwarfs, but they still fail to reproduce most of the found peculiarities.

The first derived pure spectroscopic total system mass estimates were only slightly higher than the previously derived masses from evolutionary models. Nevertheless, a comparison of these results with existing dynamical mass determinations of the system revealed a similar underprediction of the model derived masses by several sigma, as for Kelu-1 AB. These discrepancies to the existing evolutionary models, as well as the findings of different mass ratios in Chapter 2, suggest the possibility of more than one formation scenario for brown dwarfs, especially in the case of binary systems. However, the available statistics are not large enough to discriminate between the various scenarios and give a final conclusive answer.

In this thesis the effort to study brown dwarfs in the solar neighborhood yielded important individual results. The discovery of two new binary systems confirmed the preference for equal mass systems in the brown dwarf regime, while planetary mass companions to brown dwarfs seem to be rare with less than 10%. The comparison of atmospheric models with observations showed the improvements (like e. g. the inclusions of updated molecular line opacity lists) of the models in the past years to reproduce the overall spectroscopic characteristics. Furthermore, the test of evolutionary tracks from different groups yielded consistent mass predictions for the investigated binary systems. However, the two binary systems with available dynamical mass determinations revealed discrepancies between the predictions and the measurements. While for the Kelu-1 AB system an unresolved higher degree multiplicity could be a possibility to solve the discrepancy, an explanation for the ϵ Indi Bab system is still lacking. Hence, while trends in the fitted parameters could be revealed, a more accurate determination of the physical parameters of brown dwarfs will require further observations and the development of even more complete model atmospheres.

To further investigate the achieved results and shed more light on several peculiarities found, different observations are planned or already approved:
For a confirmation of the binary status of 2MASS 0337-1758 and to derive more informations on the physical properties of the secondary, follow-up observations of this system could either be derived with VLT/PARSEC + NACO SDI, which uses the CH_4 instead of the H_2O absorption feature, or again with HST/NICMOS. This time, the F110M filter together with the angular differential imaging technique (ADI) could be used to confirm the companionship and in addition the SDI technique with the F145M and F165M filter which are both sensitive to water and methane absorption. Each of these observations would automatically provide additional colors for a more precise spectral type determination of the secondary.

Upcoming HST and VLT observations of the Kelu-1 AB system include resolved optical spectroscopy, to ascertain in which component Li absorption is present and thus will help to better establish the age of the components. In addition, this will extend the individual spectral type determinations of this system into the red optical wavelength regime and provide more insight into the physical properties which cause the peculiar shapes of the components SEDs. A high-resolution near-IR radial velocity monitoring program has been started, which will provide information on the spectroscopic orbit. The aim is to determine the individual component masses and possibly reveal radial velocity signatures of the potential third component, although this depends critically on the component masses of Kelu-1 Aab. Together with the continuation of the astrometric monitoring, the upcoming results will help to refine the orbital parameters and dynamical mass determination and will make Kelu-1 AB an even more powerful benchmark object for the calibration of evolutionary models.

Beside the planned new high-resolution astrometric observations of the L / T transition binary 2MASS 0310+1648 AB, the upcoming spectroscopic observations with VLT/SINFONI and the PARSEC AO system will allow a precise spectral type determination of the individual components and to investigate the underlying spectral morphologies responsible for the flux reversal.

The next important step to reliably calibrate the evolutionary models and to better understand the underlying physics will be to find more brown dwarf binaries to enlarge the sample. High-resolution observations will then allow for empirical measurements of system and individual component masses and to draw a firm conclusion on the overall picture. The continuation of the already started PARSEC monitoring program will help

to derive more information about different orbital parameters, mass ratios, etc. for a larger number of brown dwarf binaries and therefore provide important information on increasing binary statistics and binary evolution. A recently started survey on binarity of T dwarfs might further enlarge the sample for short period systems, as well as enable insight into the specific properties of objects at the L / T transition and of those dwarfs at the coolest end.

In the near future, new instruments will potentially detect even closer and cooler brown dwarfs than known today. The Wide-field Infrared Survey Explorer (WISE) satellite (to be launched December 2009) will be operating in the mid-IR from 3.5 - 23 μm and conduct a survey of the whole sky within half a year. Particularly its first two bands (at 3.3 and 4.7 μm) are ideally suited to find very cool objects, since the resulting red colors are expected to be uniquely characteristic to select the cool brown dwarfs against background objects.

The just started Pan-STARRS project is expected to not only discover new brown dwarfs due to its unprecedented sensitivity down to $m_R \sim 24$. With its fast and 3Π sky coverage, it will provide high-precision proper motion and parallaxe measurements for a huge number of brown dwarfs. Especially the parallaxes will enable more accurate absolute magnitude determinations and place these brown dwarfs precisely in the HR - diagram, which will further help to pin down their evolution.

In about five years, the James Webb Space Telescope (JWST) with its NIRCAM, NIR-SPEC and MIRI instruments will provide diffraction limited imaging and spectroscopy covering a large wavelength range from the optical to the mid-IR (0.6 - 27 μm). Beside its many other advantages, its resolution (e. g. $\sim 0.1''$ at 5 μm) will allow to obtain resolved spectra in the mid-IR of most brown dwarf binaries for the first time. Leggett et al. (2009) and Burgasser et al. (2008b) showed that mid-IR spectra are important to better constrain the atmospheric parameters of brown dwarfs, in particular at the cooler end, and to fix the scaling of the models. Since the flux distribution in the mid-IR is very sensitive to temperature these observations will confirm the implications from the near-IR and even identify unresolved, very low-temperature binary systems.

All these missions will provide a large number of interesting new results in the coming years and will challenge the development on both, the observational and theoretical side in the field of brown dwarfs.

BIBLIOGRAPHY

Ackerman, A. S. & Marley, M. S. 2001, *ApJ*, **556**, 872

Allard, F. & Hauschildt, P. H. 1995, *ApJ*, **445**, 433

Allard, F., Hauschildt, P. H., Alexander, D. R., Tamanai, A., & Schweitzer, A. 2001, *ApJ*, **556**, 357

Allen, P. R. 2007, *ApJ*, **668**, 492

Allers, K. N., Jaffe, D. T., Luhman, K. L., et al. 2007, *ApJ*, **657**, 511

Apai, D., Pascucci, I., Bouwman, J., et al. 2005, *Science*, **310**, 834

Apai, D., Pascucci, I., Henning, T., et al. 2002, *ApJ*, **573**, L115

Baraffe, I., Chabrier, G., Allard, F., & Hauschildt, P. H. 2002, *A&A*, **382**, 563

Baraffe, I., Chabrier, G., & Barman, T. 2008, *A&A*, **482**, 315

Baraffe, I., Chabrier, G., Barman, T. S., Allard, F., & Hauschildt, P. H. 2003, *A&A*, **402**, 701

Basri, G. 1998, in Astronomical Society of the Pacific Conference Series, Vol. 134, Brown Dwarfs and Extrasolar Planets, ed. R. Rebolo, E. L. Martin, & M. R. Zapatero Osorio, 394

Basri, G., Martin, E., Ruiz, M. T., et al. 1998, in Astronomical Society of the Pacific Conference Series, Vol. 154, Cool Stars, Stellar Systems, and the Sun, ed. R. A. Donahue & J. A. Bookbinder, 1819

Basri, G. & Reiners, A. 2006, *AJ*, **132**, 663

Bate, M. R., Bonnell, I. A., & Bromm, V. 2002, *MNRAS*, **332**, L65

Becklin, E. E. & Zuckerman, B. 1988, *Nature*, **336**, 656

Beirão, P., Santos, N. C., Israelian, G., & Mayor, M. 2005, *A&A*, **438**, 251

Biller, B. A., Close, L. M., Masciadri, E., et al. 2007, *ApJS*, **173**, 143

Biller, B. A., Kasper, M., Close, L. M., Brandner, W., & Kellner, S. 2006, *ApJ*, **641**, L141

Blake, C. H., Charbonneau, D., White, R. J., et al. 2008, *ApJ*, **678**, L125

Bonaccini Calia, D., Allaert, E., Alvarez, J. L., et al. 2006, in Society of Photo-Optical Instrumentation Engineers (SPIE) Conference Series, Vol. 6272, SPIE

Bonnell, I. A., Clark, P., & Bate, M. R. 2008, *MNRAS*, **389**, 1556

Boss, A. P. 2001, *ApJ*, **551**, L167

Bouy, H., Brandner, W., Martín, E. L., et al. 2003, *AJ*, **126**, 1526

Bouy, H., Duchêne, G., Köhler, R., et al. 2004, *A&A*, **423**, 341

Brandner, W., Martín, E. L., Bouy, H., et al. 2004, *A&A*, **428**, 205

Brandner, W., Zinnecker, H., Alcalá, J. M., et al. 2000, *AJ*, **120**, 950

Burgasser, A. J. 2007a, *ApJ*, **659**, 655

Burgasser, A. J. 2007b, *AJ*, **134**, 1330

Burgasser, A. J., Burrows, A., & Kirkpatrick, J. D. 2006a, *ApJ*, **639**, 1095

Burgasser, A. J., Geballe, T. R., Leggett, S. K., Kirkpatrick, J. D., & Golimowski, D. A. 2006b, *ApJ*, **637**, 1067

Burgasser, A. J., Kirkpatrick, J. D., Brown, M. E., et al. 2002a, *ApJ*, **564**, 421

Burgasser, A. J., Kirkpatrick, J. D., Cruz, K. L., et al. 2006c, *ApJS*, **166**, 585

Burgasser, A. J., Kirkpatrick, J. D., Liebert, J., & Burrows, A. 2003a, *ApJ*, **594**, 510

Burgasser, A. J., Kirkpatrick, J. D., & Lowrance, P. J. 2005, *AJ*, **129**, 2849

Burgasser, A. J., Kirkpatrick, J. D., Reid, I. N., et al. 2003b, *ApJ*, **586**, 512

Burgasser, A. J., Liu, M. C., Ireland, M. J., Cruz, K. L., & Dupuy, T. J. 2008a, *ApJ*, **681**, 579

Burgasser, A. J., Marley, M. S., Ackerman, A. S., et al. 2002b, *ApJ*, **571**, L151

Burgasser, A. J., McElwain, M. W., Kirkpatrick, J. D., et al. 2004, *AJ*, **127**, 2856

Burgasser, A. J., Reid, I. N., Siegler, N., et al. 2007, in Protostars and Planets V, ed. B. Reipurth, D. Jewitt, & K. Keil, 427–441

Burgasser, A. J., Tinney, C. G., Cushing, M. C., et al. 2008b, *ApJ*, **689**, L53

Burningham, B., Pinfield, D. J., Leggett, S. K., et al. 2008, *MNRAS*, **391**, 320

Burrows, A. 2005, *Nature*, **433**, 261

Burrows, A., Burgasser, A. J., Kirkpatrick, J. D., et al. 2002, *ApJ*, **573**, 394

Burrows, A., Hubbard, W. B., Lunine, J. I., & Liebert, J. 2001, *Reviews of Modern Physics*, **73**, 719

Burrows, A., Marley, M., Hubbard, W. B., et al. 1997, *ApJ*, **491**, 856

Burrows, A. & Sharp, C. M. 1999, *ApJ*, **512**, 843

Burrows, A., Sudarsky, D., & Hubbard, W. B. 2003, *ApJ*, **594**, 545

Burrows, A., Sudarsky, D., & Hubeny, I. 2006, *ApJ*, **640**, 1063

Cardoso, C. V., McCaughrean, M. J., King, R. R., et al. 2008, *ArXiv e-prints*

Chabrier, G., Baraffe, I., Allard, F., & Hauschildt, P. 2000, *ApJ*, **542**, 464

Chabrier, G., Baraffe, I., Selsis, F., et al. 2007, in Protostars and Planets V, ed. B. Reipurth, D. Jewitt, & K. Keil, 623–638

Chauvin, G., Lagrange, A.-M., Dumas, C., et al. 2004, *A&A*, **425**, L29

Chauvin, G., Lagrange, A.-M., Dumas, C., et al. 2005a, *A&A*, **438**, L25

Chauvin, G., Lagrange, A.-M., Zuckerman, B., et al. 2005b, *A&A*, **438**, L29

Clarke, F. J., Tinney, C. G., & Covey, K. R. 2002, *MNRAS*, **332**, 361

Clarke, F. J., Tinney, C. G., & Hodgkin, S. T. 2003, *MNRAS*, **341**, 239

Close, L. M., Lenzen, R., Guirado, J. C., et al. 2005, *Nature*, **433**, 286

Close, L. M., Zuckerman, B., Song, I., et al. 2007, *ApJ*, **660**, 1492

Cruz, K. L., Burgasser, A. J., Reid, I. N., & Liebert, J. 2004, *ApJ*, **604**, L61

Cruz, K. L., Reid, I. N., Liebert, J., Kirkpatrick, J. D., & Lowrance, P. J. 2003, *AJ*, **126**, 2421

Cushing, M. C., Marley, M. S., Saumon, D., et al. 2008, *ApJ*, **678**, 1372

Cushing, M. C., Rayner, J. T., Davis, S. P., & Vacca, W. D. 2003, *ApJ*, **582**, 1066

Cushing, M. C., Rayner, J. T., & Vacca, W. D. 2005, *ApJ*, **623**, 1115

Cutri, R. M., Skrutskie, M. F., van Dyk, S., et al. 2003, 2MASS All Sky Catalog of point sources. (The IRSA 2MASS All-Sky Point Source Catalog, NASA/IPAC Infrared Science Archive. http://irsa.ipac.caltech.edu/applications/Gator/)

Dahn, C. C., Harris, H. C., Vrba, F. J., et al. 2002, *AJ*, **124**, 1170

Delorme, P., Delfosse, X., Albert, L., et al. 2008, *A&A*, **482**, 961

Devillard, N. 1997, *The ESO Messenger*, **87**, 19

Dupuy, T. J., Liu, M. C., & Ireland, M. J. 2008, *ArXiv e-prints*

Epchtein, N., de Batz, B., Capoani, L., et al. 1997, *The Messenger*, **87**, 27

Fischer, D. A. & Marcy, G. W. 1992, *ApJ*, **396**, 178

Folkes, S. L., Pinfield, D. J., Kendall, T. R., & Jones, H. R. A. 2007, *MNRAS*, **378**, 901

Freedman, R. S., Marley, M. S., & Lodders, K. 2008, *ApJS*, **174**, 504

Geballe, T. R., Knapp, G. R., Leggett, S. K., et al. 2002, *ApJ*, **564**, 466

Gelino, C. R., Kulkarni, S. R., & Stephens, D. C. 2006, *PASP*, **118**, 611

Gizis, J. E., Monet, D. G., Reid, I. N., et al. 2000, *AJ*, **120**, 1085

Gizis, J. E., Reid, I. N., Knapp, G. R., et al. 2003, *AJ*, **125**, 3302

Golimowski, D. A., Henry, T. J., Krist, J. E., et al. 2004a, *AJ*, **128**, 1733

Golimowski, D. A., Leggett, S. K., Marley, M. S., et al. 2004b, *AJ*, **127**, 3516

Goodwin, S. P. & Whitworth, A. 2007, *A&A*, **466**, 943

Hayashi, C. & Nakano, T. 1963, *Progress of Theoretical Physics*, **30**, 460

Henning, T. 2008, *Physica Scripta Volume T*, **130**, 014019

Ireland, M. J., Kraus, A., Martinache, F., Lloyd, J. P., & Tuthill, P. G. 2008, *ApJ*, **678**, 463

Itoh, Y., Hayashi, M., Tamura, M., et al. 2005, *ApJ*, **620**, 984

Jayawardhana, R., Ardila, D. R., Stelzer, B., & Haisch, Jr., K. E. 2003, *AJ*, **126**, 1515

Jayawardhana, R. & Ivanov, V. D. 2006, *Science*, **313**, 1279

Kalas, P., Graham, J. R., Chiang, E., et al. 2008, *Science*, **322**, 1345

Kasper, M., Apai, D., Janson, M., & Brandner, W. 2007a, *A&A*, **472**, 321

Kasper, M., Biller, B. A., Burrows, A., et al. 2007b, *A&A*, **471**, 655

Kirkpatrick, J. D. 2005, *ARA&A*, **43**, 195

Kirkpatrick, J. D., Barman, T. S., Burgasser, A. J., et al. 2006, *ApJ*, **639**, 1120

Kirkpatrick, J. D., Reid, I. N., Liebert, J., et al. 1999, *ApJ*, **519**, 802

Kirkpatrick, J. D., Reid, I. N., Liebert, J., et al. 2000, *AJ*, **120**, 447

Knapp, G. R., Leggett, S. K., Fan, X., et al. 2004, *AJ*, **127**, 3553

Köhler, R., Ratzka, T., Herbst, T. M., & Kasper, M. 2008, *A&A*, **482**, 929

Konopacky, Q. M., Ghez, A. M., Barman, T. S., et al. 2009, in American Institute of Physics Conference Series, Vol. 1094, American Institute of Physics Conference Series, ed. E. Stempels, 112–117

Kumar, S. S. 1963, *ApJ*, **137**, 1121

Lachaume, R., Dominik, C., Lanz, T., & Habing, H. J. 1999, *A&A*, **348**, 897

Lafrenière, D., Doyon, R., Marois, C., et al. 2007, *ApJ*, **670**, 1367

Lafrenière, D., Jayawardhana, R., & van Kerkwijk, M. H. 2008, *ApJ*, **689**, L153

Lagrange, A.-M., Gratadour, D., Chauvin, G., et al. 2009, *A&A*, **493**, L21

Leggett, S. K., Allard, F., Geballe, T. R., Hauschildt, P. H., & Schweitzer, A. 2001, *ApJ*, **548**, 908

Leggett, S. K., Cushing, M. C., Saumon, D., et al. 2009, *ApJ*, **695**, 1517

Leggett, S. K., Golimowski, D. A., Fan, X., et al. 2002, *ApJ*, **564**, 452

Liebert, J. & Burgasser, A. J. 2007, *ApJ*, **655**, 522

Liu, M. C., Dupuy, T. J., & Ireland, M. J. 2008, *ArXiv e-prints*

Liu, M. C. & Leggett, S. K. 2005, *ApJ*, **634**, 616

Liu, M. C., Leggett, S. K., Golimowski, D. A., et al. 2006, *ApJ*, **647**, 1393

Liu, M. C., Najita, J., & Tokunaga, A. T. 2003, *ApJ*, **585**, 372

Lodieu, N., Dobbie, P. D., Deacon, N. R., et al. 2007, *MNRAS*, **380**, 712

Looper, D. L., Gelino, C. R., Burgasser, A. J., & Kirkpatrick, J. D. 2008a, *ApJ*, **685**, 1183

Looper, D. L., Kirkpatrick, J. D., Cutri, R. M., et al. 2008b, *ArXiv e-prints*, **806**

Lowrance, P. J., Becklin, E. E., Schneider, G., et al. 2005, *AJ*, **130**, 1845

Luhman, K. L., Hernández, J., Downes, J. J., Hartmann, L., & Briceño, C. 2008, *ApJ*, **688**, 362

Luhman, K. L., Joergens, V., Lada, C., et al. 2007, in Protostars and Planets V, ed. B. Reipurth, D. Jewitt, & K. Keil, 443–457

Luhman, K. L., McLeod, K. K., & Goldenson, N. 2005, *ApJ*, **623**, 1141

Luhman, K. L., Peterson, D. E., & Megeath, S. T. 2004, *ApJ*, **617**, 565

Luhman, K. L., Whitney, B. A., Meade, M. R., et al. 2006a, *ApJ*, **647**, 1180

Luhman, K. L., Wilson, J. C., Brandner, W., et al. 2006b, *ApJ*, **649**, 894

Magazzu, A., Martin, E. L., & Rebolo, R. 1993, *ApJ*, **404**, L17

Marcy, G. W., Butler, R. P., Fischer, D. A., & Vogt, S. S. 2003, in Astronomical Society of the Pacific Conference Series, Vol. 294, Scientific Frontiers in Research on Extrasolar Planets, ed. D. Deming & S. Seager, 1–58381

Marley, M. S., Seager, S., Saumon, D., et al. 2002, *ApJ*, **568**, 335

Marois, C., Macintosh, B., Barman, T., et al. 2008, *Science*, **322**, 1348

Martín, E. L., Brandner, W., & Basri, G. 1999a, *Science*, **283**, 1718

Martín, E. L., Brandner, W., Bouvier, J., et al. 2000a, *ApJ*, **543**, 299

Martín, E. L., Delfosse, X., Basri, G., et al. 1999b, *AJ*, **118**, 2466

Martín, E. L., Koresko, C. D., Kulkarni, S. R., Lane, B. F., & Wizinowich, P. L. 2000b, *ApJ*, **529**, L37

Martin, R. G., Lubow, S. H., Pringle, J. E., & Wyatt, M. C. 2007, *MNRAS*, **378**, 1589

Masciadri, E., Mundt, R., Henning, T., Alvarez, C., & Barrado y Navascués, D. 2005, *ApJ*, **625**, 1004

Mayor, M. & Queloz, D. 1995, *Nature*, **378**, 355

McCaughrean, M. J., Close, L. M., Scholz, R.-D., et al. 2004, *A&A*, **413**, 1029

McElwain, M. W., Metchev, S. A., Larkin, J. E., et al. 2007, *ApJ*, **656**, 505

McLean, I. S., McGovern, M. R., Burgasser, A. J., et al. 2003, *ApJ*, **596**, 561

Metchev, S. A. 2006, PhD thesis, California Institute of Technology, United States – California

Metchev, S. A., Kirkpatrick, J. D., Berriman, G. B., & Looper, D. 2008, *ApJ*, **676**, 1281

Mohanty, S., Jayawardhana, R., Huélamo, N., & Mamajek, E. 2007, *ApJ*, **657**, 1064

Nakajima, T., Oppenheimer, B. R., Kulkarni, S. R., et al. 1995, *Nature*, **378**, 463

Nakajima, T., Tsuji, T., & Yanagisawa, K. 2001, *ApJ*, **561**, L119

Neuhäuser, R., Guenther, E. W., Wuchterl, G., et al. 2005, *A&A*, **435**, L13

Ofek, E. O., Oguri, M., Jackson, N., Inada, N., & Kayo, I. 2007, *VizieR Online Data Catalog*, **838**, 20412

Padoan, P. & Nordlund, Å. 2004, *ApJ*, **617**, 559

Pascucci, I., Apai, D., Henning, T., & Dullemond, C. P. 2003, *ApJ*, **590**, L111

Potter, D., Martín, E. L., Cushing, M. C., et al. 2002, *ApJ*, **567**, L133

Rabien, S., Davies, R. I., Ott, T., et al. 2004, in Society of Photo-Optical Instrumentation Engineers (SPIE) Conference Series, Vol. 5490, SPIE Conference Series, ed. D. Bonaccini Calia, B. L. Ellerbroek, & R. Ragazzoni, 981–988

Racine, R., Walker, G. A. H., Nadeau, D., Doyon, R., & Marois, C. 1999, *PASP*, **111**, 587

Rebolo, R., Martin, E. L., & Magazzu, A. 1992, *ApJ*, **389**, L83

Rebolo, R., Zapatero-Osorio, M. R., & Martin, E. L. 1995, *Nature*, **377**, 129

Reid, I. N., Burgasser, A. J., Cruz, K. L., Kirkpatrick, J. D., & Gizis, J. E. 2001a, *AJ*, **121**, 1710

Reid, I. N., Gizis, J. E., Kirkpatrick, J. D., & Koerner, D. W. 2001b, *AJ*, **121**, 489

Reipurth, B. & Clarke, C. 2001, *AJ*, **122**, 432

Rosenthal, E. D., Gurwell, M. A., & Ho, P. T. P. 1996, *Nature*, **384**, 243

Ruiz, M. T., Leggett, S. K., & Allard, F. 1997, *ApJ*, **491**, L107

Salim, S., Lépine, S., Rich, R. M., & Shara, M. M. 2003, *ApJ*, **586**, L149

Saumon, D., Hubbard, W. B., Burrows, A., et al. 1996, *ApJ*, **460**, 993

Saumon, D. & Marley, M. S. 2008, *ArXiv e-prints*

Schneider, D. P., Hall, P. B., Richards, G. T., et al. 2007, *AJ*, **134**, 102

Scholz, A., Jayawardhana, R., Wood, K., et al. 2008, *ApJ*, **681**, L29

Scholz, R.-D., McCaughrean, M. J., Lodieu, N., & Kuhlbrodt, B. 2003, *A&A*, **398**, L29

Smith, V. V., Tsuji, T., Hinkle, K. H., et al. 2003, *ApJ*, **599**, L107

Smith, W. H., Schempp, W. V., Conner, C. P., & Katzka, P. 1987, *PASP*, **99**, 1337

Stamatellos, D. & Whitworth, A. P. 2009, *MNRAS*, **392**, 413

Stassun, K. G., Mathieu, R. D., & Valenti, J. A. 2006, *Nature*, **440**, 311

Stephens, D. C. & Leggett, S. K. 2004, *PASP*, **116**, 9

Tarter, J. C. 1975, PhD thesis, AA(California Univ., Berkeley.)

Tinney, C. G., Burgasser, A. J., & Kirkpatrick, J. D. 2003, *AJ*, **126**, 975

Tinney, C. G., Burgasser, A. J., Kirkpatrick, J. D., & McElwain, M. W. 2005, *AJ*, **130**, 2326

Tsuji, T. 2002, *ApJ*, **575**, 264

Tsuji, T. 2005, *ApJ*, **621**, 1033

Tsuji, T., Ohnaka, K., & Aoki, W. 1999, *ApJ*, **520**, L119

Umbreit, S., Burkert, A., Henning, T., Mikkola, S., & Spurzem, R. 2005, *ApJ*, **623**, 940

Vrba, F. J., Henden, A. A., Luginbuhl, C. B., et al. 2004, *AJ*, **127**, 2948

Warren, S. J., Mortlock, D. J., Leggett, S. K., et al. 2007, *MNRAS*, **381**, 1400

Whitworth, A., Bate, M. R., Nordlund, Å., Reipurth, B., & Zinnecker, H. 2007, in Protostars and Planets V, ed. B. Reipurth, D. Jewitt, & K. Keil, 459–476

Whitworth, A. P. & Zinnecker, H. 2004, *A&A*, **427**, 299

Wilson, J. C., Miller, N. A., Gizis, J. E., et al. 2003, in IAU Symposium, Vol. 211, Brown Dwarfs, ed. E. Martín, 197–+

Wolszczan, A. & Frail, D. A. 1992, *Nature*, **355**, 145

Wuchterl, G. & Tscharnuter, W. M. 2003, *A&A*, **398**, 1081

York, D. G., Adelman, J., Anderson, Jr., J. E., et al. 2000, *AJ*, **120**, 1579

Zapatero Osorio, M. R., Lane, B. F., Pavlenko, Y., et al. 2004, *ApJ*, **615**, 958

ACKNOWLEDGEMENTS

A journey is best measured in friends
rather than miles

– Tim Cahill

It all started roughly 10 years ago when I decided that traveling on Earth would no longer be sufficient enough and I began to tackle my very own adventure *Travel into Space*. With sparse knowledge of how the most famous constellations look like, I started out adding knowledge and insight to my pure fascination of stars.

With this PhD thesis, the first big episode of this journey ends, and it is time to thank all those people who not only came along with me but also supported me in their very own way. A simple *Thank You*! is not enough for many cases, but it is a good start :)

First of all, I'm most grateful to Wolfgang Brandner for his supervision, guidance and patience through the past years. You shared your great astronomical knowledge to significantly improve mine, you never got tired to answer all my questions and I enjoyed the many interesting discussions we had, particularly those on the reduction and interpretation of the Kelu-1 AB spectra :) Something I'm especially thankful for, is your enduring encouragement and your willingness to even help at weekends or holidays, just because there was the need for (due to approaching deadlines etc.). This is more than one can expect from his supervisor and way more than standard. Finally, for proofreading this thesis and your suggestions to improve the content.

I'm very thankful to Prof. Thomas Henning for his supervision and giving me the great opportunity to work at the Max-Planck-Institut in Heidelberg. Special thanks for the uncomplicated and particularly very short-notice possibility to discontinue the dissertation for three months.

Further thanks go to Bertrand Goldman. With his HST grant money he provided me the great possibility to spend five months at the Space Telescope Science Institute in Baltimore as a research scholar. I'm very grateful to Keith Noll who supervised my during this time. I gained a lot of experience on Hubble data in general and NICMOS data in particular and definitely benefitted from the insight on different ways of scientific working.
Very special and deep thanks go to him and his family Amy, Zoe and Cady. You made your home my home and let me be part of your great family!

In the last few months Felix Hormuth and Viki Joergens red (at least part of) this thesis and provided many useful comments and corrections. I owe you special thanks for that! You really spent a lot of effort on it.

Many thanks to my past and present office mates: Fulvio de Bonis, Sebastian Egner, Felix Hormuth, Eva Meyer and Carolin Schnupp for the relaxed atmosphere and all those discussions far away from science.... unfortunately I still can't speak Italian but Fulvios German is now perfect ;)

Acknowledgements

Deep gratitudes to the Daidalos Watersport Team 2007: Simon, Stiki, Chris, Manu, Arne, Franky, Dennis and Lars. During a time in which I heavily doubted on my work you accepted me on the team without any "ifs ands or buts" and therefore allowed me to live another big dream of mine! This provided me the necessary distance to reignite my passion for astronomy and the joy of working in science. It will always remain an unforgettable summer. I wish you always the best wind and the biggest waves. Hang Loose :)

I'm extremely grateful to my friends: Julia, Birgit, Sarah, Sascha, the Kos-Connection Antje Z., Regina and Frank, as well as Antje Jahn and her family. With stoical calmness you tolerated me talking over and over again with deep enthusiasm about my "barbecue briquettes of the Universe". I think you learned almost as much about them as I did :) Also, you always had an open ear for my small and sometimes larger triumphs or worries, and even more understanding, when I failed to correspond with you for month on end. This is exactly what makes a friendship and I'm very, very thankful to each of you!

The final thanks go to my family. You always believed in me and supported me in every way you could. I'm deeply grateful for this!

And the journey has just begun.....

Twenty years from now
you will be more disappointed
by the things you didn't do
than by the ones you did do.
So throw off the bowlines.
Sail away from the save harbor.
Catch the trade winds in your sails.
Explore! Dream! Discover!

– Mark Twain

EHRENWÖRTLICHE ERKLÄRUNGEN

Ich erkläre hiermit ehrenwörtlich, dass ich die vorliegende Arbeit selbständig, ohne unzulässige Hilfe Dritter und ohne Benutzung anderer als der angegebenen Hilfsmittel und Literatur angefertigt habe. Die aus anderen Quellen direkt oder indirekt übernommenen Daten und Konzepte sind unter Angabe der Quelle gekennzeichnet.

Bei der Auswahl und Auswertung folgenden Materials haben mir die nachstehend aufgeführten Personen in der jeweils beschriebenen Weise unentgeltlich geholfen:

1. Neber der Betreuung durch Prof. Dr. Th. Henning, stand mir wärend der gesamten Promotionszeit Dr. W. Brander als direkter Betreuer beratend zur Seite.

2. Die in Kapitel 2 analysierten HST-Daten wurden bereits vor Beginn der Dissertation von Dr. W. Brandner beantragt. Die Datenreduktion und Analyse wurde dann jedoch von mir komplett selbständig durchgeführt.

3. Das in den Abschnitten 3.2.3 und 4.3.1 verwendete PSF Fit-Programm zur Ermittlung der astrometrischen Parameter und relativen Photometrie, wurde im Orginal von Dr. H. Bouy (IAC, Spanien) entwickelt und von mir zur Nutzung der HST/NICMOS und VLT/NACO Daten angepasst.

4. Die in Abschnitt 3.3.1 beschriebene Lösung für die Bahnparameter des Doppelsystems Kelu-1 AB und die daraus resultierende dynamisch bestimmte Systemmasse wurden in Zusammenarbeit mit Dr. R. Köhler (ZAH Landessternwarte Heidelberg) und seinem Orbit-Fit-Programm erarbeitet.

5. Die Extraktion der SINFONI Spektren von ϵ Indi Bab aus dem von der ESO erhaltenen Datencube in Abschnitt 5.2 erfolgte mit Hilfe eines bereits vorhandenen Programmes von Dr. M. Janson (MPIA). Die weitere Datenreduktion und Analyse erfolgte dann wieder mit eigenen Programmen.

Weitere Personen waren an der inhaltlich-materiellen Erstellung der vorliegenden Arbeit nicht beteiligt. Insbesondere habe ich hierfür nicht die entgeltliche Hilfe von Vermittlungs- bzw. Beratungsdiensten (Promotionsberater oder andere Personen) in Anspruch genommen. Niemand hat von mir unmittelbar oder mittelbar geldwerte Leistungen für Arbeiten erhalten, die im Zusammenhang mit dem Inhalt der vorgelegten Dissertation stehen.

Die Arbeit wurde bisher weder im In- noch im Ausland in gleicher oder ähnlicher Form einer anderen Prüfungsbehörde vorgelegt.

Die geltende Promotionsordnung der Physikalisch-Astronomischen Fakultät ist mir bekannt.

Ich versichere ehrenwörtlich, dass ich nach bestem Wissen die reine Wahrheit gesagt und nichts verschwiegen habe.

Jena, 29.05.2009

Micaela Bianca Stumpf